


Fall 2016

# An Examination of the Indentation Size Effect In FCC Metals and Alloys from a Kinetics Based Perspective Using Nanoindentation

David Earl Stegall  
*Old Dominion University*

Follow this and additional works at: [https://digitalcommons.odu.edu/mae\\_etds](https://digitalcommons.odu.edu/mae_etds)

 Part of the [Materials Science and Engineering Commons](#), [Mechanical Engineering Commons](#),  
and the [Nanoscience and Nanotechnology Commons](#)

---

## Recommended Citation

Stegall, David E.. "An Examination of the Indentation Size Effect In FCC Metals and Alloys from a Kinetics Based Perspective Using Nanoindentation" (2016). Doctor of Philosophy (PhD), dissertation, Mechanical Engineering, Old Dominion University, DOI: 10.25777/40nm-s175  
[https://digitalcommons.odu.edu/mae\\_etds/21](https://digitalcommons.odu.edu/mae_etds/21)

This Dissertation is brought to you for free and open access by the Mechanical & Aerospace Engineering at ODU Digital Commons. It has been accepted for inclusion in Mechanical & Aerospace Engineering Theses & Dissertations by an authorized administrator of ODU Digital Commons. For more information, please contact [digitalcommons@odu.edu](mailto:digitalcommons@odu.edu).

**AN EXAMINATION OF THE INDENTATION SIZE EFFECT IN FCC  
METALS AND ALLOYS FROM A KINETICS BASED PERSPECTIVE  
USING NANOINDENTATION**

by

David Earl Stegall  
B.S. August 1996, Old Dominion University  
M.E. December 2000, Old Dominion University  
M.B.A. August 2004, Old Dominion University

A Dissertation Submitted to the Faculty of  
Old Dominion University in Partial Fulfillment of the  
Requirements for the Degree of

DOCTOR OF PHILOSOPHY

MECHANICAL ENGINEERING

OLD DOMINION UNIVERSITY  
December 2016

Approved by:

A. A. Elmustafa (Director)

Gene Hou (Member)

Dipankar Ghosh (Member)

Yousuf Mohammed (Member)

Helmut Baumgart (Member)

**ABSTRACT****AN EXAMINATION OF THE INDENTATION SIZE EFFECT IN FCC METALS AND ALLOYS FROM A KINETICS BASED PERSPECTIVE USING NANOINDENTATION**

David Earl Stegall  
Old Dominion University, 2016  
Director: Dr. A. A. Elmustafa

The indentation size effect (ISE) in metals is described as the rise in hardness with decreasing depth of indentation and contradicts conventional plasticity behavior. The goal of this dissertation is to further examine the fundamental dislocation mechanisms that may be contributing to the so-called indentation size effect. In this work, we examined several metals and alloys including 99.999% Aluminum (SFE  $\sim 200 \text{ mJ/m}^2$ ), 99.95% Nickel (SFE  $\sim 125 \text{ mJ/m}^2$ ), 99.95% Silver (SFE  $\sim 22 \text{ mJ/m}^2$ ), and three alloys, alpha brass 70/30 (SFE  $> 10 \text{ mJ/m}^2$ ), 70/30 nickel copper (SFE  $\sim 100 \text{ mJ/m}^2$ ), and 7075 AlZn (SFE  $\sim 125 \text{ mJ/m}^2$ ) to study the effect of stacking fault energy on the ISE. The current work sought to address several objectives including; 1) Verify the existence of an ISE and the bilinear behavior of various FCC metals using single indentation test platform and the same tip for various stress decades: 2) Examine the thermally activated mechanisms that could contribute to the ISE via the kinetics of plastic deformation based on indentation experiments for constant load creep and load relaxation as well as classical uniaxial testing to study the coupled relationship between strain rate, dislocation density, and dislocation velocity: 3) Examine the possible contribution of stacking fault energy (SFE) on the ISE by comparing pure metals over a wide SFE range as well as the effect of alloying. We demonstrate that all the metals tested exhibit a clear ISE using a new approach that included the use of a single machine and using a single tip capable of reaching depths of  $30 \mu\text{m}$ . This eliminated any uncertainty in measurements when comparing data for any metal across the

nano to micro-range (from 0.07 *mN* to 10 *N*). It was found that the pure metals should be examined separately from the alloys when examining any dependency on SFE. Activation volume analysis, based on indentation creep experiments, was used to examine the stress dependency of the activation volume for each metal. We verified through various experiments across a wide stress range that the ISE has a kinetic signature similar to that found in uniaxial testing for work hardening. We propose an analysis of the ISE in terms of Orowan's equation which relates the strain rate to dislocation density and dislocation velocity. We performed indentation creep tests across a wide loading range to measure the strain rate sensitivity of the hardness and determine the activation volume. We found that when the data were fitted to the Orowan relation, and the GND dislocation density was assumed to increase according to strain gradient plasticity theory for an ISE, the hardness increased as the dislocation velocity decreased along with the activation volume. To confirm these observations, we developed a new indentation test protocol to perform repeated load relaxation tests in indentation to examine the dependence of dislocation velocity and density on the relaxation strain rate. We found that the relaxation data matched our assumptions that were based on the indentation creep experiments. As the hardness (stress) increases, the ratio of the dislocation velocity decreases, while the dislocation density increases, and the activation volume decreases. We fitted the dislocation velocity data to the bilinear behavior model introduced by Elmustafa and Stone (2003) and found that the dislocation velocity measurements for the pure metals showed a distinct bilinear behavior with increasing stress. The bilinear velocity data in the nano-region had a different slope compared to the data measured at deeper depths of indentation. These findings support the theory that at shallow depths of indentation the ISE is dominated by dislocation-dislocation interactions. Finally, to address the SFE issue, we conducted a variety of indentation tests including standard load

control testing and indentation creep. We showed that while a weak correlation of the ISE with SFE is observed for the pure metals tested, the influence of SFE for all metals and alloys cannot be made.

This work, in its entirety, adds to the understanding of the mechanisms that influence the ISE and contributes valuable data and methodologies for future investigators on which to draw.

Copyright, 2016, by David E. Stegall, All Rights Reserved.

This dissertation is dedicated to my children, David and Samantha.

## ACKNOWLEDGEMENTS

I want to first thank God for opening this door. I am profoundly grateful to my dissertation advisor, Dr. Abdelmageed Elmustafa, for his steadfast support, faithfulness, and commitment in the production of this work. I want to express my deep thanks and admiration for my colleagues, past and present, at the ODU/ARC Nanoindentation Lab. I thank my dissertation committee members for their guidance and valuable suggestions to improve this manuscript. Finally, I want to thank my family who supported me through these years of study, and especially my wife who has been my greatest support and without whom my life would not be complete.



## TABLE OF CONTENTS

|  | Page |
|--|------|
| LIST OF TABLES .....   | x    |
| LIST OF FIGURES .....  | xi   |
| CHAPTER .....  | 1    |
| 1. INTRODUCTION.....   | 1    |
| 1.1 Review of the Indentation Testing .....  | 2    |
| 1.2 Review of Theories to Account for the ISE .....  | 6    |
| 1.3 Review of Work Hardening and Flow Stress .....   | 11   |
| 1.4 Review of Microscopic Methodologies (TEM, EBSD).....   | 15   |
| 1.5 Review of Mechanical Methodologies .....   | 22   |
| 2. SCOPE OF WORK .....   | 23   |
| 2.1 Goals and Objectives.....  | 23   |
| 2.2 Outline of the Experimental Work .....   | 25   |
| 3. INDENTATION SIZE EFFECT IN FCC METALS: AN EXAMINATION OF<br>EXPERIMENTAL TECHNIQUES AND THE BILINEAR BEHAVIOR ..... | 30   |
| 3.1 Introduction.....  | 30   |
| 3.2 Experiments .....  | 33   |
| 3.3 Results .....  | 36   |
| 3.4 Discussion .....   | 48   |
| 3.5 Conclusions.....   | 53   |
| 4. THE ACTIVATION VOLUME OF PURE FACE CENTERED CUBIC METALS USING<br>UNIAXIAL TESTING AND NANOINDENTATION .....        | 55   |
| 4.1 Introduction.....  | 55   |
| 4.2 Experiments .....  | 60   |
| 4.3 Results .....  | 63   |
| 4.4 Discussion .....   | 66   |

|     |  |     |
|-----|--|-----|
| 4.5 | Conclusion .....   | 69  |
| 5.  | REPEATED LOAD RELAXATION TESTING OF PURE POLYCRYSTALLINE NICKEL AT ROOM TEMPERATURE USING NANOINDENTATION.....   | 70  |
| 5.1 | Introduction.....  | 70  |
| 5.2 | Experiments .....  | 71  |
| 5.3 | Results .....  | 73  |
| 5.4 | Discussion .....   | 77  |
| 5.5 | Conclusion .....   | 80  |
| 6.  | THE CONTRIBUTION OF DISLOCATION DENSITY AND VELOCITY ON THE STRAIN RATE AND SIZE EFFECT USING TRANSIENT INDENTATION METHODS AND ACTIVATION VOLUME ANALYSIS ..... | 82  |
| 6.1 | Introduction.....  | 82  |
| 6.2 | Experiments .....  | 83  |
| 6.3 | Results .....  | 87  |
| 6.4 | Discussion .....   | 93  |
| 6.5 | Conclusion .....   | 97  |
| 7.  | THE INDENTATION SIZE EFFECT AND STACKING FAULT ENERGY: ADDITIONAL PERSPECTIVES.....  | 99  |
| 7.1 | Introduction.....  | 99  |
| 7.2 | Experiments .....  | 101 |
| 7.3 | Results .....  | 101 |
| 7.4 | Discussion .....   | 105 |
| 7.5 | Conclusion .....   | 110 |
| 8.  | CONCLUSIONS .....  | 111 |
| 8.1 | Future Work.....   | 114 |
|     | REFERENCES.....  | 116 |
|     | APPENDIX A.....  | 125 |
|     | VITA.....  | 142 |

## LIST OF TABLES

| Table   | Page |
|---|------|
| 1 Calculated versus measured depths for tapping to occur using CSM.....               | 44   |
| 2 Comparison of the Hardness results from Load control and the extrapolated load..... | 76   |
| 3 Creep versus Load Relaxation .....  | 96   |
| 4 Normalized SFE for Pure FCC metals and Alloys .....                                 | 102  |

## LIST OF FIGURES

| Figure  | Page |
|---|------|
| 1 Load depth curve.....   | 3    |
| 2 Schematic of a typical SEM.....   | 16   |
| 3 Schematic of typical EBSD Setup .....   | 17   |
| 4 Schematic of a typical TEM .....  | 20   |
| 5 CSM and load control data to $\sim 25 \mu\text{m}$ .....  | 36   |
| 6 CSM and load control data from surface to $2 \mu\text{m}$ .....   | 37   |
| 7 Typical $\alpha$ -brass CSM hardness versus depth curve identifying the three regions of changing hardness as articulated by Almasri et al.[61] ..... | 38   |
| 8 Schematic of an indent and associated plastic zone in a pure nickel sample having a grain size of $\sim 100 \mu\text{m}$ .....                        | 39   |
| 9 High Berkovich Tip XP-Series Method on pure polycrystalline nickel.....   | 41   |
| 10 Standard Berkovich Tip XP-Series Method on pure polycrystalline nickel.....  | 42   |
| 11 Load-depth curves for $\alpha$ -brass and fused silica.. .....   | 43   |
| 12 Hardness depth curves for various E/H ratio metals.....  | 45   |
| 13 High Load Berkovich Tip New G-Series Method on pure polycrystalline nickel.. .....   | 47   |
| 14 Standard Berkovich Tip New G-Series Method on pure polycrystalline nickel.. .....  | 47   |
| 15 Comparison of hardness versus depth for pure nickel.....   | 50   |
| 16 BiLinear behavior from Nano to Micro scale using a single tip.....   | 52   |
| 17 Grain sizes of 120, 97, and $100 \mu\text{m}$ for Al, Ag, and Ni.....  | 61   |
| 18 Stress-strain curves for Al, Ag, and Ni.....   | 63   |
| 19 Activation volume versus hardness for Al.....  | 64   |
| 20 Activation volume versus hardness for Ag.....  | 65   |
| 21 Activation volume versus hardness for Ni.....  | 66   |
| 22 Incremental load relaxations versus time for maximum loads of $500 \text{ mN}$ and $50 \text{ mN}$ . .....   | 73   |

| Figure  | Page |
|---|------|
| 23 Load versus displacement curve using the load control test protocol with 5 incremental unloading segments. ....                  | 74   |
| 24 Load versus displacement curve using the load control test protocol modified for repeated load relaxations. ....                 | 75   |
| 25 Hardness (stress) relaxations versus time compared with the ratio of $v/v_o$ and $\rho/\rho_o$ for the 50 mN maximum load .....  | 79   |
| 26 Hardness (stress) relaxations versus time compared with the ratio of $v/v_o$ and $\rho/\rho_o$ for the 500 mN maximum load ..... | 80   |
| 27 Strain rate sensitivities of the hardness for pure Al, Ni, Ag.....   | 86   |
| 28 Load relaxation curves for all 3 metals at 50 and 500 mN. ....   | 87   |
| 29 Velocity and normalized activation volume versus H for Al. ....  | 89   |
| 30 Velocity and normalized activation volume versus H for Ag.....   | 90   |
| 31 Velocity and normalized activation volume versus H for Ni. ....  | 91   |
| 32 Results of repeated relaxation tests for Al. ....  | 92   |
| 33 Hardness versus depth metals and alloys.....   | 102  |
| 34 Magnitude of the ISE for pure metals and alloys .....  | 103  |
| 35 Bi-linear behavior for pure metals and alloys.....   | 104  |
| 36 $V^*$ versus hardness normalized to the reduced modulus.....   | 105  |
| 37 SEM image of $\alpha$ -brass indentation.....  | 108  |
| 38 SEM image of aluminum indentation .....  | 109  |
| 39 SEM image of silver indentation .....  | 109  |

## **CHAPTER 1**

### **INTRODUCTION**

Deviations from the conventional theories that govern the plasticity of metals have been the source of fundamental research for decades. Those deviations that are length scale dependent have been of particular significance in recent years due to the exponential growth in the so called nanotechnology sector. The rapid change in integrated circuit technology is the most notable driver in this field which has seen a doubling of the density on circuit components integrated on silicon substrates every few years, from the hundreds of microns in the mid twentieth century to the tens of nanometers at present. To facilitate these advancements, testing methodologies have been developed to characterize the mechanical properties of materials, including metals, at the sub-micron and nanometer scales. These methodologies generally strive to relate the properties measured for small volumes of material to those measured at macro-scale which are based on classical techniques including tensile, creep, fracture, and hardness testing. The hardness test is uniquely suited for examining small volumes of material given its design and relatively simple execution. In light of the interest in establishing mechanical properties at diminishing length scales a well-known phenomenon noted in indentation testing referred to as the indentation size effect (ISE) has been the source of debate for many years. The ISE is generally described as an increase in hardness with decreasing depth of penetration. The relevance of understanding the mechanisms that govern the ISE is significant given it contradicts conventional plasticity theories of indentation whereby the hardness is expected to be load independent for self-similar indenters.

This chapter summarizes the development of indentation testing and the traditional theories developed to relate hardness to other stress strain behavior. A brief overview of the strain gradient plasticity theory developed to account for the ISE is presented. This is followed

by a short overview of techniques including transmission electron microscopy and electron backscattered diffraction techniques developed to visually observe dislocation mechanisms that could be contributing to the ISE in metals. Finally, a brief review of the experimental work and methods using techniques such as instrumented indentation to examine deformation mechanisms governing deformation and plastic flow at the nanoscale.

### **1.1 Review of the Indentation Testing**

The hardness of a material is generally measured by pressing a rigid indenter into the surface of a sample at a defined load. Most indenters are diamond fabricated with a spherical, conical, or pyramidal shape. Testing devices are usually classified based on; (1) the impressed load being either macro ( $\lll 10\text{ N}$ ), micro (typically  $\sim 100\text{ mN} \leq x \leq 10\text{ N}$ ), or in more recent years nano ( $\ggg 100\text{ mN}$ ); (2) the type of measurement being either one that is based on the dimensions of the indentation (Brinell, Vickers, and Knoop) or one that is based on depth of penetration (Rockwell and Instrumented Indentation (IIT) or nanoindentation) [1].

Prior to the development of IIT, the hardness derived using classical microhardness testers required that the contact area from the residual impression of an indenter be measured under magnification. This became a limiting factor for establishing hardness at very shallow depths of indentation due to the difficulty in accurately measuring the contact area for very shallow indents. IIT, or nanoindentation, is based on the simultaneous monitoring of both displacement and load allowing for the hardness and modulus of a material to be measured continuously throughout the indentation cycle. A typical system consists of a magnetic coil providing load on a shaft supported by springs with a diamond tip at the opposite end. The displacement is usually monitored using parallel capacitive plates. The entire system is calibrated

to precisely measure the stiffness of the sample and machine. Based on continuous monitoring, the load versus displacement histories can be plotted similar to Figure 1.

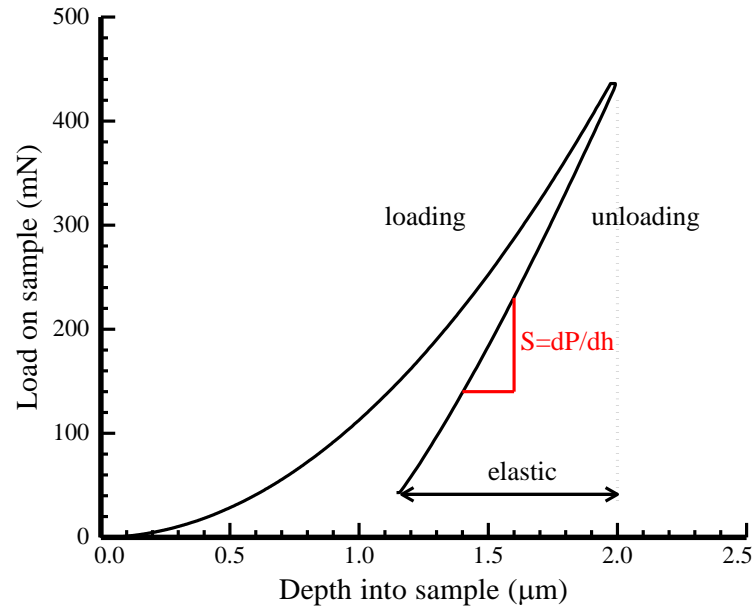


Figure 1 Load depth curve

A technique, commonly known as the Oliver-Pharr method, has been widely used for the analysis and derivation of hardness and modulus using IIT data [2]. This method uses the stiffness measured as the change in force over the change in displacement on the unloading side of the curve as shown schematically in Figure 1. The basis of the Oliver Pharr method is realized by the ability to determine the contact depth from the measured displacement minus the ratio of the force divided by the stiffness as given in Equation 1[3].

$$h_c = h - \varepsilon \frac{P}{S} \quad (1)$$

In Equation 1,  $h_c$  is the contact depth,  $h$  is the measured displacement,  $\varepsilon$  is a constant related to the indenter geometry,  $P$  is the measured force, and  $S$  is the stiffness. The power of this relation



is noticeably that the contact depth, and thus contact area, can be determined without the need to visually measure the residual impression under magnification. This facilitates measurements at very small scales. The contact area is based on the indenter geometry and has been analytically derived as a function of the contact depth. At this stage of the analysis the hardness can be calculated based on the load divided by the contact area at any depth and load. Similarly, this method allows for the determination of the modulus based on the relation given by Equation 2 that defines the so called reduced modulus  $E_r$  [2, 3].

$$E_r = \frac{\sqrt{\pi}S}{2\beta\sqrt{A}} \quad (2)$$

The Young's modulus is related to the reduced modulus and the modulus of the indenter as well as Poisson ratio of the indenter and sample, according to Equation 3 [2, 3].

$$E = \left[ \frac{1-\nu^2}{E_r} - \frac{1-\nu_i^2}{E_i} \right] \quad (3)$$

The Oliver-Pharr method has been successfully implemented for the determination of hardness and modulus for many materials, both brittle and elasto-plastic, using the standard load control protocol similar to that employed for traditional microhardness testing. In particular, the load control protocol relates to the calculation of hardness and modulus at a specific load and depth. An additional protocol known as continuous stiffness measurement (CSM) was developed to measure hardness and modulus as a function of depth also using the Oliver Pharr method. The CSM introduces a slight harmonic oscillation on the indenter shaft, usually resulting in less than two nanometers displacement, and measures the dynamic response at each unloading oscillation. The CSM can be thought of as a series of loading/unloading displacement curves, similar to that shown in Figure 1, for a single loading/unloading based on LC protocol, but is distinct in that the

hardness and modulus can be calculated at each cycle. The change in stiffness is essentially the elastic rebound of the material for each successive cycle.

It is recognized that the measurement of hardness is essentially the materials resistance to deformation given it is not a unique fundamental material property but is relevant to the derived mechanical performance and in the case of metals, is associated with the flow (or yield) stress and work hardening behavior [4]. It is with this understanding that care be taken when attempting to derive a relationship between hardness and yield stress due to the dissimilar nature of the stress and strain states when comparing uniaxial tension and indentation. While the hardness test is simple in its execution, a mathematical solution describing the deformation field around the indentation is required to develop its relation to flow stress [5]. To this end, a great deal of the research performed in the first half of the twentieth century was devoted to the development of models relating hardness in indentation to the flow stress for non-strain hardening and strain hardening metals using different indenter geometries. One of the foundational definitions of hardness is known as the Meyer hardness and is defined as the load divided by the area of contact and has units of stress in Newtons [6]. The well-known Meyer Law was developed from this definition of hardness using a power law relation between the load and the depth based on constants related to work hardening and predicts that for a geometrically self-similar indenter the hardness would remain constant regardless of load [1, 6]. Similarly, much research was devoted to the pursuit of a relation between hardness and flow stress based on different indenters. The relationship, now commonly referred to as the Tabor relation, where the hardness is generally equal to three times the yield (flow) stress was experimentally found to be accurate regardless of indenter type and prior material condition [1, 7].

The traditional theories that govern indentation plasticity predict that for an indenter possessing a self-similar geometry the hardness would not be dependent on load, or depth of penetration. This observation has been shown to be incorrect for very low loads and shallow depths of penetration for many materials most notably metals. A prevailing theory based on dislocation hardening due to strain gradients beneath the indenter was accepted as being responsible for the ISE.

## **1.2 Review of Theories to Account for the ISE**

The size effect in indentation has been experimentally observed for microhardness tests well over sixty years and reported by various researchers [8-12]. These types of observations resulted in an abundance of research over the years to isolate the physical anomalies or specific material mechanisms responsible for the ISE. An example of a physical explanation included surface distortion due to oxides or mechanical polishing. This idea was subsequently ruled out by careful experimentation that showed the ISE is present in both electro-polished and mechanically polished specimens of the same material [13].

The most widely accepted explanation is that the ISE is based on some fundamental material behavior most likely associated with dislocation mechanisms in the vicinity of the indenter tip [14]. It was proposed that strain gradients beneath the indenter introduced an abundance of geometrically necessary dislocations (GND) that are required to maintain compatibility in the lattice and that these dislocations provide the hardening responsible for the ISE [11, 15-19]. A model was developed by Nix and Gao based several factors including; on a constant material length that is related to an intrinsic material length scale; with the length between dislocations; the concept of GND loops that are accommodated within a hemispherical

volume under the indenter; and the Taylor dislocation hardening model [20, 21]. The Taylor relation is given as follows:

$$\tau = \alpha G b \sqrt{\rho_g + \rho_s} \quad (4)$$

where  $\tau$  is the flow stress,  $\alpha$  is a constant 0.33,  $G$  is the shear modulus,  $b$  is the Burgers vector, and  $\rho$  is the dislocation density. This relation defines the dependence of the flow stress with the square of the sum of the GND and statistically stored dislocation (SSD) densities. The GND density scales with the strain gradient whereas the SSD density scales with the effective strain. This equation is then related to the Tabor relation where the hardness is generally equal to three times the flow stress yielding equation 5.

$$H = 3\alpha G b \sqrt{\rho_g + \rho_s} \quad (5)$$

It is assumed that the GND density is confined to a hemispherical volume beneath the contact of the indenter. Nix and Gao surmised that the GND scale with the strain gradient while the SSD scale with the effective strain thereby the GND are constrained by the radius of contact in accordance with the Taylor dislocation hardening model [21]. This led to equation 6 which is based on the geometry of the indenter and has particular significance given the GND are inversely proportional to the depth  $h_c$ .

$$\rho_g = \frac{\tan^2 \theta}{2bh_c} \quad (6)$$

Finally, Nix and Gao relate the above equations to form the following:

$$\frac{H}{H_o} = \sqrt{1 + \frac{h^*}{h}} \quad (7)$$

And;

$$H_o = 3\alpha Gb\sqrt{\rho_s} \quad (8)$$

where  $H_o$  is the bulk hardness at depths where SSD dominate, and  $h^*$  is the length scale required for the ISE given by;

$$h^* = \frac{81}{2} b\alpha^2 \tan^2 \theta \left(\frac{G}{H_o}\right)^2 \quad (9)$$

It is noted that when the experimental data were fitted to Nix and Gao model, the data depart from the linearity at shallow depths of indentation contrary to what the model predicts. Other researchers confirmed this deviation when comparing different materials [22, 23]. Simulations were developed to analytically model the behavior and ascertain the source of the deviation for the nanohardness data. Huang et al concluded that the discrepancy between the Nix Gao model and experimental data was based on a combination of the indenter tip radius at small depths and the misrepresentation of the size of the storage volume for the GNDs [24]. A modified material length scale  $h^*$  was subsequently proposed to correct for the radius of the plastic zone when accommodating GND's in lieu using the radius of contact as given in Equation 6 above leading to Equation 10 [23].

$$\rho_g = \frac{3}{2} \frac{1}{f^3} \frac{\tan^2 \theta}{bh_c} \quad (10)$$

The parameter  $f$  was analytically derived based on the maximum strain gradient beneath the indenter in the contact region and was reported to be on the order of 1.5 to 2 based on material examined [23]. This equation enhanced the estimate of the GND density in the plastic zone and partially corrected for the discrepancy in the Nix Gao model.

An alternate approach was developed by Elmustafa and Stone to fit experimental data across the nano to micro scale that is similar in its approach to the above but based its GND estimation on the following from Ashby;

$$\rho_g = \frac{4\Gamma}{bh_c} \quad (11)$$

where,  $\Gamma$  is the strain in the plastic zone estimated at about 19%,  $b$  times  $h_c$  is the characteristic length over which the gradient exists [25]. This estimation of the GND density was first introduced by Ashby and used by Ma and Clark in their model for single crystalline silver [11, 26]. It is noted that the difference between the calculated GND density when comparing Equation 10 and Equation 11 is  $\sim 1.0$  when considering a Berkovich tip having an included angle of  $65.3^\circ$  and  $f \approx 2.1$ . The Taylor dislocation hardening model is used along with the sum of the GND and SSD densities shown in Equation 4. In this model the hardness is approximately the hardness at yield plus 9 times the flow stress in shear and is given in Equation 12 (where  $\lambda=9$ ).

$$H = H_f + \lambda\sigma \quad (12)$$

Combining Equation 8 with Equation 4 and Equation 12 yields the following;

$$\frac{(H-H_f)^2}{4\Gamma\lambda^2\alpha^2G^2b} = \frac{b\rho_s}{4\Gamma} + \frac{1}{h_c} \quad (13)$$

This model shows that the hardness increases inversely in proportion with decreasing depth of indentation. A plot of the left hand side of Equation 13 versus  $h_c^{-1}$  should result in a straight line having a slope equal to 1. This equation has been called the bilinear behavior model and Elmustafa and Stone concluded that at shallow depths of indentation the left hand side of Equation 13 exhibits a distinct change in slope from deeper indentation depths and attributed this change to dislocation-dislocation interactions at the shallow depth of indentation [27].

The strain gradient plasticity based model including the various enhancements have been successfully fitted to the nano and microhardness data for numerous single crystal and polycrystalline metals. Among the most significant enhancements was the introduction of mechanism based strain gradient plasticity theory (MBSGPT) where an intrinsic material length scale was introduced to account for GND interaction on specific slip systems around the gradient [21, 28]. It is now widely accepted that excessive GND's are responsible for the ISE hardening and that sharp strain gradients accommodate the hemispherical volume beneath the indentation. To further understand how dislocation mechanisms interact and affect the kinetics of deformation additional experimental techniques are required to be employed. The subsequent sections present alternate methodologies for examining the dynamics of dislocation content, movement, and interaction. The first approaches are based on techniques to visually examine dislocation structures and movement by observation using electron microscopy. The second set of methodologies utilize techniques that infer dislocation movement and interaction by employing mechanical tests used to measure the flow stress.

### 1.3 Review of Work Hardening and Flow Stress

The resistance to deformation and the required increase in stress and strain is known as work hardening. The ability of a metal to work harden is based on the density of dislocation networks interacting with each other as well as other structural barriers, i.e. lattice friction, grain boundaries, and precipitate atoms, to impede motion during straining [4]. Many theories have been developed to account for work hardening including Taylor, a dislocation hardening model, which led to Equation 4 and was based on the concept of dislocation pileup at obstacles and boundaries. Taylor originally derived the expression based on the square root density of the dislocations to model the observed parabolic hardening curve [4]. Work hardening can be visually examined for face centered cubic (FCC) metals by a simple shear stress shear strain curve derived from a uniaxial tensile test; therefore, they are attractive to study. There are three regions of the curve designated as Stage I, Stage II, and Stage III that have been defined to describe the work hardening behavior. Stage I is typically characterized as the beginning at the hardening where the dislocations are thought to move easily through the crystal without much added stress due to a low density and few obstacles and is thus referred to as easy glide and has a linear nature with low hardening rate [4, 29]. Stage II is characterized by a higher rate of linear hardening with slip extending to secondary systems and a greater number of barriers that rapidly increase the dislocation multiplication and sources. This stage is relatively independent of stress and temperature and thus the primary mechanism for hardening is predominantly due to dislocation pileup according to the Taylor dislocation hardening model [4, 29]. Stage III is characterized by a region of decreased rate of hardening due to the so called “dynamic recovery” whereby dislocations are eliminated by mutual annihilation or escaping at a free surface and is a strong function of temperature [4, 29]. Many FCC metals exhibit all three stages of work



hardening but some factors can affect the presence and limits of each stage. These factors will be discussed later in this section.

In the case of a polycrystalline FCC metal the flow stress curve consists of two distinct regions starting with an elastic deformation where the stress increases linearly with strain times the Young's modulus for the metal obeying Hooke's law. When the proportional limit is reached the metal enters a nonlinear region where the stress and strain are characterized by the familiar power law relationship for strain (work) hardening given in Equation 11 [29].

$$\sigma_f = K\epsilon^n \quad (14)$$

In Equation 14, the flow stress is defined by a power law relation comprised of a strength constant  $K$  times the strain raised to a power term  $n$  called the "strain (work) hardening coefficient". The value of  $n$  has particular significance in classifying metals based on their propensity to work harden. When a strain rate based test is performed, a similar parameter known as the strain rate sensitivity (SRS),  $m$ , can be derived using Equation 15.

$$m = \left( \frac{\partial \ln \sigma}{\partial \ln \dot{\epsilon}} \right) \quad (15)$$

From a strain rate change or stress relaxation test a power law is established and is given by Equation 16 [29].

$$\sigma_f = C\dot{\epsilon}^m \quad (16)$$

The SRS  $m$  also is useful in relating dislocation behavior with thermally activated processes as a fundamental parameter used in calculating the so called activation volume which will be introduced in the following Section. Also, the flow stress is known to increase with increasing strain rate and thus work hardening is strongly associated with  $m$  [4].

The plastic deformation of metals is an irreversible process that is based on the movement, accumulation, and storage of dislocations whose motion has been impeded by some

barriers. The barriers are typically local, angstrom level, or longer range, over tens of nanometers range, and it is the distribution and type of barriers that are responsible for the hardening of the metal during straining. In the case of dislocations it is the shear stress,  $\tau$ , acting on preferential slip planes that is the driving mechanism for plastic deformation and flow. An increase in  $\tau$  is required for the continued movement of dislocations during straining and thus plastic deformation. The shear stress is a function of several variables including strain, structure, strain rate, and temperature. There are two basic components that  $\tau$  is dependent upon on, one having a thermal sensitivity ( $\tau^*$ ) and the other being athermal ( $\tau^a$ ) [4, 29, 30]. The athermal component does not depend on temperature nor strain rate and thus is associated with long range obstacles and stress fields and finds no benefit from thermal activation to overcome obstacles and long range barriers [4, 29, 30]. The thermal component is temperature and strain rate dependent and is assisted by thermal fluctuations (vibrations) to overcome short range barriers resulting from impurities, solute atoms, lattice friction, forest dislocations, that tend to be a few atomic layers in distance [4, 29, 30]. The ratio of the thermal and athermal components ( $\tau^*/\tau^a$ ) commonly referred to a Cottrell-Stokes law, in Stage I is typically on the order of 1 and on the order of 0.1 for Stage II [4].

There are two important thermodynamic factors that assist in the motion of dislocations and thus the ability for FCC metals to work harden, thermal activation and stacking fault energy. Thermal activation assists plastic deformation (flow) by providing the energy necessary for a dislocation to climb, or move past, an obstacle in the active slip plane. First, the activation area is the atomic area characterized by the thermally activated process sweeping dislocation during plastic deformation. The activation area is defined as the length of the dislocation times the Burgers vector. When the activation area is multiplied by the distance to be overcome

due to an obstacle then the volume associated with thermal activation is given which is known as the activation volume  $V^*$  [4]. Dieter explains that study of the thermal activation process as it relates to plastic deformation is fundamental to validating dislocation processes in metals and the activation volume  $V^*$  in particular can provide information concerning the rate controlling mechanisms given its dependence on stress [29]. The calculation of  $V^*$  from mechanical tests provides a link to establish the dominance of long range and short range mechanisms during deformation and is typically given by Equation 17.

$$V^* \approx K_b T \left( \frac{\partial \ln \dot{\epsilon}}{\partial \ln \tau} \right)_T$$

In Equation 17,  $V^*$  is equal to the Boltzmann constant  $K_b$ , times the absolute temperature in Kelvin, times the partial natural log of the strain rate  $\dot{\epsilon}$ , divided by the partial of the shear stress  $\tau$ , at constant temperature [31]. The value of  $V^*$  is typically given on units of the cubic Burgers vector  $b^3$  and its magnitude is related to various dislocation mechanisms including climb, cross slip, glide, intersection forest dislocations, etc. [4, 31].

The second thermodynamic factor, the stacking fault energy  $\gamma_{sf}$ , is the energy required for a dislocation to “cross” to an adjacent slip plane in the presence of an obstacle and is unique to FCC metals. When a dislocation moves in the slip plane, it can disassociate into two partial dislocations and interrupt the stacking sequence of the atomic arrangement. For an FCC metal, the closest packed plane is the (111) plane and is typically denoted by the abbreviated packing (ABC/ABC/ABC...) sequence and a stacking fault is characterized by an interruption of the packing sequence due to the disassociated partials resulting in (ABC/AC/ABC...) where AC represents an unstable energy state [4, 29]. The width of the stacking fault ribbon determines the energy needed to cross slip and is impacted by factors including chemical composition and the addition of alloying. Metals having a high stacking fault energy,  $\gamma_{sf}$ , such as aluminum (~200

$mJ/m^2$ ) possess a narrow width stacking fault and can easily facilitate cross slip of dislocations while a metal having a low  $\gamma_{sf}$  such as silver ( $\sim 22 mJ/m^2$ ) possess a larger stacking fault width which inhibits cross slip. Additionally, an alloy such as alpha brass work hardens easily and possesses a very low  $\gamma_{sf}$  ( $<10 mJ/m^2$ ) with limited ability to cross slip, due to alloying [4, 29]. Therefore, the work hardening of metals and alloys can be examined based on  $\gamma_{sf}$  [4, 29]. The salient point of examining FCC metals in terms of  $V^*$  and  $\gamma_{sf}$  is that either of these two thermodynamic parameters give evidence for the signature of dislocation dominated mechanisms being responsible for the deformation process in terms of dislocation motion.

Krausz and Eyring describe two distinct methodologies traditionally used to examine deformation mechanisms in crystalline materials by dislocation movement that includes those based on visual observation, known as direct methods, and those that infer dislocation movement and structure based on measuring the flow stress during testing, known as indirect methods [31]. Both methodologies are based on the well-known Orowan's equation given in Equation 18 [31].

$$\dot{\epsilon} = b\rho\vec{v} \quad (18)$$

In Equation 18,  $\dot{\epsilon}$  is the strain rate,  $b$  is the Burgers vector,  $\rho$  is the average dislocation density, and  $\vec{v}$  is the average dislocation velocity. The density and velocity of dislocations, as a function of strain rate, are dependent on the same variables that affect thermal activation including temperature, stress, strain, and crystal structure [31]. These methodologies will be reviewed in the following two sections.

#### **1.4 Review of Microscopic Methodologies (TEM, EBSD)**

To examine the dislocation movement by direct means, the methods of choice in recent years has been to use either scanning electron microscopy (SEM) utilizing a high resolution electron backscattered diffraction (HREBSD) or by transmission electron microscopy (TEM)

techniques. A brief introduction to these techniques as well as recent experimental work regarding dislocation behavior around indentations is provided in this section.

The SEM is a microscope that utilizes an electron beam to image the surface of a conducting specimen at very high magnifications. The electron beam is typically generated using a powerful filament that is accelerated through a column of magnets that focus the beam to a very precise spot while under vacuum. The electron beam raster's back and forth over the specimen and penetrates the near surface layers. The reflected, or back scattered, beam is captured by a detector and an image of the surface features is produced on a monitor. The SEM has an incredible depth of field and is considered the best equipment today that has a spatial resolution of a few nanometers. A schematic of a typical SEM is given in Figure 2.

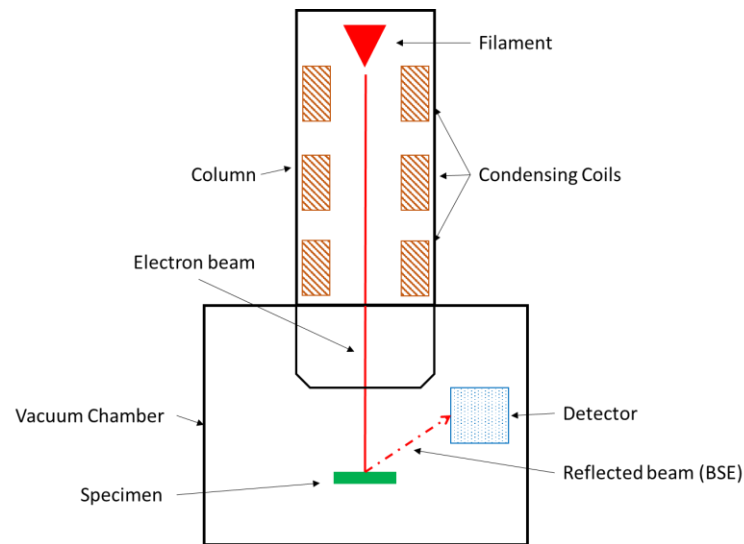


Figure 2 Schematic of a typical SEM

When the SEM is coupled with a charged couple device (CCD) camera, the backscattered electrons can be collected and characteristic patterns can be imaged that are analogous to Kikuchi lines [32]. The sample is typically rotated at an angle to the CCD camera similar to that one shown graphically in Figure 3.

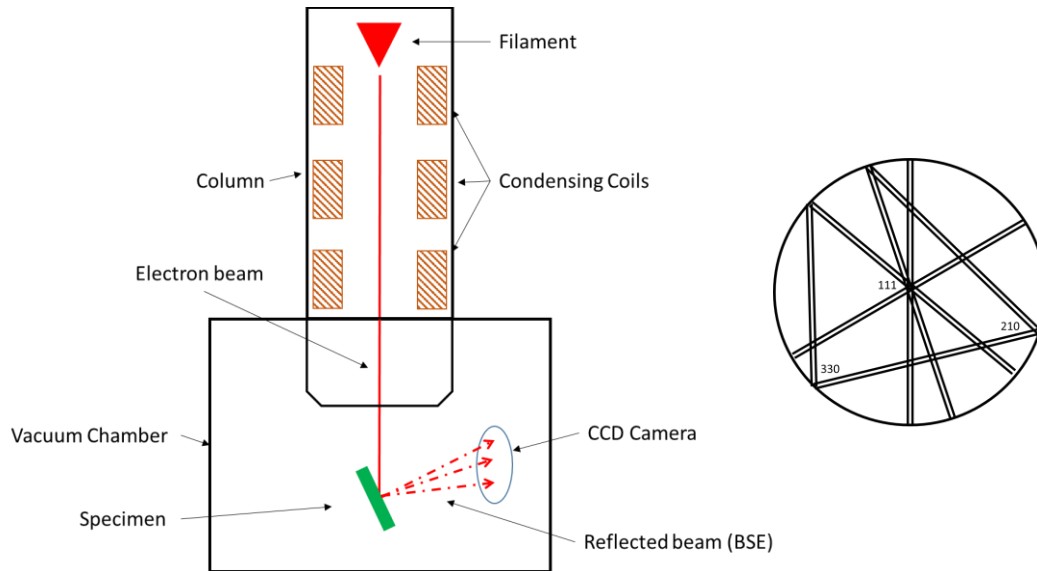


Figure 3 Schematic of Typical EBSD Setup

The hypothetical pattern on the right of Figure 3 is a representation of an EBSD patterning showing details of the crystal phases that are present in the sample which represent Kikuchi lines. With the use of computer technology, a technique known as Orientation Image Mapping (OIM) reveals many characteristics of the microstructure for a polycrystalline sample [32].

One such characteristic that is of particular interest is the measurement of strain based on observed lattice rotations due to gradients and GND structure resulting from plastic deformation. The specific mathematical framework that supports this measurement is beyond the scope of this work but has been covered in detail in the literature [33-39]. The ability of EBSD to estimate

GND densities based on the stored strain energy measured by lattice rotation makes it a desirable technique to examine the ISE. There have been a number of researchers that have reported on using EBSD to investigate the plastic zone around indentations for single crystal metals that exhibit an ISE [40-44]. The common findings of these efforts revealed that significant changes in the lattice rotation, or gradient in strain, are observed when comparing the volume beneath the indenter for shallow to deep indents that correlate to the ISE based on the MBSGP theory. It is noted that each of these studies relied on the use of a focused ion beam (FIB) to mill out the section through the indentation for EBSD examination. It is unclear if the ion beam may induce damage to the surface being milled and thereby lead to problems interpreting the data gathered by EBSD. This is a possible source of error for these types of examinations given the beam can lead to reorientation of grains that are necessary for OIM mapping and subsequent GND calculations. Mayer et al. discussed in detail the positive and negative effects that FIB may have on various materials including FCC metals [45]. In particular Mayer et al. pointed out that Gallium ( $\text{Ga}^+$ ) ions have been shown to cause reorientation of surface grains for fine grained FCC metals to form Ga intermetallic compounds. They showed several examples of Ga induced FIB damage to copper grains to depths of several hundred nanometers, well beyond the expected depth range for the ion doses imparted on the sample, and the resultant reorientation of grains using EBSD OIM [45]. It was further noted by Mayer et al. that similar reorientation based on FIB was observed for other FCC metals including aluminum, gold, and nickel. They conclude that caution should be exercised when using FIB to prepare samples for microstructural examinations due to the effects of beam exposure on reorientation of grains and possible misinterpretation of data gathered from EBSD OIM [45]. These types of sources of error when using FIB to prepare samples are mentioned to point out the possible issues when interpreting

EBSD data for GND estimations when cross sections through indentations were used as the basis for examining the ISE. In contrast, Kysar and coworkers have produced various studies beneath wedge indentations for copper and aluminum single crystals and examined the resulting cross section via EBSD [46]. The cross section was cut and subsequently electro-polished to remove any induced deformation. They produced very high resolution maps showing increased densities of GND's, on the order of  $10^{14} m^{-1}$ , in the zone directly beneath the indenter. The GND density tends to decrease for deeper indentations towards the bulk properties. They concluded that the copper sample showed an increased lattice rotation compared to the aluminum at equivalent depth of indentation and that there is a very high GND density directly beneath the indents [46]. These findings also support the MBSGP theory for the ISE being governed by the high density of GND's.

Based on these results, EBSD continues to be a powerful tool for conducting examinations of the influence of GND density in the plastic zone beneath indentations. There are however issues yet to be resolved to precisely construct the patterns necessary for lattice curvature assessments near the length scale of dislocations. A detailed study for using high resolution EBSD, the relevant issues encountered, and a novel set of approaches to address some of these issues is provided by Ruggles [47]. What is clear is that EBSD can provide an estimation of GND density based on data inferred from lattice rotations but that some uncertainty still exists. Further, EBSD does not provide specific information regarding dislocation sources or structural interactions. For more detailed analysis, the transmission electron microscope (TEM) is typically used.

The TEM differs from the SEM in that the electron beam penetrates the sample and produces an image that exposes through the thickness structure within the sample. In TEM, the



sample is generally a thin slice of material having a thickness on the order of micrometers. The sample is usually prepared by ion milling followed by controlled thinning of the cross section by acid etching. The etching also removes any disturbed layers from the milling process. The sample is loaded into the TEM mid-span of the column and the electron beam is focused at a point on the thin section. The electron beam passes through the sample and an image of the cross section is produced. A simple sketch of a TEM is given in Figure 4.

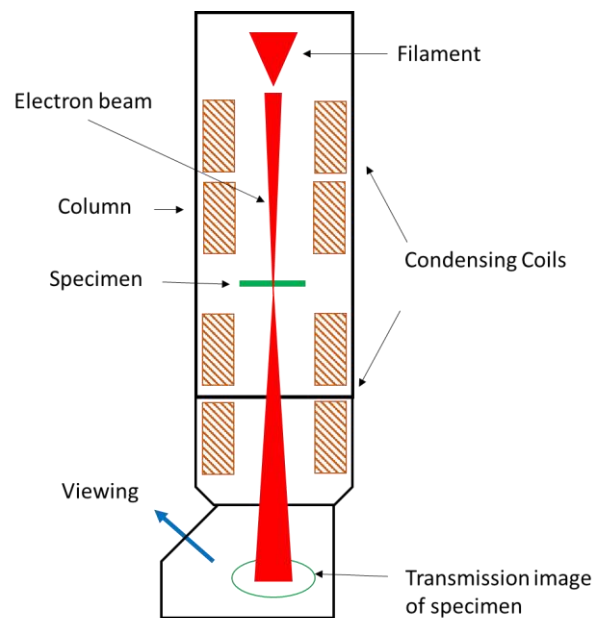


Figure 4 Schematic of a typical TEM

The volume immediately around and beneath a single indentation has been examined using TEM in some cases in conjunction with SEM/EBSD and has been documented by many researchers [11, 40, 42, 48-52]. Many of these studies examined the residual indentation posttest and required some form of milling operation to reveal the volume of material beneath the indenter. The work by Graca et al. was unique in that the indentations were made in an electron transparent area of a thin polycrystalline nickel coating using a self-similar diamond pyramid

indenter in an atomic force microscope (AFM) [52]. Furthermore, they attempted to interpret and correlate the results of their experiments using established theories for the ISE. From the TEM images of the indented regions they were able to report specific details about the resultant dislocation structures. In particular, they reported that plastic zone beneath the indent is accommodated by distinct mechanisms including a high dislocation density directly around the indentation, the presence of loops and helical dislocations propagating outward from the inner region, and the emission of straight line dislocations [52]. They articulated that the high dislocation density region closest to the indent was formed by sessile, immobile, dislocations resulting from pinning which was primarily considered responsible for the ISE. They further pointed out that the dislocations emanating outward from the plastic zone could be contributing somewhat to the ISE but to a lesser extent as the ones closest to the center of the indentation [52]. They concluded that the ISE is caused by a dislocation mechanism as anticipated by the Nix-Gao relation although the observed size of the plastic zone was larger than that model would predict [52].

Based on the above review, the use of TEM to directly image dislocation structures provides insights into how specific dislocation structures and types manifest to influence the plastic deformation responsible for the ISE. TEM allows for individual dislocation sources and structures to be identified as well as the extent to which they extend beyond the deformed zone. However, this type of experimental techniques require specialized equipment and great effort to prepare samples suitable for examination. This resulted in a limited number of materials that were selectively studied and most are single crystal. Therefore, methods based on the mechanical measure of flow stress continue to be developed to provide a more convenient means to infer

dislocation content and mobility that can be compared to the observed dislocation content based on TEM and to the density estimations provided by EBSD.

### **1.5 Review of Mechanical Methodologies**

The measure of plastic flow based on uniaxial tensile tests, constant load creep testing, stress/load relaxation testing, and strain rate jump testing can be used to indirectly infer the statistical average dislocation movement based on the Orowan's equation 18 [31]. Based on the estimations of the strain rate sensitivity, activation volume, dislocation density, and velocity, one can infer basic information concerning the interactions and structure of dislocations that govern the mechanisms that influence the kinetics of deformation. The most common experiments that are used to examine these parameters are transient type strain rate change, constant strain relaxation tests, and constant load creep tests performed in uniaxial tension at the macroscale. The remainder of this dissertation describes the implementation of similar types of experiments that have been adapted for indentation testing.

## CHAPTER 2

### SCOPE OF WORK

#### 2.1 Goals and Objectives

The goal of this dissertation is to further examine the fundamental dislocation mechanisms that may be contributing to the indentation size effect. An abundance of research has been conducted on single crystal FCC metals, however, only limited work has been done using polycrystalline metals. While much of the focus has been on visualizing the dislocation content associated with indentations at various depths up to  $2 \mu m$  using techniques including EBSD and TEM, to the best of my knowledge no work has been accomplished to examine dislocation mechanisms that may contribute to the ISE using a single indentation machine and tip capable of reaching from the nano to the micro scale. The current work sought to address the following objectives;

1. Verify the existence of an ISE and the bilinear behavior of various FCC metals using single indentation test platform and the same tip for various stress decades.

Motivation: This work is unique in that to date no other research has been published that provides indentation data on a wide variety of polycrystalline metals and alloys using a single test platform with the same tip for increasing stress decades. Further, this research uses equipment that has the capability of applying loads, using both the CSM and basic load control technique, which range from the  $.07 mN$  to  $10 N$ , or from the nano to the micro range. This capability, coupled with a special Berkovich tip fabricated to have a usable

geometry to 30  $\mu\text{m}$ , will address the issues faced by other researchers that used two different machines with two different tips.

2. Examine the thermally activated mechanisms that could contribute to the ISE via the kinetics of plastic deformation based on indentation experiments for constant load creep and load relaxation as well as classical uniaxial testing to study the coupled relationship between strain rate, dislocation density, and dislocation velocity.

Motivation: Dislocation cross slip and glide are thermally activated processes that drive the kinetics of deformation. This work will build on previously established research using well established techniques including activation volume and implications of Cottrell-Stokes law to examine the relationship between thermally activated processes and the ISE. This work will seek to examine, in greater detail, some of the more fundamental variables (including strain rate, dislocation densities, and dislocation velocity) that may contribute to the specific mechanisms governing thermally activated processes at low temperature for the different metals and will seek to establish relationships between each variable and the ISE.

3. Examine the possible contribution of stacking fault energy on the ISE by comparing pure metals over a wide SFE range as well as the effect of alloying.

Motivation: The work hardening of metals is primarily influenced by the ability of dislocations to cross slip during plastic deformation. Cross slip is known to be an activated process requiring an expenditure of energy to

overcome long range barriers. Elmustafa et al. examined the influence of SFE on the ISE using pure aluminum (high SFE) and alpha brass (low SFE) and concluded that the ISE was not affected by SFE [53]. However, their work considered only two polycrystalline metals and the conclusion was based on an examination of the magnitude of the ISE. The research presented herein postulated that a comparison of a pure metal and an alloy may not be appropriate for examining possible trends in ISE behavior based on SFE. Therefore, several metals and alloys of variable SFE were selected to test a wide set for a complete analysis. This aspect of the research will attempt to better understand the influence of stacking fault energy (SFE) on the indentation size effect (ISE) for several pure metals and alloys based on indentation experiments.

## **2.2 Outline of the Experimental Work**

This section describes the individual experimental work performed to accomplish this dissertation. The first set of experiments were designed to verify the ISE and the bilinear behavior for several FCC metals and the results are presented in Chapter 3 and were published in the Journal of Materials Research [54]. This work consisted of two basic components, a qualitative and a quantitative approach, and established the framework for the following experiments described in this dissertation. The qualitative component consisted of utilizing a single indentation machine and single tip to conduct all the different experiments. This approach eliminated any uncertainty in measurements when comparing data for any metal across the nano to micro-range (from 0.07 *mN* to 10 *N*). The work also incorporated a quantitative aspect in that

it added several pure metals and alloys that were chosen based on SFE and included 99.999% aluminum (SFE  $\sim 200 \text{ mJ/m}^2$ ), 99.95% nickel (SFE  $\sim 125 \text{ mJ/m}^2$ ), 99.95% silver (SFE  $\sim 22 \text{ mJ/m}^2$ ), and an alloy, alpha brass 70/30 (SFE  $> 10 \text{ mJ/m}^2$ ). Later studies included two additional alloys, nickel copper 70/30 (SFE  $\sim 100 \text{ mJ/m}^2$ ), and 7075 aluminum (SFE  $\sim 125 \text{ mJ/m}^2$ ). The addition of several different metals provided a larger dataset to draw conclusions concerning various aspects that may influence the ISE. Two separate test protocols were utilized in this work, load control and CSM. The CSM suffers what is known as “tapping” when testing soft metals having a high E/H ratio. The CSM experiences tapping by repeatedly losing contact with the surface of the specimen until an appreciable depth is reached. Additional experiments were conducted near grain boundaries to assess the possible influence of dislocation pile up on the CSM protocol. It was found that the issues related to CSM deviations at shallow depths of indentation were the result of machine error and the presence of grain boundaries had no effect. All the metals tested showed a clear ISE and all were found to depict a bilinear behavior. This proved that the ISE is real in each metal based on the qualitative approach that utilized the same machine and tip to conduct the experiments. Finally, the number of metals tested provided more data to satisfy the quantitative component to be used for additional investigations based on SFE. It was found that there was a weak correlation between the alignments of the metals based on SFE when fitted to the bilinear behavior model but additional alloys were required to draw any firm conclusion.

Based on the findings of the work described in Chapter 4, it was concluded that pure metals and alloys should be compared separately. Therefore, the work in Chapters 4, 5, and 6 focused on pure metals; whereas in Chapter 7 we examine the experimental research for both pure metals and alloys and the possible influence of SFE.

The experiments described in Chapter 4 are based on comparisons of the stress dependence of  $V^*$  derived from uniaxial and indentation creep tests for the pure metals. The content of this chapter were published in the journal Materials Research Express [55]. Tensile test data for each metal were obtained using conventional uniaxial testing. The tensile stress was converted to hardness and  $V^*$  was computed. Constant load indentation creep tests were performed at various loads that cover the nano to micro regime and  $V^*$  was computed. Finally, literature data sets from conventional uniaxial testing was included for comparison. In each case, the data for each metal converged to a linear curve. The  $V^*$  showed a clear dependence on hardness and was consistent with the theory of the accumulation of dislocations with strain hardening which results in smaller activation area swept out by dislocations during activation.

Following the work presented in Chapter 4, it was postulated that information concerning the dislocation density and the velocity of dislocation could be examined based on  $V^*$  since both the Orowan Equation 18 and Equation 17, for  $V^*$ , are based on strain rate which can be measured experimentally. It was further hypothesized that in the presence of an ISE, where the density of dislocations is known to increase based on MBSGP theory that the velocity of dislocations should slow in the region where size effects dominate. The work presented in Chapters 5 and 6 address this aspect of the research.

Chapter 5 provides the details for the development of a new experimental indentation technique, based on classical uniaxial experiments, for conducting constant strain repeated load relaxation experiments using nanoindentation. This method did not exist in the control software for the nanoindenter and was developed as part of this research. The content of Chapter 5 was published in the journal Applied Physics Letters [56]. The purpose of developing this technique was to develop a separate approach from the constant load indentation creep experiments to



verify observations of dislocation density and velocity based on the Orowan's equation (Equation 18) and the  $V^*$ . It was found that for a nickel sample when  $H$  increases,  $V^*$  decreases, the ratio of dislocation density increases, and the ratio of the dislocation velocity decreases.

The work in Chapter 6 describes constant load indentation creep and load relaxation tests that were performed on several FCC Al, Ag, and Ni metals that exhibit indentation size effect (ISE) to examine the coupled relationship between the activation volume  $V^*$  at specific loads, the dislocation density, and the dislocation velocity ( $v$ ) from kinetics based perspective. The work described in this chapter is currently under review for publication in the Journal of Materials Research. The influence of the indentation size effect on the dislocation velocity and the activation volume is thoroughly examined using the two independent indentation creep and load relaxation experiments. This work is carried upon the general experimental and theoretical hypothesis that the indentation size effect is driven by a dislocation mechanism, specifically the increase in the geometrically necessary dislocation density at shallow depth of indentation due to the presence of a large strain gradient. Geometrically necessary dislocations (GNDs) dominate the materials propensity to harden when their density exceeds the density of statistically stored dislocations (SSDs) and are primarily considered responsible for the size effects. Based on the pre-established bilinear behavior and the decrease of the activation volume with hardening due to dislocation-dislocation interaction in indentation creep experiments by Elmustafa and Stone [13, 27] it is demonstrated that the dislocation velocity exhibits a bilinear behavior when plotted versus hardness using the Orowan's relation [25]. Ag and Ni distinctively depict a bilinear behavior in the dislocation velocity with hardness, however Al exhibited a rather linear behavior. This can be explained by the fact that Al exhibits higher stages of work hardening at a much lower applied stress levels.

The research presented in Chapter 7 examines the possible influence of the SFE on the magnitude of ISE for various metals and alloys. As discussed in Chapter 4, when plotted based on the bilinear behavior model it was found that pure metals and alloys exhibited different behavior suggesting that different mechanisms were impacting the ISE. Therefore, the effect of SFE on the magnitude of ISE was investigated for pure metals Al, Ni, and Ag along with alloys of alpha brass (70/30 CuZn), Monel (70/30 CuNi), and 7075 Aluminum (95/5 AlZn). The SFE is known to impact alloys differently from pure metals based on the content of the solute. The effect of other interfacial phenomenon, including deformation twinning, on the ISE is also briefly examined.

Finally, Chapter 8 summarizes the objectives and primary conclusions of this dissertation and recommendations for future work.

## CHAPTER 3

### INDENTATION SIZE EFFECT IN FCC METALS: AN EXAMINATION OF EXPERIMENTAL TECHNIQUES AND THE BILINEAR BEHAVIOR

#### 3.1 Introduction

The nano/micro-mechanical behavior of metals has been the focus of intense research for well over fifty years. In the past much emphasis was placed on micro-scale measurements due to perceived errors in very near surface or nano-scale measurements [17]. This interest is driven in large part by the emerging “nano” technology sector that continues to push the envelope for designing structures at the micro and nano scale. It has been well established that the flow stress of metals can be characterized by measuring the hardness using microindentation but the research was limited to the micro range. Over the past two decades advances in characterization equipment and techniques, such as Instrumented Indentation Testing (IIT) and continuous stiffness measurement (CSM), have revolutionized the ability to probe surface layers accurately to less than fifty nanometers. The use of IIT to characterize the properties of materials at depths as shallow as 20 nm or less has become very popular in recent years [57]. This technique is used to measure the very near surface hardness and elastic modulus of materials and can be used for bulk or composite (thin film) systems.

The hardness of a material is generally defined as the ability of a material to resist plastic deformation and has particular significance in polycrystalline metals as it is related to the flow stress (yield) and the tensile stress. The flow in a metal takes place when plastic deformation occurs as result of a specific loading condition. In this case when an indenter is pushed into the metal using hardness testing, a measure of the flow stress can be determined using the familiar relation where hardness equals three times the flow stress. When attempting to characterize the

mechanical behavior of metals for both bulk and thin films, it has long been known that at small scales the hardness is observed to increase with decreasing depth of indentation for certain metals as demonstrated by Ma and Clarke and Nabarro et al. [11, 19]. To account for this size effect several theories have been proposed by Fleck et al., Gao et al., Huang et al., including strain gradient plasticity (SGP) that includes an intrinsic length scale to replace conventional plasticity models [16, 21, 28]. The basic framework proposed by the SGP has been modified in part by several researchers over the years but the essential foundation lies in the belief that the ISE is governed by the presence of geometrically necessary dislocations (GNDs) within the plastic zone for indentations in the nano-scale range (generally taken to be less than  $1 \mu m$ ). Gao et al. developed a widely used relationship between microhardness and depth that has been used to describe the ISE based on the Taylor Dislocation Hardening model (TDH) and a characteristic length scale [21]. The Taylor Dislocation Hardening (TDH) model is used to relate the flow stress dependence on the presence of GNDs and statistically stored dislocations (SSDs) where the GNDs scale with the strain gradient, while the SSDs scale with the effective strain. When microhardness data are fitted to the Nix Gao model it remains linear but when nanohardness data are introduced the fit is no longer linear [21]. This phenomenon has been noted by several investigators including Kim et al. and Durst et al. when comparing hardness data across scales [22, 23]. An attempt to understand this breakdown led others to develop simulations to analytically model the behavior and ascertain the deviation for the nanohardness data. The simulation developed by Huang et al. concluded that there are two main factors for the discrepancy between the Nix Gao model and data from nanoindentation [21, 24]. The first factor is due to the indenter tip radius at small depths and the second one is due to the storage volume for the GNDs.

In this work, we examine the ISE for several FCC metals including 99.999% Aluminum, 99.95% Nickel, 99.95% Silver, and 70/30 Copper Zinc alloy ( $\alpha$ -brass) using a single Berkovich indenter tip on the same test machine. This machine is capable of providing loads that resulted in depths that extend from the nano range to the micro range ( $50\text{ nm}$  to  $25\ \mu\text{m}$ ) respectively. These metals were chosen based on their stacking fault energy (SFE) with  $\alpha$ -brass having a very low SFE of  $>10\text{ mJ/m}^2$  and aluminum having a very high SFE of  $200\text{ mJ/m}^2$ . Two metals with intermediate SFE, nickel ( $125\text{ mJ/m}^2$ ) and silver ( $22\text{ mJ/m}^2$ ), were also chosen. The plastic deformation of FCC metals is directly influenced by the SFE. The SFE is a measure of the distance between partial dislocations and has a direct impact on the ability of dislocations to cross slip during plastic deformation. The lower the SFE the larger the separation between partial dislocations and thus cross slip and dynamic recovery are inhibited. The SFE impacts pure metals differently from alloys.

It is our belief that no other work has been published to date that examines the ISE of polycrystalline metals using the same hardness machine with a single tip that covers the range mentioned above ( $50\text{ nm}$  to  $25\ \mu\text{m}$  depth of indentation). There have been several investigations of the ISE in single crystal metals including Ma and Clarke and some researched polycrystalline metals Elmustafa and Stone using nanoindentation testers in the near surface range with a Berkovich shaped indentation tip and traditionally microhardness testers in the micro-range with a Vickers indenter [11, 58]. Elmustafa et al. concluded that when the data from microindentation tests are plotted along with nanoindentation data for  $\alpha$ -brass and pure aluminum samples and fitted to the TDH model the nano data produced a shallower slope when compared to the microindentation data [59]. The microindentation data correlated well with the TDH model and the data exhibited a slope approximately close to one based on the model. They referred to this

change in slope as “bilinear behavior”. However, because they used two different tips and two machines to collect the data there was some question regarding whether the actual cause of the bilinear behavior was mechanism based or due to the use of two different tips. The current work was conducted to address the existence of an ISE and to verify the bilinear behavior of these metals using a single tip.

### 3.2 Experiments

Four metals were chosen for this research according to their stacking fault energy. A plate of  $76.2\text{ mm} \times 76.2\text{ mm} \times 3.175\text{ mm}$  was obtained from Kamis Inc. for each metal. The metals chosen were 99.999% Aluminum, 99.95% Nickel, 99.95% Silver, and 70/30  $\alpha$ -brass (Cartridge Brass C26000). Two samples were cut from each plate to a size suitable for nanoindentation testing.

The aluminum samples were annealed at  $344^\circ\text{C}$  for 30 minutes and then air cooled to ambient temperature resulting in a grain size of  $120\ \mu\text{m}$ . The nickel samples were annealed at  $750^\circ\text{C}$  for 60 minutes and then air cooled to ambient temperature resulting in a grain size of  $100\ \mu\text{m}$ . The silver samples were annealed at  $350^\circ\text{C}$  and then air cooled to ambient temperature resulting in a grain size of  $97\ \mu\text{m}$ . The  $\alpha$ -brass samples were stress relieved at  $260^\circ\text{C}$  and then air cooled to ambient temperature resulting in a grain size of  $63\ \mu\text{m}$ .

The samples were polished using an Allied Multi-Prep automated polishing system that can actively monitor the amount of material removed by means of a calibrated micrometer attached to the polishing head. This system can accurately control the speed, rotation, flatness, and load on the specimen to provide a high quality surface. The polishing procedure used for these metals is given in Tayon et al. [60]. This type of polishing procedure has been used in lieu of electro-polishing for electron backscattered diffraction analysis and is capable of producing a nearly

strain free surface resulting in a deformed layer of less than 50 *nm*. The minimal deformation on the surface of a sample resulting from the use of this polishing technique is acceptable for nanoindentation testing. Properties at these shallow penetration depths are generally more scattered due to the effect of environmental noise, errors in tip calibration, surface roughness, and thermal drift. Therefore, the results in this study are focused on penetration depths that exceed the thickness of this deformed layer caused by polishing.

Indentation tests were carried out on each sample using an XP Nanoindenter, from Agilent Technologies, outfitted with a high load option that allows testing to loads up to 10 *N* (1 *kg* force). The indentation tests were carried out using two different test protocols to compare and verify the ISE results. The first test technique was a traditional quasi-static load control test. During this test the nanoindenter presses the stylus into the sample at a constant rate to a defined load and then holds at that load for a dwell time of ten seconds and then unloads. The stiffness of contact is determined from the slope of the load-depth curve during the unloading segment of the test and the data were used to determine the mechanical properties of the sample by the Oliver-Pharr analysis [2]. The load control experiments were conducted with loads ranging between 0.07(10<sup>-3</sup>) *N* to 10 *N*. This test technique provides the hardness and modulus at a specific load and penetration depth.

The second test protocol used the continuous stiffness measurement (CSM) technique. The CSM technique produces the evolution of hardness and elastic modulus as a continuous function of penetration depth into the surface by superimposing a small harmonic force oscillation (usually resulting in a harmonic displacement oscillation of 2 *nm* or less) on the tip during the loading cycle. This allows the stiffness of contact, and subsequently the mechanical properties of the sample to be continuously evaluated by analyzing the harmonic force and

harmonic displacement data, as detailed in Oliver and Pharr [3]. The tests using the CSM were conducted to achieve the maximum depth possible in each specimen, typically  $25\ \mu\text{m}$ .

The calibration and verification of the tip area function for the Berkovich shaped tip of a penetration range up to  $30\ \mu\text{m}$  requires several steps. We performed a preliminary calibration procedure recommended by Agilent Technologies for an initial  $2\ \mu\text{m}$  of geometry using a fused silica standard. This procedure has been widely cited in similar research involving nanoindentation experiments where indentation tests are performed on a reference material with known mechanical properties. Using the resulting data (load, displacement, and stiffness) the lead term of the tip is fixed and the residuals between the contact area and contact depth are minimized as demonstrated by Oliver and Pharr [2]. The tip calibration (or area-function calibration) is the process of determining best-fit coefficients for the Oliver Pharr function given by Oliver and Pharr [2]. This area function is then verified by performing indentation tests to maximum penetration depths for different materials such as tungsten and high strength steel (AISI 4340) where the tip shape can be readily verified over the entire penetration range using well known standards.

Arrays of five indentation tests were conducted for each load with proper spacing between adjacent indents. The initial indentation tests were performed on the as-polished surface of each sample. At the beginning no etching was performed on the samples to reveal grain boundaries or microstructure morphology. As discussed later, we performed indentation tests on a Ni sample that had been etched using a 50/50 Nitric Acetic solution to reveal the grain boundaries.



### 3.3 Results

We chose to employ both the CSM and load control protocols to verify the ISE for each metal. Our expectation was that the continuous hardness line from the CSM would trace through the discrete data points for hardness obtained using the load control test protocol, however, we noted a deviation from this expectation at very shallow depths for all the metals tested. The CSM data are plotted against the load control data for all the samples in Figure 5 agree very well from about  $1\ \mu\text{m}$  to  $25\ \mu\text{m}$  depth.

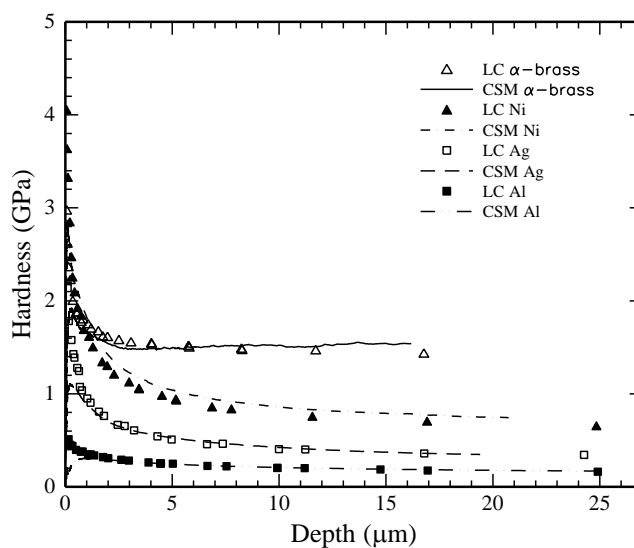


Figure 5 CSM and Load Control data to  $\sim 25\ \mu\text{m}$

A closer inspection of the data from the surface to about  $2\ \mu\text{m}$  shown in Figure 6 reveals that the hardness measured using the CSM deviates from the hardness measured using load control at depths less than  $500\ \text{nm}$ . Therefore, we conclude that the data from the load control

protocol display a conventional ISE, whereas the data from the CSM protocol at depths below 500 nm are not.

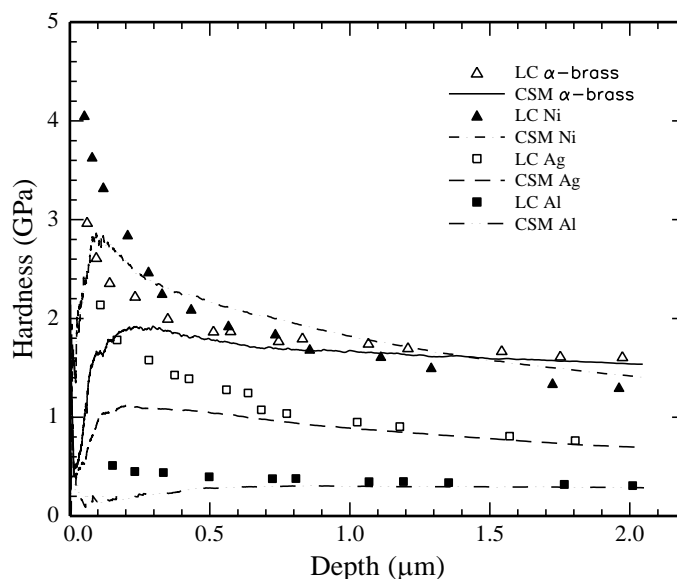


Figure 6 CSM and Load Control data from surface to 2  $\mu\text{m}$

A review of recent research indicates that there are several opinions as to the exact cause of the deviation in the CSM data at very shallow depths, i.e. tapping effect. Of particular interest and relevance to this work are two differing proposed sources for the tapping effect when using the CSM for indentation experiments on FCC metals. The first theory to be examined involves the possible interaction of the indentation with a grain boundary resulting in a localized hardening due to several sources including solute and/or interstitial pinning of dislocations related to the Hall-Petch effect [61-64]. Next, we investigated the possibility that the CSM is responsible for this behavior based on research that was conducted by Pharr et al. on FCC metals having a high modulus to hardness ( $E/H$ ) ratio [65].

The effect of grain boundary strengthening on the hardness of metals, both FCC and BCC, has been widely studied and well documented in the literature [66-71]. In many studies the increase in hardness around a grain boundary was attributed to solute and/or interstitial pinning of dislocations whereas in other studies it was attributed to slip transmission across the grain boundary. In particular, Almasri and Voyiadjis reported similar hardness versus depth behaviors for nanoindentation tests of pure silver, nickel, copper, and aluminum polycrystalline samples [61]. Their work presented results of indentation experiments on FCC metals to examine the indentation size effect and was further discussed by Voyiadjis and Peters [64]. They employed an XP Nanoindenter with a Berkovich tip utilizing the CSM test protocol. They identified three regions where the ISE of the hardness changes similar to that shown in Figure 7 for our  $\alpha$ -brass data.

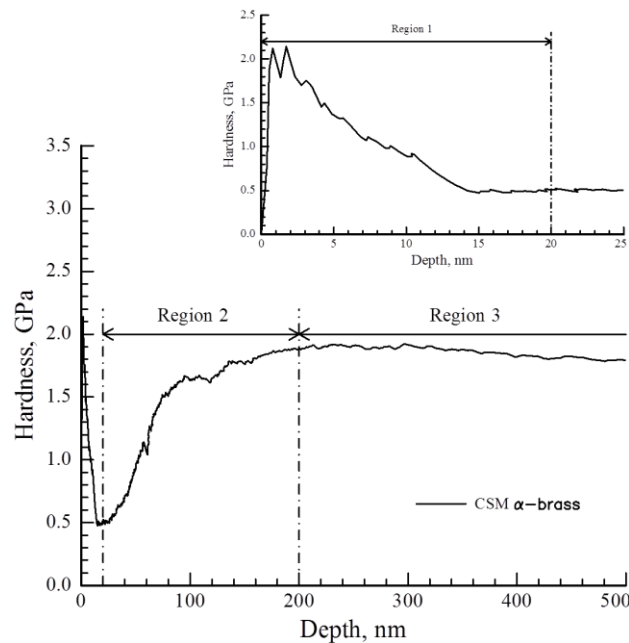


Figure 7 Typical  $\alpha$ -brass CSM hardness versus depth curve identifying the three regions of changing hardness as articulated by Almasri et al.[61] Region 1 is shown in the inset figure to a depth of ~25 nm.

They referred to Regions I and III, where the hardness decreases with increasing depth, as being dominated by the SGP mechanism. They also concluded that Region II was dominated by grain boundaries acting as barriers to dislocation movement resulting in an increase in hardness with increasing depth. The hardening effect is driven by the volume of the plastic zone beneath the indenter increasing in size until it is obstructed by the grain boundaries as shown in Figure 8.

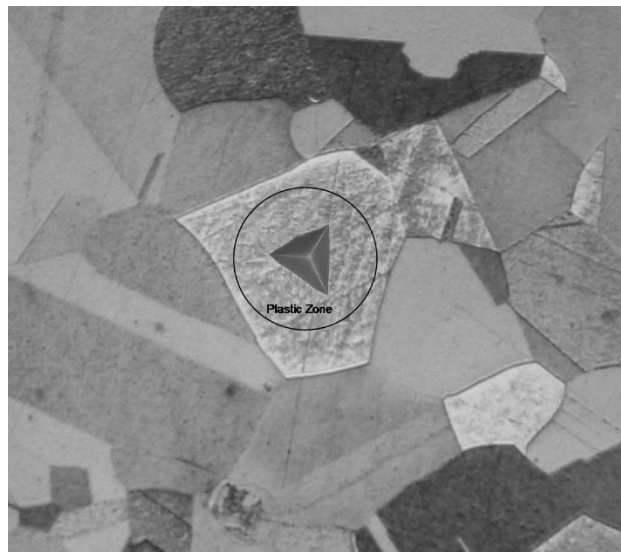


Figure 8 Schematic of an indent and associated plastic zone in a pure nickel sample having a grain size of  $\sim 100 \mu\text{m}$ . The plastic zone is generally assumed to be 2.5 times the diameter of the indent.

However, because the indentation process continues, the number of GND's continues to be introduced into the plastic zone resulting in an increase in hardness. These observations are based on work presented by Yang and Vehoff where the dependence of ISE was investigated for several nickel samples having grain sizes of  $850 \text{ nm}$ ,  $1350 \text{ nm}$ , and  $80 \mu\text{m}$  [48]. It was concluded that at grain sizes below  $1350 \text{ nm}$  the material did not exhibit a true ISE whereas at  $80 \mu\text{m}$  the material did show an ISE. These observations make sense given at smaller grain sizes as the

indentation progresses into the material the plastic zone increases until it reaches the grain boundary. The effective strain gradient remains high until the indentation crosses over the grain boundary therein the gradient is relaxed and the plastic zone continues to grow again. When the grain size is large enough to accommodate the entire plastic zone generated by the indentation, without any influence from grain boundaries, the material showed a classic ISE with continuously decreasing hardness with increasing depth. Almasri and Voyiadjis also noted that the hardness can be affected by impurities and their concentrations as cited by Sayan et al. in a study of the microhardness behavior of NaCl [61, 72]. Therefore, based on their conclusions it would seem that this behavior is caused by factors related to the specimen chemistry and structural morphology. We anticipate that the hardness will continuously increase with decreasing depth due to ISE. Apparently, Almasri and Voyiadjis conclude that the ISE could be impacted by different mechanisms in these three regions despite the fact that the hardness fails to increase with decreasing depth [61].

As stated previously, our initial tests were conducted on the as-polished surface of each sample. To investigate the effect of a grain boundary on the hardness we performed a series of tests on a pure Ni sample where we made three indents at varying distances from the grain boundary and near the center of the grain. These tests were conducted in a manner similar to those reported by Britton et al. for commercially pure iron [73]. We etched the surface of the Ni sample to reveal the grain boundaries under the microscope. Each indentation was made using the standard Testworks© XP CSM protocol with a maximum depth of  $2\ \mu\text{m}$  a strain rate of  $0.05/\text{s}$ , and a hold time at maximum depth of 10 seconds. We also performed the tests using a new standard Berkovich tip, having a usable shape to about  $3\ \mu\text{m}$  on one grain and for comparison our previously used tip for high loads, capable of reaching depths up to  $30\ \mu\text{m}$  on

another similarly sized grain. The results of the tests are shown in Figures 9 for the high load tip and Figure 10 for the low load tip. It is clear that the tapping effect is present for all indentations regardless of location with respect to the grain boundary.

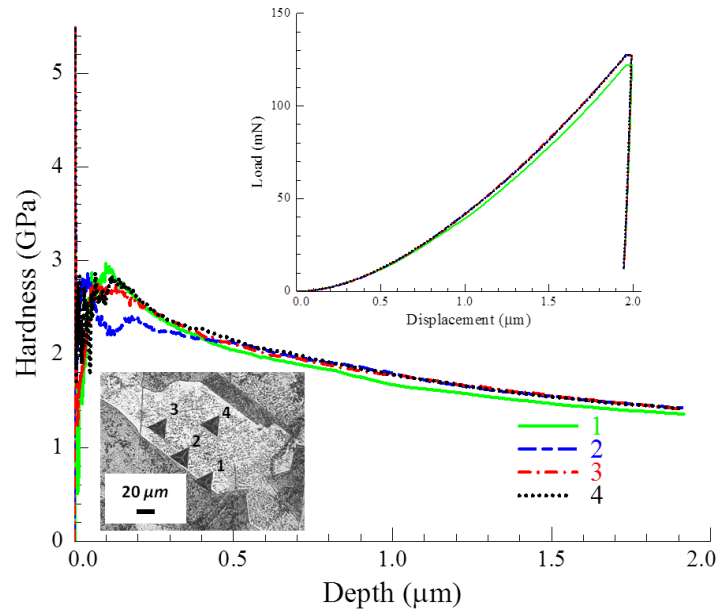


Figure 9 High Load Berkovich Tip XP-Series Method on pure polycrystalline Nickel. The Hardness versus depth curve shows a clear tapping effect for all indentations regardless of location to grain boundary. Inset upper right shows the load displacement curves for each test. Inset lower left shows micrograph of indentations near grain boundary.

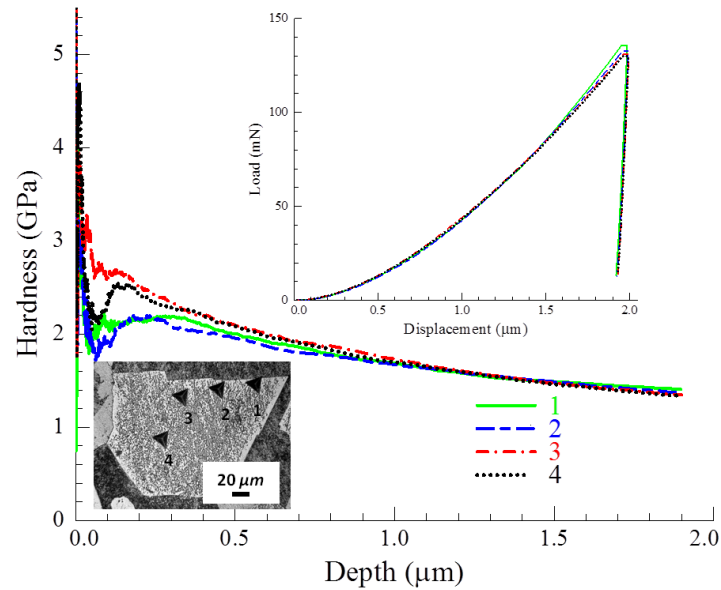


Figure 10 Standard Berkovich Tip XP-Series Method on pure polycrystalline Nickel. The Hardness versus depth curve shows a clear tapping effect for all indentations regardless of location to grain boundary. Inset upper right shows the load displacement curves for each test. Inset lower left shows micrograph of indentations near grain boundary.

Pharr et al. also observed a similar behavior for soft metals with high modulus to hardness ( $E/H$ ) ratios, such as single crystal copper, where the hardness increases and suddenly decreases before it increases back again unexpectedly at shallow depths less than 500 nm [65]. They reported this behavior when testing a very soft metal, single crystal copper. It was noted that this behavior is expected for metals having a high contact stiffness with very little elastic rebound when using the CSM protocol. We confirmed this postulate as can be seen in Figure 11, where fused silica exhibits a significant amount of elastic rebound on the unloading side of the curve and has a very low  $E/H$  ratio. The FCC metals exhibit almost no elastic rebound on the unloading side which is indicative of a high  $E/H$  ratio metal.

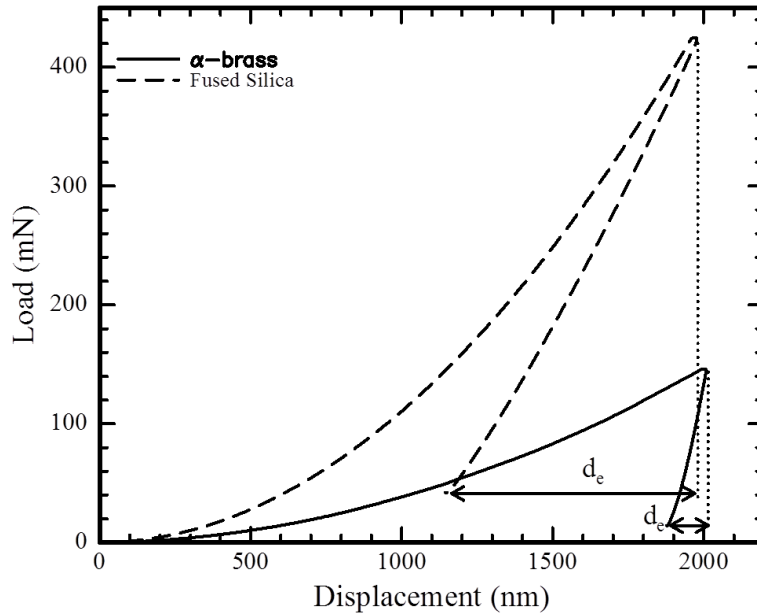


Figure 11 Load-depth curves for  $\alpha$ -brass and Fused Silica. The elastic rebound is denoted by  $d_e$ .

Pharr et al. stated that the stiffness, which for an elastic contact is given by the ratio of the load amplitude to the displacement amplitude, can be measured continuously during the loading cycle [65]. It is assumed that the amplitude of the oscillation, usually 2 nm or less, has no significant effect on the overall loads and displacements. They determined that this assumption does not hold for soft metals with high E/H ratios. Pharr et al. concluded that at shallow depths, the dynamic unloading produces errors in load and displacement that result in the indenter lifting off the surface during the CSM oscillation cycle and produces noisy unreliable data [74]. The drop in the hardness occurs because the force oscillation that is required to generate the commanded displacement oscillation, which is between 1 nm and 2nm by default, is too large to be supported by the material and this causes loss of contact with the sample. Stiffness is, therefore, measured too low because for a given force oscillation the measured displacement is much larger than the elasticity of the material can actually support. Since stiffness is defined as



the harmonic force divided by the harmonic displacement, the resulting hardness and modulus readings will be lower than the actual values.

Pharr et al. developed a model for predicting the maximum and minimum depth to which the “tapping” can be expected to occur for a high ratio (E/H) metal having a clear ISE [65]. The tapping depth can be determined from equation 20 given below which stems from the Gao et al. model [21]:

$$h_{tap} = \frac{1}{2} \left( \sqrt{h^* + \frac{4}{\pi} \frac{K^{2/m} E_r^2}{\tan^2 \Psi H_o^2} \Delta h^2} - h^* \right) \quad (19)$$

where  $h_{tap}$  is the maximum, or minimum, depth that tapping can be expected to occur based on the reduced modulus  $E_r$ ,  $H_o$  is the bulk hardness, the indenter geometry  $\psi$ ,  $h^*$  is a material dependent characteristic length,  $K$  and  $m$  are constants, and  $h$  is related to the contact depth.

The calculated versus measured CSM tapping depths for the metals tested in this study are shown in Table 1.

Table 1 Calculated versus measured depths for tapping to occur using CSM

| Material     | E/H Ratio | Minimum Calculated Tapping Depth (nm) | Minimum Measured Tapping Depth (nm) | Maximum Calculated Tapping Depth (nm) | Maximum Measured Tapping Depth (nm) |
|--------------|-----------|---------------------------------------|-------------------------------------|---------------------------------------|-------------------------------------|
| Fused Silica | 7.8       | 7                                     | 4                                   | 7.4                                   | 30                                  |
| 4340 Steel   | 40        | 25                                    | 10                                  | 40                                    | 40                                  |
| Alpha Brass  | 47        | 30                                    | 30                                  | 70                                    | 110                                 |
| Niobium      | 69        | 50                                    | 20                                  | 74                                    | 80                                  |
| Silver       | 71        | 40                                    | 30                                  | 200                                   | 200                                 |
| Nickel       | 89        | 50                                    | 30                                  | 200                                   | 150                                 |
| Aluminum     | 260       | 145                                   | 50                                  | 500                                   | 500                                 |

We expanded the application of this model to hardness data from several materials other than the FCC metals described above to demonstrate the “tapping” effect. We chose fused silica, which has a very low E/H, pure niobium, which has a BCC structure and moderate E/H ratio, and we chose a 4340 steel with a BCC structure and moderate E/H ratio. The results of these metals are shown in Figure 12. It can be seen that the fused silica exhibits very little to no tapping while the niobium and 4340 steel samples exhibit some “tapping” to depths less than 70 nm. It is also noted that the fused silica shows no ISE whereas the other metals do show a clear ISE. This is expected given the mechanical behavior of fused silica is not dislocation dependent.

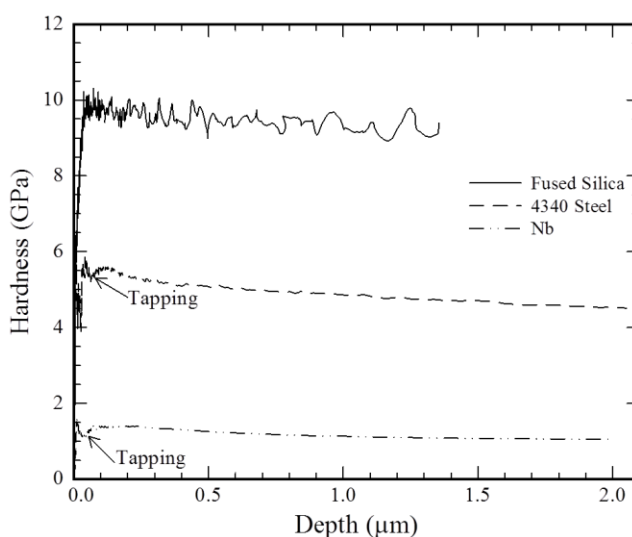


Figure 12 Hardness Depth Curves for various E/H ratio metals.

When comparing the data for each FCC metal, and including the reference samples, we could predict when the tapping would occur to within less than 20 nm. Pharr et al. stated that when using the CSM for high E/H ratio soft metals the loss of contact with the surface due to tapping can only be minimized but not eliminated [74]. They further provide for a correction to the force-displacement stiffness data to minimize the tapping effect in high E/H ratio metals. The

correction is applied to the calculation of the Load on Sample and the Displacement into Surface. Specifically, the square root of two times the Harmonic Force to the Load on Sample and the square root of two times the Harmonic Displacement to the Displacement into Surface Channel. This correction only minimizes the tapping effect therefore; it is for this reason that they recommend either not using CSM for characterizing the ISE of soft metals or using exceedingly small harmonic displacement oscillation sizes. We conclude through our research that beyond the predicted tapping range it is acceptable to use of both CSM and load control data.

We repeated the experiments on the etched Ni sample along grain boundaries as described in the previous section, but this time we used new G-Series CSM methods included in the Nanosuite© software package provided by Agilent. Nanosuite© is the latest driver interface for the XP Nanoindenter and replaces the previous Testworks© interface. The correction for Load on Sample and Displacement into Surface, mentioned above, have been incorporated into the latest CSM methods included with the Nanosuite© software. The tests were set up exactly as before except this time a 1  $\mu\text{m}$  depth was used for the standard Berkovich tip while a 2  $\mu\text{m}$  depth was used for the high load Berkovich tip. This change was added to compare the difference in depths along the grain boundary. The results of the new G-Series CSM test methods are shown in Figures 13 and 14 for the high load and standard load Berkovich tips respectively. It is clear that the corrections have significantly improved the shallow depth results for all the indentations regardless of location with respect to the grain boundary.

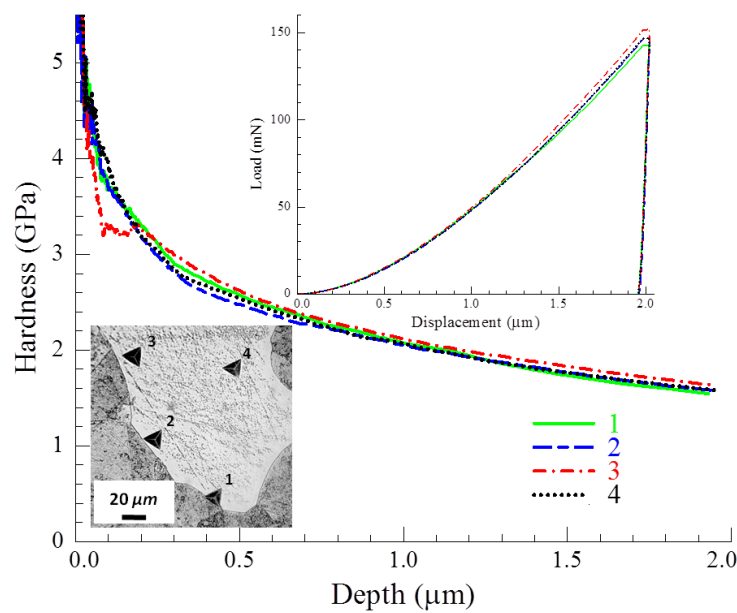


Figure 13 High Load Berkovich Tip New G-Series Method on pure polycrystalline nickel. The Hardness versus depth curves show significantly minimized tapping effect for all indentations regardless of location to the grain boundary. Inset upper right shows the load displacement curves for each test. Inset lower left shows micrograph of indentations near grain boundary.

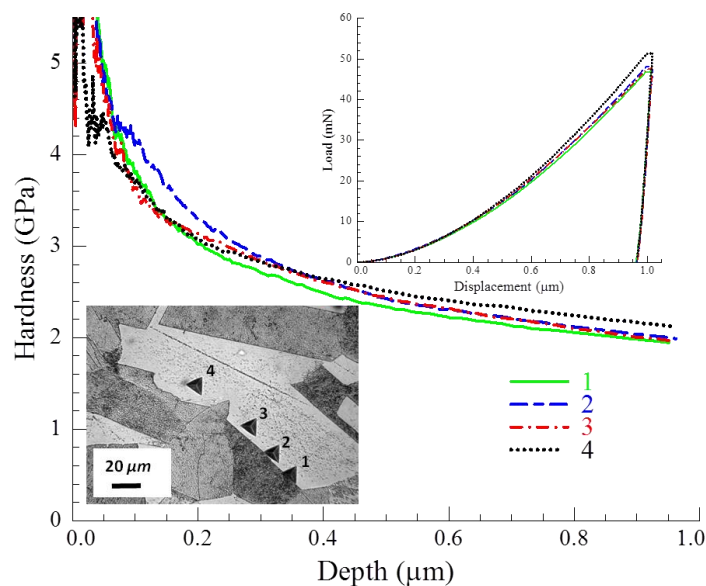


Figure 14 Standard Berkovich Tip New G-Series Method on pure polycrystalline nickel. The Hardness versus depth curves show significantly minimized tapping effect for all indentations regardless of location to the grain boundary. Inset upper right shows the load displacement curves for each test. Inset lower left shows micrograph of indentations near grain boundary.

### 3.4 Discussion

We have observed a deviation from the expected increase in hardness with decreasing depth that characterizes the ISE for several FCC metals using the CSM protocol. This deviation is not supported as a physically based phenomenon when using the traditional load control protocol which shows a continued increase in hardness with decreasing depth as shown in Figure 10. We could neither confirm nor deny the location of the indentations on the as polished surface of the samples to ascertain what effect the grain boundary could be having on the results. Therefore, we conducted several experiments using the XP based CSM protocol on the etched Ni samples at increasing distance from a grain boundary and found that the deviation in hardness at shallow depths is present regardless of location or tip used. We then used the G-Series CSM protocols that employed a correction which minimized the error associated with the measurements of Load on Sample and Displacement into Surface at shallow penetration depths along the grain boundary for the same Ni sample using the same two tips. We found that the deviation was significantly minimized. The CSM and load control data had much better agreement at very shallow depths of penetration.

The increase in hardness due to grain boundary interaction has been well established in the literature for BCC metals [62, 68, 70, 73, 75, 76]. However, for FCC metals the results are less conclusive [67, 73, 77, 78]. Both Wo and Ngan (2004) and Britton et al. (2009) conducted grain boundary experiments on FCC metals and found that the hardness was not directly affected by the presence of a grain boundary [67, 73]. Britton et al. (2009) explained that in the case of FCC Cu it would be expected to have slightly higher grain boundary strengthening as compared to BCC metals given the fewer available slip systems [73]. However, FCC metals show no pop-in events on the load-depth curve that are associated with grain boundary interaction. This

observation was attributed to an ease of slip transfer across the grain boundary for FCC Cu whereas in BCC metals there is typically dislocation locking due to Cottrell atmospheres associated with interstitial impurities. Referring to Figures 9, 10, 13, and 14 we show that the load depth curves show no strain burst or pop-in behavior that is typically associated with grain boundary interaction in BCC metals [67, 73]. Wo and Ngan (2004) also reported that they found that there was no significant statistical difference in the load depth curve and associated hardness near selected grain boundaries for  $\text{Ni}_3\text{Al}$  as compared to the grain interior [67].

Finally, in Figure 15, we compared data from the grain interior for each method and tip to previous data collected on the as-polished surface of Ni, along with Ni data taken by Voyiadjis and Peters (2010) that were reported to be near a grain boundary [64]. The tapping effect is present in all cases when using the XP CSM protocol. The data for the sample from Voyiadjis and Peters (2010) do depict higher overall hardness, but that is likely due to the difference in polishing procedures used that left the sample in a more work hardened state [64]. The magnitude of the tapping effect in the hardness and depth, were in good agreement with all the samples shown.

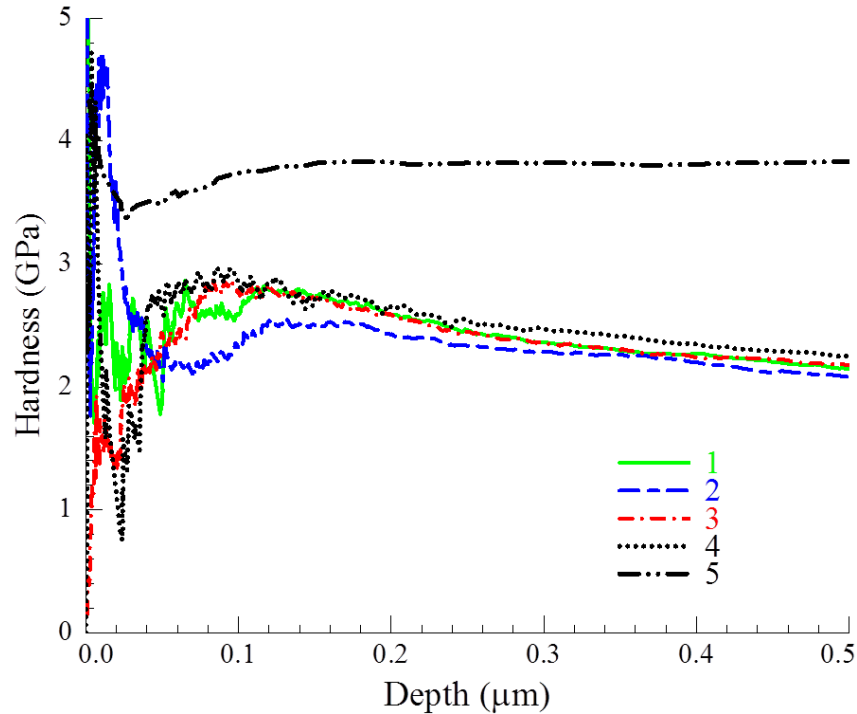


Figure 15 Comparison of Hardness versus Depth for pure nickel. 1. HL Berkovich Tip XP Method (Center Grain), 2. Standard Berkovich Tip XP Method (Center Grain). 3. HL Berkovich Tip XP Method (As Polished Surface). 4. Standard Berkovich Tip XP Method (As Polished Surface). 5. Voyadjis and Peters<sup>19</sup> Data Nickel (Acta Mech 211, 2010)

If the CSM protocol is used to study the ISE then discrete data points obtained using a load control method should be used in the shallow range for verification. Based on the experimental evidence given above, we have determined that for the metals presented in this study, the deviations between the CSM and load control hardness data at very shallow depths are a result of the CSM tapping as articulated by Pharr et al. [74]. We have verified that the ISE in these metals by showing that the hardness obtained by the load control test protocol in the shallow “tapping” range decrease with increasing depth and further over the entire plunge by both methods, CSM and load control.

## Indentation Size Effect and Bi-Linear Behavior

We wanted to examine the resulting hardness behavior and the ISE of several metals, having different SFE, using a single indenter tip. We used two different testing protocols (CSM and load control) to verify the ISE and in doing so identified a deviation between the hardness at shallow depths that had been previously examined by Pharr et al.[65]. The hardness data for all four FCC metals investigated are shown in Figure 16 fitted to the Elmustafa and Stone model for the bilinear behavior [58]. The model is described in detail by Elmustafa et al. and plots the hardness as a function of the reciprocal of the depth and accounts for the contribution of GNDs and the strain gradient [59]. In this model, which is given below by Equation 20;  $H_f$  is the hardness due to friction stress associated with the drag of dissociated dislocations and their interactions with point defects;  $\rho^s$  is the density of statistically stored dislocations,  $\lambda \approx 9$  is a constant that relates the flow stress in shear to the hardness;  $\Gamma \approx 19\%$  is the shear strain in the plastic zone beneath the indenter;  $G$  is the shear modulus;  $b$  is the burgers vector;  $\beta = 1$ ;  $\alpha \approx 0.33$  is a constant.

$$\frac{H_1^2}{C_1^2} = \frac{\rho^s}{C_2} + \frac{1}{D} \quad (20)$$

where:

$$H_1 = H - H_f$$

$$C_1 = \frac{2\sqrt{\Gamma}\sqrt{b}\lambda\alpha G}{\sqrt{\beta}}$$



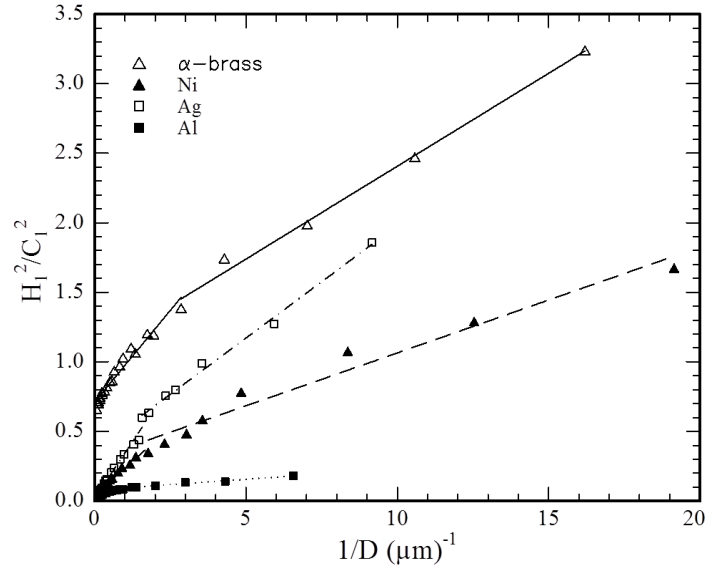


Figure 16 BiLinear Behavior from Nano to Micro Scale using a single tip.

A plot of  $H_I^2/C_I^2$  versus  $1/D$  should result in a straight line having a slope equal to one regardless of the depth. The slope of the nanoindentation data have a notably different from the microhardness data. Also, it can be seen that the slopes for each metal in the nano-region are different which is consistent with the findings of Elmustafa et al. [59]. As seen in Figure 16, the bilinear behavior is clearly evident regardless of indenter geometry, including the tip radius above 20 nm. We conclude that tip issues do not contribute to the discrepancy in the Nix Gao relation or the Elmustafa Stone model for the bilinear behavior [21, 58]. This finding provides experimental support for the finite element simulations developed by several investigators to study the indenter tip radius effect in the micro/nano indentation hardness in FCC metals. This finding also validates the observation of Elmustafa et al. in which they determine that there is no plausible explanation to support the hypothesis that indenter geometry would have an effect on the bilinear behavior [59]. Furthermore, the research presented in this paper would seem to also validate the conclusions that Elmustafa et al. articulate that the SGP collapses at small scales and

further supports the notion that the bilinear behavior of these FCC metals could very well be attributed to the presence of long range shear stresses induced by GND's [59].

### 3.5 Conclusions

- We have verified that the bilinear behavior for pure Al and  $\alpha$ -brass is mechanistic in nature and is observed regardless of the type of the self-similar indenter tip employed.
- The XP CSM protocol resulted in erroneous hardness readings at very shallow depths due to the errors in the reported Load on Sample and Displacement into Surface and the so called “tapping” of the stylus as articulated by Pharr et al. [65]. We performed indentation tests along grain boundaries with the XP CSM methods using TestWorks and found the under reported errors in the shallow depth data regardless of the proximity to a grain boundary. We performed indentation tests along grain boundaries with the G-Series CSM methods using Nanosuite and found that the tapping issue is significantly minimized compared to the XP data regardless of the proximity to a grain boundary.
- We also compared two different Berkovich tips, one new standard Berkovich tip having no tip blunting from previous use, and one high load Berkovich tip that was previously used. There was no significant difference in the tapping effect.
- An examination of the Load Depth curves show no significant “pop-in” events or “strain burst” type behavior regardless of location that is typically associated with grain boundary hardening for BCC metals.
- Our data agree with Britton et al. (2009) for Cu, as well as Wo and Ngan (2004) for Ni<sub>3</sub>Al that FCC metals do not exhibit hardening effects due to interaction with the grain boundary interface [67, 73]. Only BCC metals show this type of behavior where there is a propensity for dislocation pinning and locking due to the Cottrell atmospheres associated

with interstitial atoms. Also, for FCC metals there is little resistance to slip transfer across grain boundaries.

- We compared data from the grain interior for each method and tip to previous data collected on the as-polished surface of Ni, along with Ni data taken by Voyadjis and Peters (2010) that were reported to be near a grain boundary and showed that the tapping effect is present in all cases [64].
- We therefore conclude that the apparent hardening/softening behavior at shallow depths for the FCC metals examined in this research is due to the errors associated with the XP CSM protocol and the so called tapping effect for high E/H metals.
- Despite the fact that the SFE of the single metals tested (Al, Ni, and Ag) depicted limited correlation with the magnitude of the ISE, the impact of interfacial energies including the stacking fault energy of the solid solution alloys (Cu-Zn, Al-Zn, and Ni-Cu) will be examined later.

**CHAPTER 4**

**THE ACTIVATION VOLUME OF PURE FACE CENTERED CUBIC METALS**

**USING UNIAXIAL TESTING AND NANOINDENTATION**

**4.1 Introduction**

It is well established that the activation volume decreases with increasing stress in uniaxial experiments [5, 79-84]. The mechanisms that are associated with the increase of the activation volume with decreasing stress are regarded as solid solution strengthening mechanisms. The activation volume,  $V^*$  has traditionally been derived from uniaxial tensile tests and can be measured using indentation techniques with the advent of instrumented indentation. Recently indentation creep experiments were employed for materials at low homologous temperature to examine deformation mechanisms [85-88]. Using indentation creep experiments, it was concluded that the activation volume decreases with increasing hardness from nanoindentation experiments and the data from nanoindentation experiments extrapolate into the uniaxial testing data [25, 58].  $V^*$  is defined as the Burgers vector ( $b$ ) times the area swept out by dislocations during thermal activation,  $V^*$  is given as Equation 21

$$V^* = \frac{9K_b T}{m_H H} \quad (21)$$

where  $K_B$  is Boltzmann's constant,  $T$  is the absolute temperature,  $H$  is the hardness, and  $m_H$  is a strain rate sensitivity of the hardness. The factor 9 is to convert the flow stress in shear to hardness (hardness is  $9 \times$  the flow stress in shear). The strain rate sensitivity of the hardness  $m_H$  is given by Equation 22;

$$m_H = \left. \frac{\partial \ln H}{\partial \ln \dot{\epsilon}_H} \right|_{h_c} \quad (22)$$

where  $m_H$  is evaluated at constant plastic depth,  $h_c$ , to eliminate hardness measurement

brasses and the results were compared with Cu at different strains [79]. Butt and Feltham (1984) studied the activation volume in polycrystalline  $\alpha$ -brasses of various grain sizes, % Zn content, and different Cu purity over a wide range of strains and at three different temperatures [79]. The data suggest that solute atoms impeded dislocation glide only up to small percentage values of uniaxial strain whereas at high strains i.e. larger than 4%,  $V^*\sigma$  (activation volume  $\times$  flow stress) for  $\alpha$ -brass and single crystal Cu coincided and the dislocations/dislocations interaction, which leads to strain hardening, dominated the kinetics of deformation [79].  $V^*/b^3$  for single and polycrystalline Cu exhibited similar behavior to the  $\alpha$ -brasses and single crystal Cu in [79] and the effect of work hardening directly affected the activation volume [84]. Similar trends were also observed for Al and it was found that  $m_\sigma$  (strain rate sensitivity of the flow stress  $\times$  flow stress) is directly related to  $V^*$  through Equation 23 [80].

The strain rate sensitivity  $m_\sigma$  in a uniaxial tension or compression test is given by

$$m = \left. \frac{\partial \ln \sigma}{\partial \ln \dot{\epsilon}} \right|_\epsilon \quad (23)$$

and the corresponding activation volume in a uniaxial tension or compression experiment is given by

$$V^* \approx 3K_b T \left( \frac{\partial \ln \dot{\epsilon}}{\partial \ln \sigma} \right)_T \quad (24)$$

In review of Equations 21 and 24 it can easily be concluded that the uniaxial tension or compression activation volume data can be transformed to activation volume hardness data by employing a factor of 3 that takes into account the conversion from flow stress to hardness. The motivation of coalescing the uniaxial data with the nanoindentation data is to investigate deformation mechanisms at different length scales and to link bulk material properties to their surface counterparts. It is plausible to validate Butt and Feltham (1984) connotation by

extrapolating the data to the nanoscale or subsurface properties provided that such a material exhibits indentation size effect where the hardness increases with size or depth of indentation [79]. In studies of indentation hardness, several researchers had observed an indentation size effect in polycrystalline and single crystals FCC and BCC materials [11, 16-18, 20, 25, 58, 89]. Strain gradient plasticity theories (SGP) were developed to address situations where size effects might be important and cannot be expressed by the classical plasticity theory. It is suggested in the SGP theory, with respect to the relationship between the flow stress in shear and the dislocation density of Taylor's dislocation hardening model (TDH), that dislocation flow is a combination of statistically stored dislocations (SSDs) and geometrically necessary dislocations (GNDs). The SSDs scale with the effective strain and the GNDs scale with the strain gradient [25, 58]. Elmustafa and Stone demonstrated, based on indentation creep experiments, that the ISE in  $\alpha$ -brass and Al has a kinetic signature identical to the one produced by work-hardening, when the data were analyzed using activation volume approach [25,58]. They concluded that the ISE is caused by an increase in dislocation density at shallow depths, which is in agreement with the strain gradient plasticity theories. The commonality between Elmustafa and Stone, Bochniak, and Butt and Feltham is that the activation volume decreases with stress/hardness as the deformation is dominated by dislocation/dislocation interaction [25, 58, 80, 79]. It is also widely reported in the literature that materials with coarse grain depict a size effect caused by accumulation of dislocations due to strain gradient for indentations of increasingly small size [58]. On the other hand materials that tend to exhibit stress enhancement due to grain refinement i.e., nanocrystalline and ultrafine grained materials (average grain size < 100 nm) do not depict a size effect. Similarly, for uniaxial tensile testing, nanocrystalline and ultrafine grained materials do not experience either elongation or strain hardening which is not the case for coarse grained

polycrystalline metals [90, 91]. In contrast to coarse grained materials where dislocations accumulate and the density of dislocations increases, the density of dislocations in nanocrystalline and ultrafine grained materials saturates due to dynamic recovery or due to the annihilation of dislocations into the grain boundaries [92]. The indentation size effect resulting from accumulation of dislocations due to strain hardening is key to the fundamental principle that the activation volume decreases with hardening since the activation area becomes significantly small. For nanocrystalline materials, one would expect the activation volume to maintain a fixed value with strain hardening in nanoindentation experiments by inspection of Equation 1 since the hardness does not change from shallow to deep indents due to the lack of a size effect. Similarly, for nanocrystalline and ultrafine grained materials, the activation volume will not change because these materials do not experience strain hardening in conventional uniaxial testing.

The topic of the relationship between hardness and activation volume as discussed in the literature and mentioned above is primarily focused on bulk materials using classical tensile or compressive uniaxial experiments. It is commonly accepted that the decrease in the activation volume with increasing stress is governed by solute solution interaction only for small percentage of uniaxial strains whereas for high strains dislocations/dislocations interaction dominates the crystal rheology [79-84]. This was shown to be true only for bulk materials when tested in uniaxial tension or compression. Elmustafa and Stone have demonstrated using nanoindentation that this concept can be extended to surface properties for Al and alpha brasses and concluded that at high strains the activation volume decreases due to dislocations/dislocations interactions for materials that exhibited indentation size effect i.e., the indentation size effect possess a kinetic signature similar to the one that produced by strain

hardening [25, 58]. Elmustafa and Stone demonstrated this using Al, a high stacking fault energy material (SFE) and alpha brasses a low SFE using low load nanoindentation Berkovich indenter tip and a microhardness Vickers' tester for intermediate loads [25, 58]. While only the nanoindentation equipment can be used in load control (creep) experiments to measure the strain rate sensitivity of the hardness and thereafter calculate the activation volume, the microhardness Vickers tester could not be used for such experiment and the strain sensitivity of the hardness could not be verified and it was borrowed from the nanoindentation experiments. There were always questions as whether the results reached from using two separate machines equipped with different tip geometries and one machine cannot even be used in creep experiments could be accepted to conclude that activation volume decreases with hardness for surface layers [25, 58]. Elmustafa and Stone initially thought that the indentation size effect was influenced by the SFE which led to their testing of an FCC in Al (high SFE) and an alloy in alpha brasses (low SFE) materials which led to their conclusion that the activation volume decreases with hardness [25, 58]. To the best of our knowledge, it was only the first time that this concept emerged for surface layers and was concluded from a test of only one FCC material in Al. In order to expand this concept to surface layers of other FCC materials it was decided to test Ag and Ni in addition to the already tested Al materials. Because of these issues it was also decided in this research that a single machine with a single tip geometry can be used to probe properties across a wide range of length scales while maintaining the average strain beneath the indenter constant. Unlike FCC materials, the activation volume for bcc and intermetallic materials is insensitive to the level work hardening and remains constant with increasing stress [85, 93, 94].

Using activation volume analysis, we propose to explore deformation mechanisms in Al, Ag, and Ni FCC metals from uniaxial testing data and compared with activation volume data



measured using indentation experiments. Indentation creep experiments were conducted using a Nanoindenter XP equipment outfitted with a high load attachment that is capable of applying loads of up to 10 *N*. The combination of the standard XP head coupled with the high load attachment enabled us to conduct experiments that extended from the nano to the micro scale using a single Berkovich diamond indenter tip. The range of loads extended between 30  $\mu N$  and 10 *N* with nanoindentation being used for loads as low as 30  $\mu N$  which correspond to indents below 50 *nm* and high loads for depths as high as 30  $\mu m$ .

## 4.2 Experiments

We tested samples of Al, Ag, and Ni FCC pure metals using conventional tensile testing as well as indentation creep experiments using a nanoindenter equipped with a load as high as 10 *N*. Two sets of samples were prepared from each material for each test, uniaxial tensile test specimens as well as test coupons for nanoindentation experiments. Polycrystalline Al (99.999%), Ag (99.95%), and Ni (99.95%) plates were heat treated to an annealed temperature of 344, 350, and 750 °C respectively. The corresponding grain sizes were 120, 97, and 100  $\mu m$  as shown in Figure 17. The rationale for choosing coarse grained over nanocrystalline or ultrafine grained metals is to rule out any stress enhancement due to grain refinement. Also, nanocrystalline and ultrafine grained metals do not exhibit strain hardening and dislocations annihilation at the grain boundaries is conceivable in addition to saturation of dislocations due to dynamic recovery. All of these are key factors for the activation volume to vary with stress or hardness.

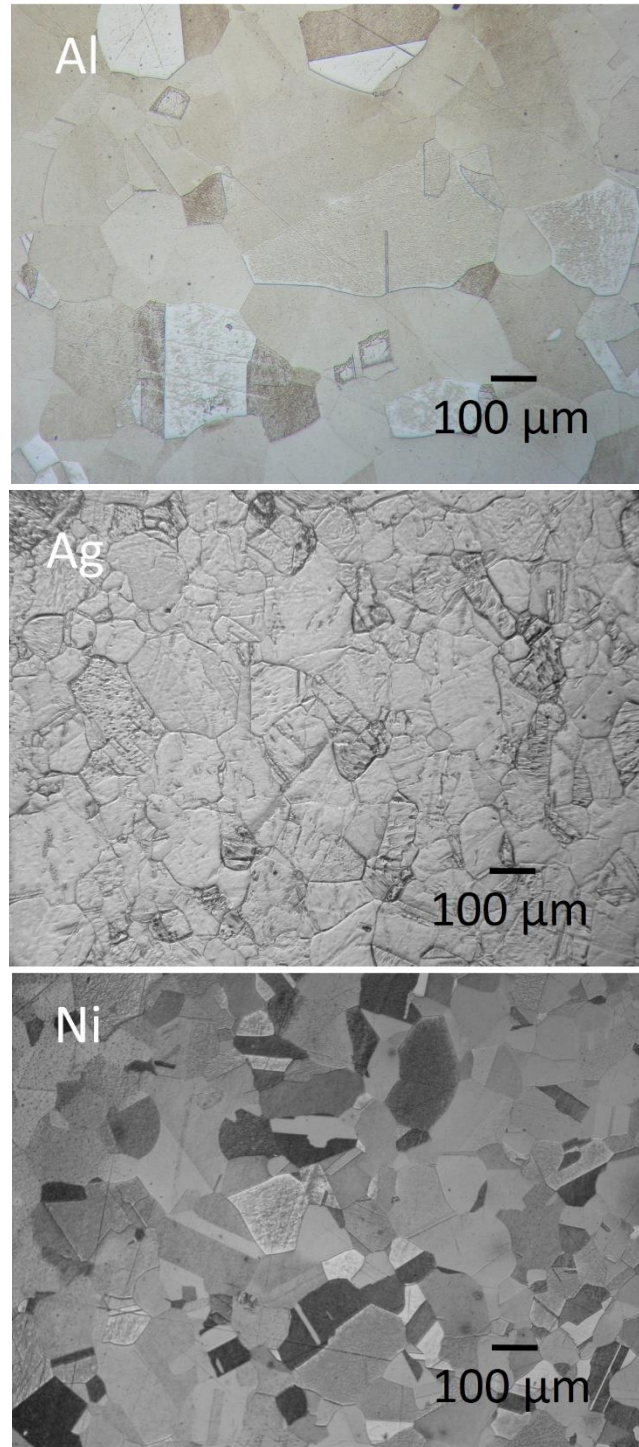


Figure 17 Grain sizes of 120, 97, and 100 μm for Al, Ag, and Ni.

For nanoindentation testing, two samples, 1.9 cm X 1.9 cm X 0.32 cm, were cut from each plate and were mechanically ground and polished to provide flat near deformation free

surfaces of less than 50 *nm* in residual surface deformation. The polishing procedure used was originally developed for the preparation of electron backscattered diffraction (EBSD) specimens that require minimal surface deformation. Constant load control (LC) and continuous stiffness method (CSM) indentation tests were conducted for each material with proper spacing between adjacent indents to avoid prior plastic deformation from preceding indents. Each sample was tested at loads ranging from 0.3 *mN* to 10 *N* using the LC protocol and to a depth of at least 25 $\mu$ *m* using the CSM protocol.

The uniaxial tensile test specimens were machined from each plate having a gage length of 25 *mm*, width of 6.25 *mm* and a thickness of 3.175 *mm*. A 98 *kN* (22 Kips) MTS servo-hydraulic tensile machine was used in displacement control to test the specimens at a rate of 0.05 in/second and the samples were pulled until failure by separation. The tensile specimens had a stochastic monochrome speckle pattern applied to allow 3-D photogrammetry using digital image correlation (DIC) tracking at 2 *Hz* for strain computation. The load was recorded simultaneously with the DIC system to generate stress strain curves. The resulting stress-strain curves for each metal are shown in Figure 18 and represent the engineering stress strain. The data presented in this figure corresponds to strains computed at a point near the region where necking occurred. The DIC technique used for this research was similar to that described in [95] for tensile testing.

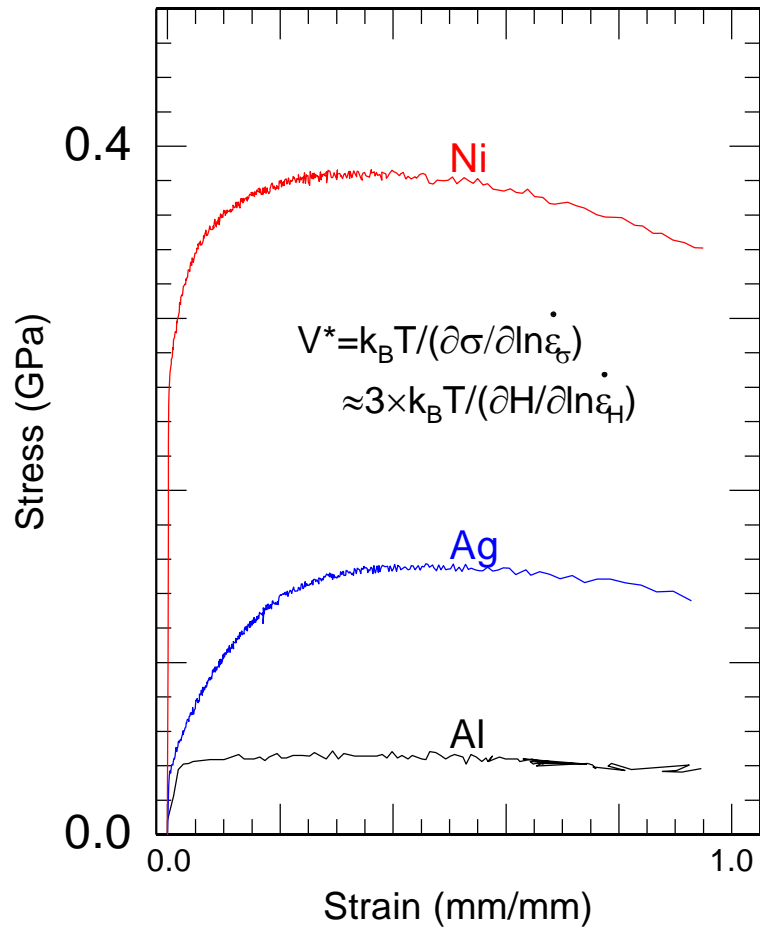


Figure 18 Stress-strain curves for Al, Ag, and Ni.

### 4.3 Results

Using data obtained in the indentation creep experiments for  $m$ , and based on the values of  $mH = \partial H / \partial \ln \dot{\epsilon}_{eff}$  as shown in Equation 22 above we generate plots of  $V^*/b^3$  versus  $H$  for the three metals as shown in Figures 19, 20, and 21. The data cover a wider range of loads and depths when compared to the data reported by Elmustafa and Stone for Al [58].

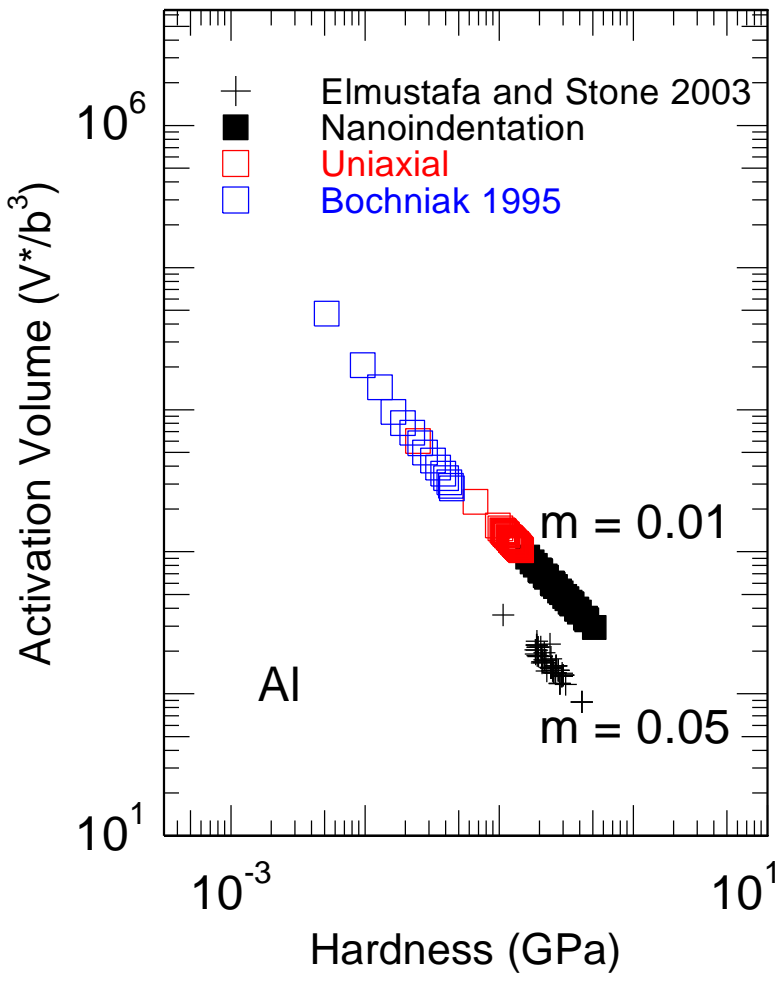


Figure 19 Activation volume versus hardness for Al.

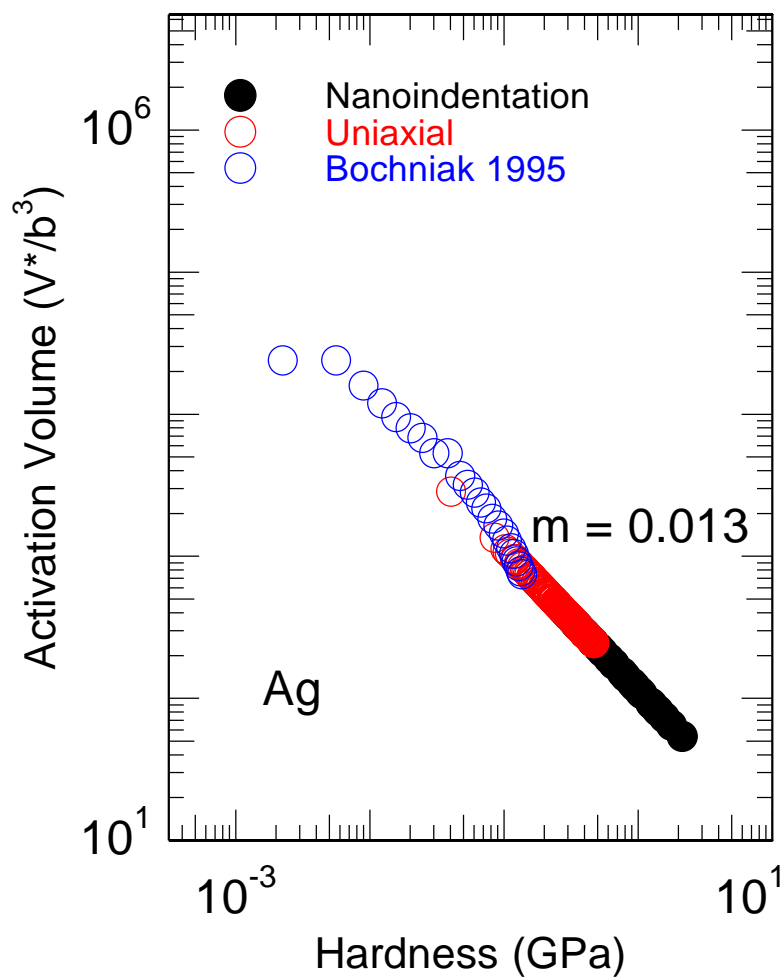


Figure 20 Activation volume versus hardness for Ag.

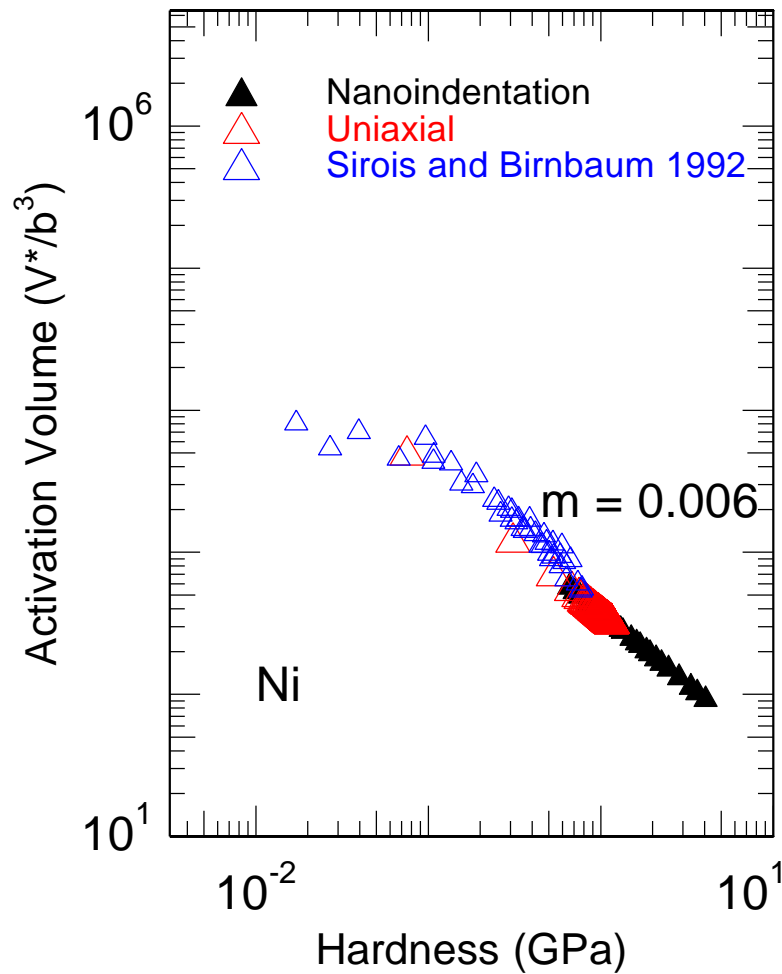


Figure 21 Activation volume versus hardness for Ni.

#### 4.4 Discussion

The stresses of the stress-strain curves (Figure 18) of the uniaxial testing were converted to activation volume data by multiplying the stresses by a factor of 3 to take into account the relationship of the flow stress to hardness. It is noted that the activation volume based on the tensile test data was calculated directly from the continually changing stress from the stress strain curves (Figure 18) for a single test specimen whilst the activation volume based on indentation was based on multiple tests at various loads resulting in discrete hardness values. The

comparison is made to show that the relative effect of work hardening through both regimes is similar and the current uniaxial data that are converted to activation volume versus hardness nicely fill out the decades of activation volume dependence on stress/hardness between the two regimes. The  $m$  value that is used in these calculations is the same value that is derived from the nanoindentation and high load indentation data as is defined in Equation 23. Surprisingly the normalized activation volume calculated from the uniaxial testing data appreciably collapsed to the nanoindentation data which represent data as shallow as 30 nm and as high as 25  $\mu\text{m}$  in addition to the literature data [80, 82] despite the fact that the  $m$  value that is used in these calculations is not measured from the uniaxial testing experiments. This in turn validates the strain sensitivity value that is measured using nanoindentation and high load indentation experiments. The strain rate sensitivity of the hardness,  $m$ , remains constant during work hardening of a material according to the modified Cottrell-Stokes Law [96]. It can be seen in Figures 19, 20, and 21 that the activation volume drops with increasing hardness for both test methods establishing the familiar signature of work hardening behavior. The nanoindentation data which include both shallow and high loads data, the uniaxial data, and the literature data which represent conventional uniaxial testing data overlap each other. From the data of Figure 19 for Al, we notice that  $V^*/b^3$  decreases as the hardness increases for the range of loads that include all different tests including the uniaxial tensile test data by Bochniak [80]. These data are very similar to those presented by Elmustafa and Stone for Al [58]. The nanoindentation data of Elmustafa and Stone (2003) offset the Bochniak (1995) data as well as the current data. Elmustafa and Stone (2003) offered the presence of vacancies generated during deformation in Al at room temperature as a possible explanation for the discrepancy between their data and the data from Bochniak (1995) [58, 80]. They continued to argue that the presence of vacancies in



deformation is likely to increase the rate sensitivity of the flow stress. The strain rate sensitivity (SRS) of the hardness of Elmustafa and Stone data was measured as  $m \approx 0.05$  [58]. The SRS of the hardness for the current data is reported as  $m \approx 0.01$ , and is in good agreement with previously reported data [97, 98]. This SRS caused the data to follow the same trend as the Bochniak data and collapsed to the current uniaxial data [80]. In addition, the SRS of the hardness was measured for Ni in the current work as  $m \approx 0.006$ , in agreement with previously reported values [99, 100]. Finally, the SRS of the hardness for Ag was  $m \approx 0.013$  for the current work which also agrees well with [101].

$V^*/b^3$  for Ag from Bochniak and for Ni from Sirois and Bimbaum is initially nearly constant, Figures 20 and 21, as a function of work hardening at the lower levels of hardness [80, 82]. Then at a hardness level of 0.08 *GPa* and 0.1 *GPa* for Ag and Ni respectively,  $V^*/b^3$  begins to decrease as the hardness increases. Butt and Feltham attributed this transition to a change from kinetics governed by dislocation-solute interactions to kinetics governed by dislocation–dislocation interactions as the latter becomes more important at higher levels of stress [79]. It is to be noted that  $V^*/b^3$  for Al did not experience the same transition Ag and Ni experienced, from initially nearly constant to a certain level of hardness and then gradually decrease with an increase in hardness. This can be explained by the fact that Al, a high stacking fault energy (SFE) material compared to Ag and Ni, the stress for dislocations to cross-slip during activation is much less than that for Ag and Ni. Al exhibits higher stages of work hardening at a much lower applied stress levels. On the other hand Ag and Ni, intermediate and low SFE materials, require a higher activation energy for dislocations to cross-slip during activation. Cu, another low to intermediate SFE material, for example exhibited stage III work hardening at a hardness level of 0.05 *GPa* for polycrystals [83].

#### 4.5 Conclusion

- $V^*/b^3$  from uniaxial testing data compared well with  $V^*/b^3$  data measured using nanoindentation equipped with high capability that reached 10 N for Al, Ag, and Ni FCC metals.
- $V^*/b^3$  vs.  $H$  data extrapolated into literature data from conventional uniaxial testing.  $V^*/b^3$  is shown to be sensitive to  $H$ .
- Accumulation of dislocations due to dislocations/dislocations interaction resulted in smaller activation area swept out by dislocations during activation explains the decrease in  $V^*/b^3$  with strain hardening.
- SRS of the hardness of Elmustafa and Stone data, measured as  $m \approx 0.05$ , which resulted in offsetting the current data and the literature data of  $V^*/b^3$  versus hardness was higher than SRS of the hardness for the current data ( $m \approx 0.01$ ) which is in agreement with the literature [80].
- Since the strain sensitivity value  $m$  that is used in the calculation of  $V^*/b^3$  vs.  $H$  for the uniaxial testing data is measured from the nanoindentation and high load indentation data and the data collapsed to a single curve including literature data [81, 82] this validates the  $m$  value that is measured from nanoindentation and high load indentation experiments.

## CHAPTER 5

### REPEATED LOAD RELAXATION TESTING OF PURE POLYCRYSTALLINE NICKEL AT ROOM TEMPERATURE USING NANOINDENTATION

#### 5.1 Introduction

A plastically deforming crystalline solid is subject to various competing atomistic processes that contribute to the flow stress and the ability for the material to work harden. In the case of metals, these processes are primarily governed by the mechanisms that influence the movement of dislocations and their direct dependence on stress and temperature. The use of single transient tests (either constant load or constant strain) to study the deformation mechanisms in plastically deforming crystalline materials has been examined extensively using techniques primarily developed for monotonic uniaxial test machines [102, 103]. These tests have provided the capability for the measurement of two key quantities, the strain rate sensitivity of the stress ( $m$ ) and the activation volume ( $V^*$ ), which are used to characterize the kinetic aspects of plastic deformation [83, 104-107]. These two quantities are important for determining the macroscopic deformation mechanisms that are operating but provide little information on the specific microscopic processes that can be contributing to the flow stress. To address this, repeated transient tests (either repeated stress relaxations or creep) were developed to study the contribution of specific dislocation mobility mechanisms on the flow stress and in particular the relative influence of the thermally activated and athermal components [30, 108, 109].

In recent years, the use of instrumented indentation testing (nanoindentation) to conduct similar transient tests (constant load or constant strain) and develop meaningful relationships with those performed in a uniaxial machine has been well documented in literature [110-112]. Caijun et al. explained that the precaution when using these methods is in the interpretation of

the data given the complex stress state that exists in indentation that is not present in traditional uniaxial tests [110]. However, they provide a detailed analysis of different transient tests in indentation and conclude that meaningful power law creep parameters can be measured and are comparable to those measured in a uniaxial test. In addition, there have been multiple researchers who have used single transient methods to determine  $m$  and  $V^*$  for a variety of materials and have reported general agreement with those measured in uniaxial tests [13, 113-115]. While examining the relationship between the indentation size effect (ISE) and  $m$  and  $V^*$ , Stegall and Elmustafa concluded that using activation volume analysis from nanoindentation based on single transient creep tests  $V^*$  decreased with increasing hardness (or stress) while the strain rate sensitivity of the hardness was relatively constant regardless of load for a variety of FCC metals and alloys [116]. These results were similar to the ones reported in the literature in prior uniaxial tests [79, 80, 117]. In this work, we present a methodology developed to perform repeated load (stress) relaxation tests using nanoindentation to obtain information about the relative mobility and density of dislocations. The measurement of dislocation densities and their interaction at varying load levels are keys to better understand the mechanisms that control the so called ISE.

## 5.2 Experiments

The material chosen for this research was 99.95% pure polycrystalline Nickel. Two samples were cut to sizes suitable for indentation testing and annealed at 750 °C and followed by air cooling resulting in an average grain size of  $\sim 100 \mu\text{m}$ .

A Nanoindenter XP (Agilent Technologies, Inc., Santa Clara, CA) equipped with a three-sided diamond Berkovich probe was used to conduct the repeated load (stress) relaxation tests. The Berkovich indenter was specifically fabricated to have a useful shape to about  $30 \mu\text{m}$  for higher load (deeper depth) experiments. The test protocol was designed to initiate repeated

loading cycles, each of which was followed by relaxation hold period of 30 s. During the relaxation hold segment the load was adjusted continuously to maintain the indentation depth constant and equal to the maximum value attained at the end of the preceding load segment. The displacement tolerance and the small incremental step load size for the dynamic calculation of the load during relaxation segment were adopted to achieve a constant indentation depth during relaxation period. Great care was taken to capture the final displacement upon termination of the loading cycle; this final displacement was used as the set-point for control during the relaxation hold segment. The tolerance and increment step size were varied for the different repeated loading cycles of the tests to minimize the noise during the relaxation phase. The load limit was varied from 50 *mN* to 500 *mN*. In this paper we only report on the 50 *mN* and 500 *mN*. The time to load for the first loading cycle was set at 20 s and the same loading rate was followed for subsequent cyclic loadings. Only the final relaxation segment is followed by the unloading cycle and the unloading rate was set equivalent to the loading rate. Figure 22 shows a typical set of repeated relaxations for tests at two different maximum loads, 50 *mN* and 500 *mN*.

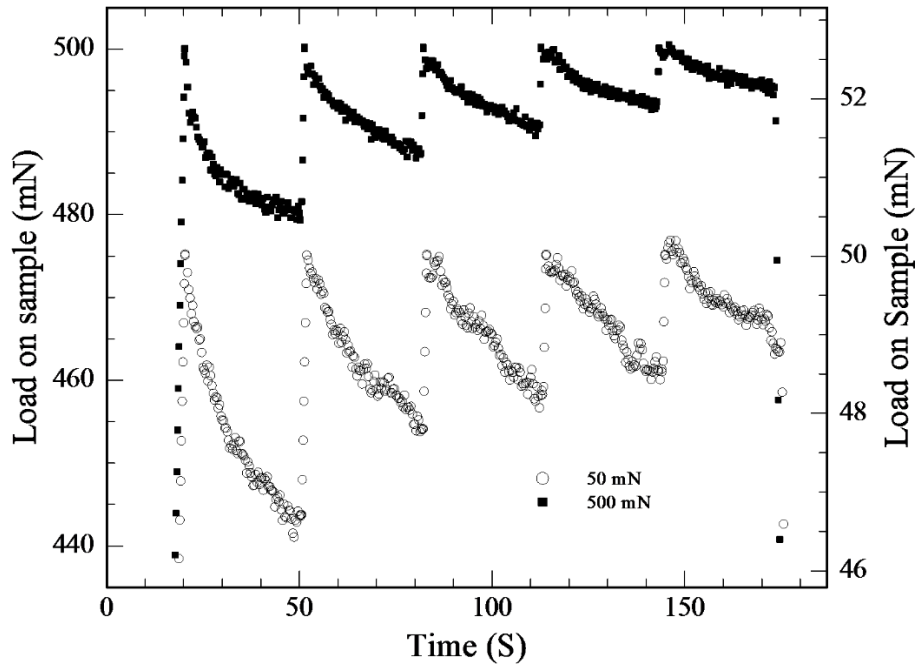


Figure 22 Incremental load relaxations versus time for maximum loads of 500 *mN* and 50 *mN*.

### 5.3 Results

The stiffness of contact was determined by the slope of the load and displacement curves during the unloading segment of the test and the data were used to determine the mechanical properties by the Oliver–Pharr analysis [3]. The nanoindenter continuously records displacement, load, and time throughout the plunge. The hardness is calculated based on contact depth at the point of unloading following the end of the hold segment for a standard load control test. To accomplish this, the contact depth was extrapolated through the hold segment using the as calculated values provided by the test protocol at the end of the hold time at the point of unloading. The contact depth was determined by establishing the stiffness through the hold segment according to

$$S = \sqrt{\frac{4P}{\pi\left(\frac{H}{E_r}\right)}} \quad (25)$$

where  $S$  is the stiffness,  $P$  is the load,  $H$  is the hardness and  $E_r$  is the reduced modulus.

Based on Equation 26 we were able to back out the stiffness values at different load levels. Next, the contact depth was calculated using Equation 1, Chapter 1 Section 1.2, and subsequently the contact area by Equation (27). The hardness is determined from the load and the contact area where

$$A_c = f(h_c) \quad (26)$$

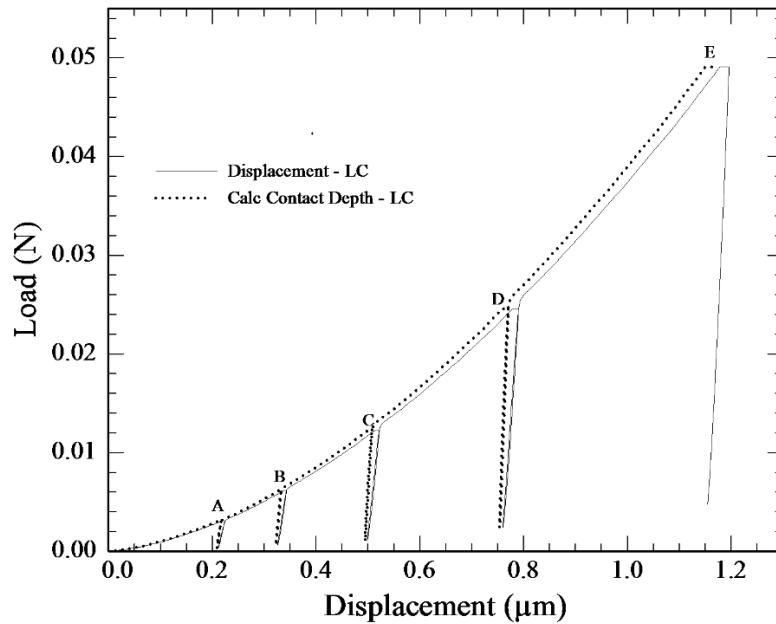


Figure 23 Load versus displacement curve using the load control test protocol with 5 incremental unloading segments.

The dotted line shows the calculated contact depth while the hardness calculated at each unloading are represented by A through E and are given in Table 2.

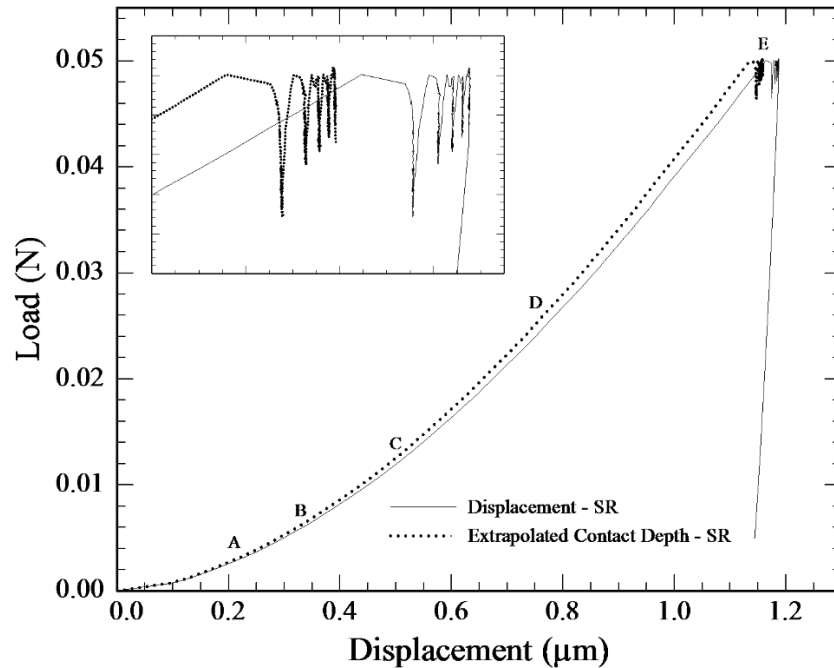


Figure 24 Load versus displacement curve using the load control test protocol modified for repeated load relaxations.

Figure 23 shows the indentation load versus the displacement for a 50 *mN* load control experiment with five incremental loading steps identified as A through E. The load displacement curve is represented by the solid line and the dotted line shows the extrapolated contact depth. To confirm that the extrapolated values in Figure 24 were derived correctly, the hardness values were calculated using the load corresponding to the intermediate increments A through D of Figure 23 since the hardness value at E is automatically retained by the machine. It was found that the hardness values correlate well with the load control method and the results are indicated in Table 2.



Table 2 Comparison of the Hardness results from Load control and the extrapolated load

| Interval | Hardness (GPa) |              |
|----------|----------------|--------------|
|          | Measured       | Extrapolated |
|          | LC             | SR           |
| A        | 2.60           | 2.58         |
| B        | 2.22           | 2.19         |
| C        | 1.93           | 1.93         |
| D        | 1.67           | 1.71         |
| E        | 1.46           | 1.46         |

The purpose of this work was to develop a technique capable of examining the coupled relationship between  $V^*$  and the components controlling the dislocation mobility using nanoindentation. Some researchers have argued that attempting to perform repeated relaxation testing in indentation is problematic to obtain valuable results due to the complex state of strain ahead of the indenter [118]. We demonstrated that a repeated relaxation indentation experiment can be implemented to equivocally generate results similar to those obtained using traditional uniaxial experiments [30, 109, 118]. Further, we have shown that the hardness (stress) can be determined with confidence at various load levels by extrapolation of the contact stiffness using the Oliver and Pharr analysis allowing for the precise monitoring during the relaxation hold segments. Therefore, we believe using repeated relaxation indentation experiments can be used to examine dislocation mechanisms that may be influencing the ISE. Based on this perspective, we are specifically interested in establishing relationships between dislocation density and velocity in the presence of an ISE.

## 5.4 Discussion

In dislocation plasticity, the activation volume represents the volume in which dislocations are mobile during thermal activation. In terms of the measured hardness, the apparent activation volume is generally defined by Equation 22, Chapter 4 Section 4.1, and linked to the strain rate sensitivity of the hardness by Equation. 23 [13]. In these equations  $k_B$  is Boltzmann's constant,  $T$  is the absolute temperature (K),  $H$  is the hardness,  $\dot{\epsilon}$  is the strain rate, and  $9$  is a factor that represents the Taylor factor and the ratio of hardness to yield strength. It can be seen that the activation volume is a rate dependent quantity. The Orowan equation is represented by Equation 18 (Chapter 1, Section 1.3) and shows that the strain rate is a function of the density of a moving dislocation  $\rho_m$  with an average velocity  $v$ . Caillard and Martin showed that when Equation. 22 and Equation 18 are combined,  $V^*$  is examined based on the relative contributions of the  $\rho_m$  and  $v$ , but it is not possible to discern which is dominating the stress [30]. We modified their relationship to take into account the ratio of the flow stress to hardness and the corresponding result is given by

$$V^* = 9K_b T \left( \frac{\partial \ln \rho_m}{\partial H} + \frac{\partial \ln v}{\partial H} \right) \quad (27)$$

The activation volume  $V^*$  is classically determined based on Equation 22 from a single transient creep or load relaxation test [112]. However, in order to examine the contribution of the rate of the dislocation density to the hardness and the rate of the dislocation velocity to the hardness as given by Equation 28, we need to define  $V_r$ , a phenomenological activation volume and  $V$ , activation volume of the dislocation velocity which are both needed for the stress relaxation analysis according to Caillard and Martin [30]. The first of these is  $V_r$  which is experimentally determined in conjunction with a time constant  $C_r$  to characterize the logarithmic nature of the relation. The second value  $V$  is a measure of the dislocation density moving between the

beginning and end of successive relaxations. Therefore,  $V_r$ ,  $C_r$  and  $V$  can be defined by the relations given in Caillard and Martin [30] and modified here to account for hardness as

$$\Delta H = \left( \frac{-9K_b T}{V_r} \right) + \left( \frac{1+t}{C_r} \right), \quad (28)$$

$$V^* = \frac{9K_b T}{\Delta H} \left( \ln \frac{\dot{\epsilon}_{i2}}{\dot{\epsilon}_{f1}} \right).$$

In order to investigate the ISE from an activation volume of the dislocation velocity perspective,  $V$ , a parameter  $\Omega$  which represents the ratio  $V_r$  to  $V$  needs to be defined to draw the relationship between  $\rho_m$  and  $v$

$$\Omega = (1 + \beta) \left( 1 + \frac{K_r}{M} \right). \quad (29)$$

where the value of  $K_r$  is the work hardening coefficient and  $M$  is the combined modulus of the machine and the specimen [30]. The value of  $C_r$  is used to determine the ratio of  $\rho_m/\rho_{m0}$  that describes the change in the mobile dislocation density over the transient to the initial mobile dislocation density. This ratio is given by [30]

$$\left( \frac{\rho_m}{\rho_{m0}} \right) = \left( \frac{C_r}{C_{r+t}} \right)^{\frac{\beta}{1+\beta}}. \quad (30)$$

Finally, according to Caillard and Martin [30], the ratio of the dislocation velocity  $v$  can be determined using the relationship given in

$$\left( \frac{\rho_m}{\rho_{m0}} \right) = \left( \frac{v}{v_0} \right)^{\beta}. \quad (31)$$

Figures 25 and 26 show the change in hardness with the ratios for the mobile dislocation density and velocity versus time for the repeated transients of a 50 *mN* and 500 *mN* maximum loads respectively.

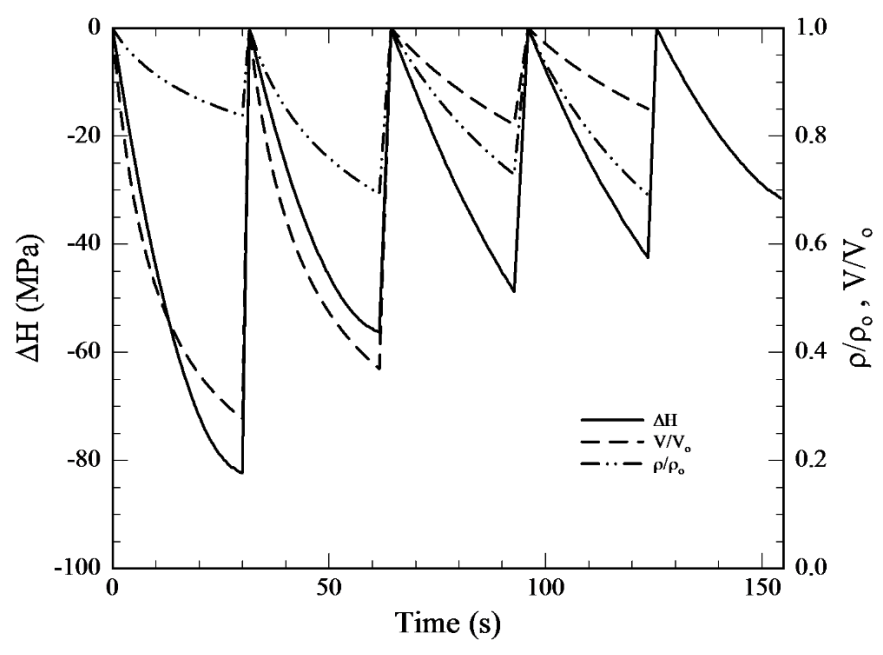


Figure 25 Hardness (stress) relaxations versus time compared with the ratio of  $v/v_0$  and  $\rho/\rho_0$  for the 50 mN maximum load

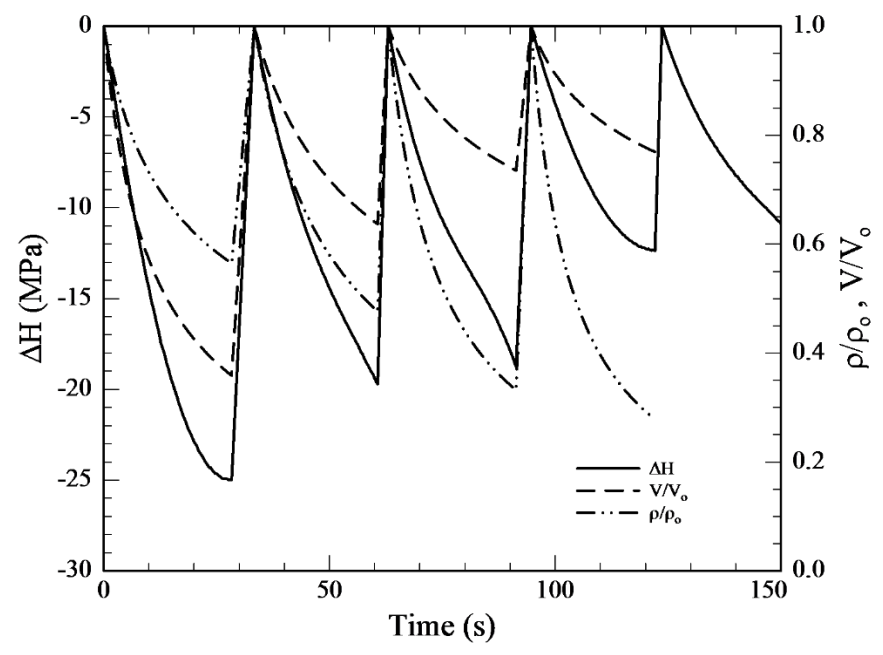


Figure 26 Hardness (stress) relaxations versus time compared with the ratio of  $v/v_0$  and  $\rho/\rho_0$  for the 500 mN maximum load

The data in these figures show that the dislocation velocity increases as the dislocation density decreases over each successive transient. The magnitude of the activation volume of the dislocation velocity,  $V$ , was found to be on the order of  $\sim 30b^3$  at 50 mN and  $\sim 70b^3$  at 500 mN for the first relaxation segments. The value of  $V$  at 500 mN of  $\sim 70b^3$  is comparable to the value of  $\sim 100b^3$  reported by Wang et al. for bulk polycrystalline Ni obtained in a uniaxial relaxation test [118]. Further, they reported that in general the value of  $V$  tended to be a factor of two smaller than  $V_r$  for their experiments [118]. We found a similar trend in our data where the ratio of  $V_r/V$  ( $\Omega$ ) according to Equation 31, was on the order of 2 for the first relaxation, but in our case the ratio tends to increase with successive relaxations. We associate this increase in  $\Omega$  to be influenced by the ISE.

## 5.5 Conclusion

The purpose of this work is to develop an experimental technique for indentation, beyond that of single transient creep, capable of generating data to examine the coupled relationship between  $V$ ,  $\rho$ , and  $v$  for metals that exhibit an ISE. We have presented a method for performing repeated hardness (stress) relaxation tests using nanoindentation and have demonstrated that this experimental technique can generate results similar to those obtained using traditional uniaxial experiments. Specifically, we derived the activation volume of the dislocation density  $V$ , the phenomenological activation volume  $V_r$ , which reasonably compare to previously published values for polycrystalline nickel in tension utilizing established closed form solutions. We found that the ratio of the initial to the final dislocation density decreases with increasing depth of indentation while the dislocation velocity increases. This finding would seem to indicate that as the depth of indentation decreases; the velocity of mobile dislocations is directly inhibited by the

increase in the dislocation density and is at a minimum consistent with the accepted theory that the ISE is governed by a dislocation mechanism. A complete examination of the possible relationship between these results and the ISE along with additional pure metals will be covered in Chapter 6.

## CHAPTER 6

### THE CONTRIBUTION OF DISLOCATION DENSITY AND VELOCITY ON THE STRAIN RATE AND SIZE EFFECT USING TRANSIENT INDENTATION METHODS AND ACTIVATION VOLUME ANALYSIS

#### 6.1 Introduction

The tendency for some metals, especially FCC metals, to exhibit a size effect under specific loading conditions including indentation and torsion has been the focus of intensive research to understand the fundamental mechanisms that control this phenomenon [11, 16, 18, 20, 74]. It is widely accepted that the indentation size effect (ISE) is caused by accumulation of geometrically necessary dislocations (GNDs) resulting from strain gradient for shallow indents [26, 54]. For single crystal metals and alloys, transmission electron microscopy (TEM) and electron beam scattering diffraction (EBSD) techniques were extensively used to scan and examine deformation maps within the plastic zone [41, 49-51, 119]. In TEM image analysis, it was found that the hardness decreases or increases with increasing indentation depth suggesting that there is a local interaction between dislocations and grain boundaries in single grains [48]. At smaller indentation depths range, the hardness may decrease with increasing indentation depth due to the classical ISE where the motion of dislocations nucleated below the indenter is not influenced by the surrounding interfaces [48]. From EBSD kernel average misorientation maps, regions with large orientation gradients typically indicate significant lattice curvature, and hence high GNDs density which are key to the presence of an ISE [120]. Another perspective on the study of the ISE which is based on kinetics of deformation was presented by Elmustafa and Stone, 2003 [58]. Using activation volume analysis based kinetics they concluded that the ISE gives rise to dislocation strengthening mechanisms that are similar to mechanisms that are responsible for testing specimens with different work hardening levels [58]. It is well established

that the activation volume decreases with increasing stress in uniaxial experiments [79, 80]. The mechanisms that are associated with the increase of the activation volume with decreasing stress are regarded as solid solution strengthening mechanisms whereas the ones that are associated with the decrease of the activation volume with increasing stress as dislocation-dislocation interaction. From nanoindentation experiments, Elmustafa and Stone, 2003 concluded that the activation volume also decreases with increasing hardness and the data extrapolate into the uniaxial testing data [58].

In the present work, we seek to expand our understanding of these observations by examining, in greater detail, some of the more fundamental variables (including strain rate, dislocation densities, and dislocation velocity) measured using indirect methodologies that may contribute to the specific mechanisms governing thermally activated processes at low temperature for different pure polycrystalline metals. We further seek to establish how the coupled relationships between each variable contribute to the ISE.

## **6.2 Experiments**

Polycrystalline Aluminum (99.999%), Nickel (99.95%), and Silver (99.95%) plates were procured from Kamis Inc. and subsequently heat treated to an annealed state to obtain grain sizes listed in Table 1. Two samples, 1.9 cm X 1.9 cm X 0.32 cm, were cut from each plate and were mechanically ground and polished to provide flat near deformation free surfaces of less than 50 nm in residual surface deformation. The polishing procedure used was originally developed for the preparation of electron backscattered diffraction (EBSD) specimens that require minimal surface deformation.

Indentation creep and load relaxation experiments were conducted using a Nanoindenter XP from Agilent. This particular equipment was outfitted with a high load attachment for the XP



head that was capable of applying a load of up to 10 *N*. The combination of the standard XP head coupled with the high load attachment allowed for experiments to be performed that extended from the nano to the micro scale using a single Berkovich diamond indenter tip. The Berkovich tip was fabricated to have a useful shape for higher load experiments resulting in depths beyond 30  $\mu\text{m}$ . Five indentation tests were conducted at increasing loads with proper spacing between adjacent indents to avoid prior plastic deformation from preceding indents. The indentation tests were performed on the as-polished surface of each sample with no etching to reveal grain boundaries or microstructure morphology. We have shown in previous research that the hardness, and the magnitude of ISE, are not significantly affected by the presence of grain boundaries in FCC metals [54].

As presented in Chapter 3, we verified that each of the pure metals examined exhibited a clear indentation size effect using the traditional load control (LC) as well as the continuous stiffness method (CSM) protocols [54]. Each sample was tested at loads ranging from 0.07 *mN* to 10 *N* using the LC protocol and to a depth of at least 25  $\mu\text{m}$  using the CSM protocol. In addition to the data obtained from the LC protocol to test the ISE, we leveraged off the same tests to gather constant load creep data over a specific hold time, typically 10 seconds, at the maximum load. The indenter tip is driven to the maximum load and held constant during the hold segment while the change in displacement is recorded thus providing the data needed to examine the creep behavior.

To assess certain material properties, such as the strain rate sensitivity (SRS) of the hardness, the instantaneous hardness should be determined during the hold segment. For the standard LC protocol, the instantaneous hardness during the hold segment must be extrapolated from the point of unloading at the end of the hold segment. The hardness is calculated by

dividing the load by the area of contact. The displacement, load, and time are continuously captured throughout the indentation hold segment. In order to use the hold segment data to calculate the instantaneous hardness, the contact depth (not the displacement) is required. The contact depth is used to calculate the contact area and the hardness is determined based on Oliver Pharr method, 2004 [3]. The contact depth was defined in Equation 1 (Chapter 1 Section 1.2). The hardness and the reduced modulus are obtained from each unloading segment to calculate the contact stiffness using Equation 25, Chapter 5 Section 5.3.

To compute the SRS and to assess the possible impact of different hold times, a series of creep indentation tests were performed at 50  $mN$ , with hold times of 20  $s$ , 60  $s$ , and 120  $s$ , at a constant indentation strain rate of 0.05  $s^{-1}$ . The strain rate sensitivity of the hardness can be calculated using Equation 22 (Chapter 4 Section 4.1). The strain sensitivity  $m$  as defined by Equation 22, which is determined from the slope of the plots of the hardness and the strain rate for each metal is shown in Figure 27. In this particular case, the SRS of the hardness for Al, Ag, and Ni is 0.01, 0.013, and 0.006 whereas the literature values from uniaxial testing for the same materials were reported as 0.01, 0.009 and 0.004 respectively [97-101].

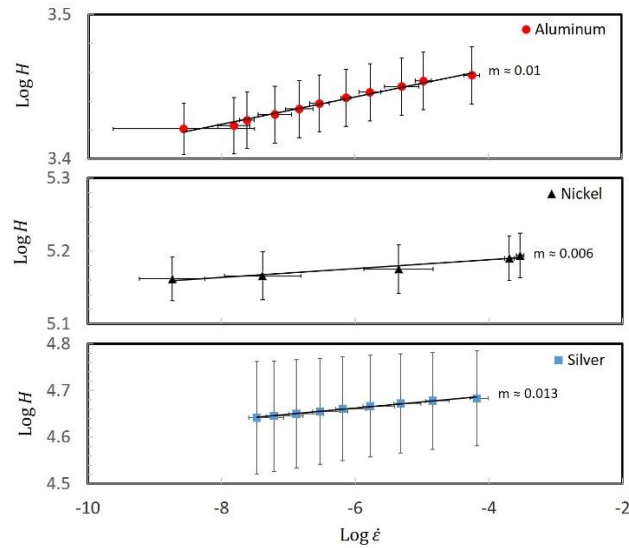


Figure 27 Strain Rate Sensitivities of the Hardness for Pure Al, Ni, Ag

In contrast to the indentation tests where the load is held constant while the displacement changes with time (i.e. creep), a different protocol was developed to perform constant strain experiments where the displacement is held constant while the load continues to relax with time (load relaxation LR). The details of this protocol and the results of the technique for the Nickel samples were reported previously [56]. An approach similar to that described in the previous section for establishing the instantaneous hardness during the hold segments was used for this protocol and verified as elucidated in Caillard and Martin [30]. The LR protocol was developed to provide a single or repeated load relaxations over a specific hold time (strain being constant) similar to classical repeated stress relaxation tests for uniaxial specimens [30]. A typical set of load relaxation versus time curves for all three metals is shown in Figure 28 for tests conducted at 50  $mN$  and 500  $mN$ , respectively.

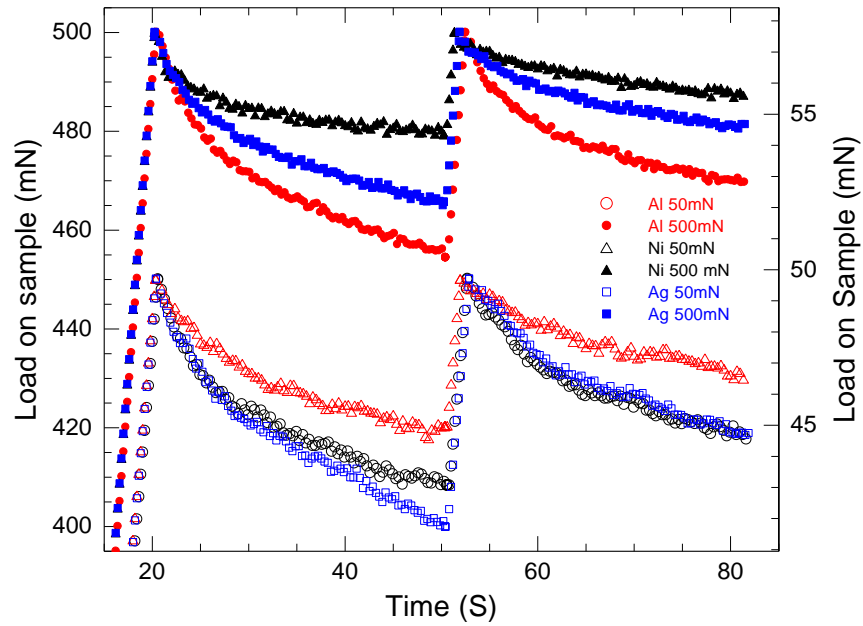


Figure 28 Load Relaxation Curves for all 3 metals at 50 and 500 mN.

### 6.3 Results

Transient tests including creep and load relaxation are typically employed to examine specific rate dependent deformation mechanisms of materials that are thermally activated [104, 118]. The use of indentation methods to perform these types of tests has been well documented. In general, certain parameters including those that are used in determining power law creep, SRS, and activation volume have been shown to be in agreement with classical uniaxial tests [110, 115, 121]. The parameters that can be determined from transient type tests can be interpreted as powerful indicators that describe the deformation kinetics, in which the activation volume and the SRS are of significant importance. In the case of constant load creep experiments Elmustafa and Stone, have demonstrated, by multiplying the value of  $m$  by the hardness, one can obtain the

equivalent of  $mH$  or  $\partial H / \partial \ln \dot{\epsilon}_{eff}$  [13]. Furthermore, they showed that the ISE can also be observed when the metals are compared on a plot of  $mH$  versus load or size [13].

Using the values of  $mH$ , the activation volume can be calculated using the procedure given by Stone and Yoder [85] and given in Equation 21 (Chapter 4 Section 4.1). The activation volume is typically described as the area swept out by dislocations ahead of plastic deformation. We performed indentation creep experiments at specific loads ranging from 0.07 mN to 10 N. Using Equation 21 (Chapter 4 Section 4.1), the hardness and the average SRS of the hardness, the activation volume,  $V^*$  corresponding to a specific load case was determined. The activation volume normalized to the cubic Burgers vector versus hardness corresponding to each load case is shown in Figure 29, Figure 30, and Figure 31 for each metal. In addition, the dislocation velocity has been approximated and plotted versus hardness in Figure 29, Figure 30, and Figure 31.

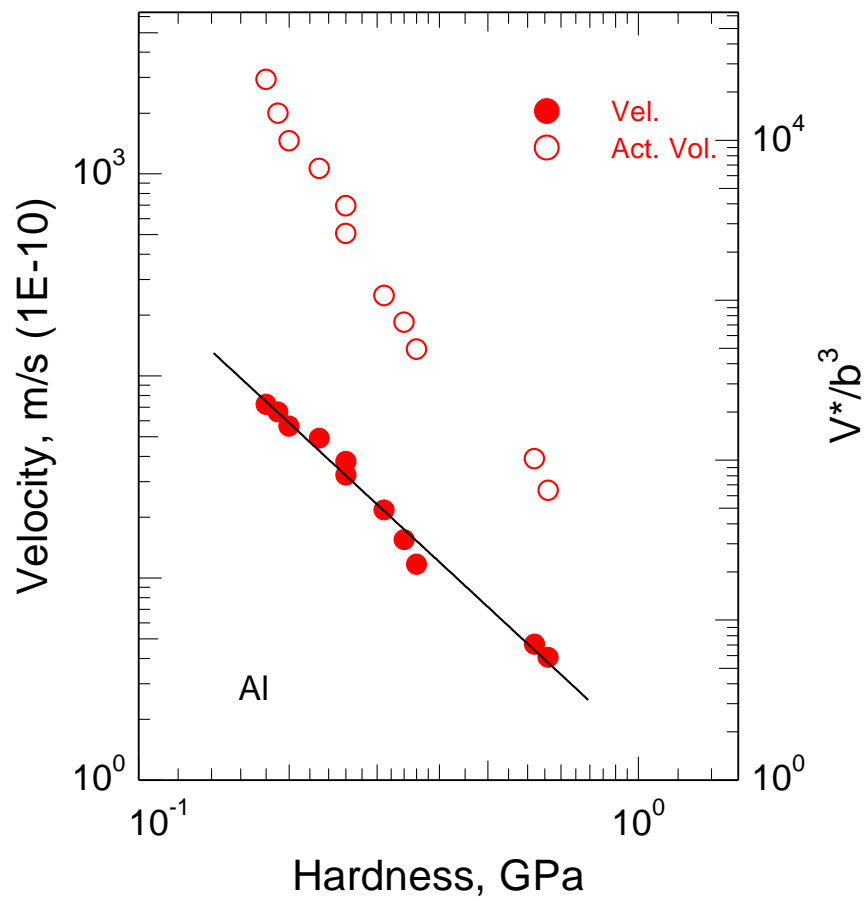


Figure 29 Velocity and normalized activation volume versus H for Al.

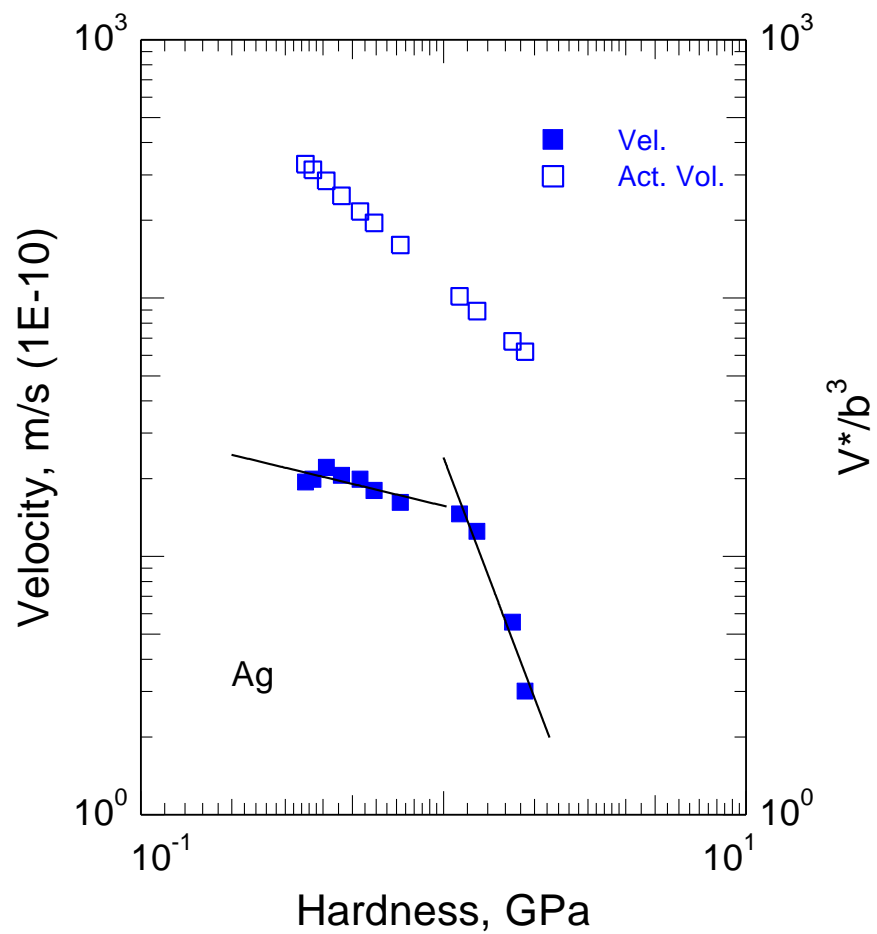


Figure 30 Velocity and normalized activation volume versus H for Ag.

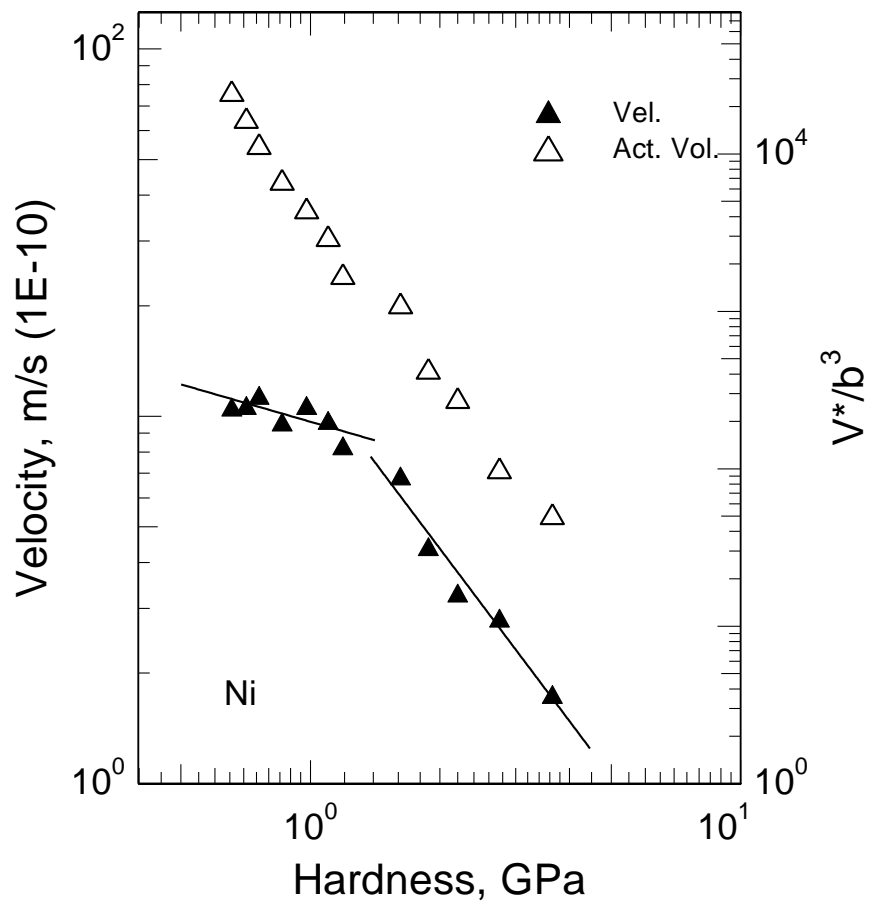


Figure 31 Velocity and normalized activation volume versus H for Ni.



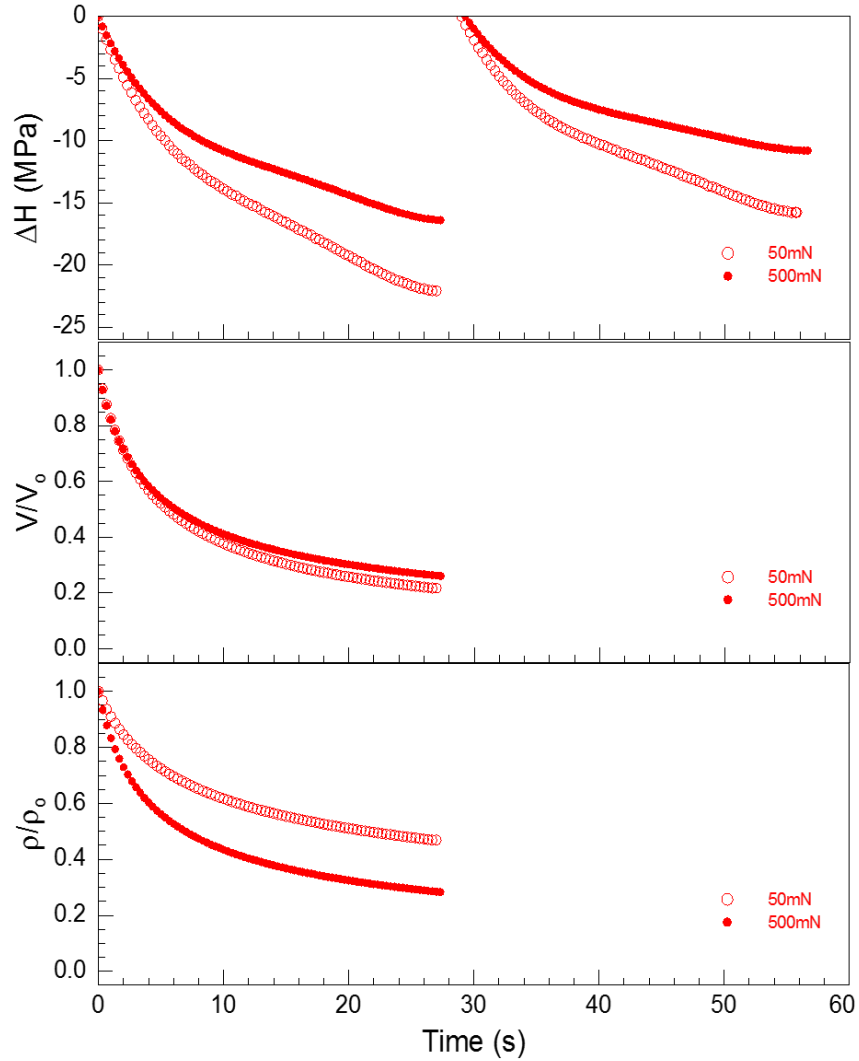


Figure 32 Results of repeated relaxation tests for Al.

Load relaxation data have been traditionally used to examine more fundamental aspects of the flow stress that contribute to kinetics of deformation including the thermal and athermal components of the flow stress. Figure 32 shows the change in hardness, the ratio of the dislocation velocity, and the ratio of the dislocation density versus time for repeated relaxation tests at 50 *mN* and 500 *mN* for Al. The data for the Ag and Ni samples depict similar results and therefore only the Al data are shown in Figure 32 to demonstrate the trends. Since the GNDs,

which are believed to be responsible for the ISE, dominate the crystal plasticity at shallow depths of indentation, it is reasonable to use the GNDs portion of the total dislocation density for the calculation of the ratio of the dislocation velocity at shallow depth of indentation up to  $1.0 \mu\text{m}$ . However, for deeper depths of indentation, it is more plausible to use the total density of dislocations to calculate the ratio of the dislocation velocity.

#### **6.4 Discussion**

The measure of dislocation dynamics, interactions, and movement has traditionally required the use of physical direct methodologies under magnification such as etch pit and TEM [31]. These techniques require specific equipment and expertise but also provide the most direct experimental data regarding the movement of dislocations in solids. In the absence of the availability of these techniques, other more indirect methodologies have been developed to infer the movement of dislocations that are based on traditional uniaxial testing where changes in strain rate can be accurately controlled [30]. The tests of primary use are those that are based on some transient in either load, displacement, or strain rate that can be fit to some logarithmic set of equations that describe the state of deformation. It is noted that the Orowan's relation relates the strain rate to the density of dislocations and the dislocation velocity as given by Equation 18 (Chapter 1 Section 1.3). The dislocation density  $\rho$  is defined herein as the total dislocation density and not the mobile dislocation density. According to Courtney, 1990, it is appropriate to use the total dislocation density provided the velocity is examined relative to this population as stated in Equation 18 [122]. This assumption is acceptable given that the methodologies utilized in this research serve to approximate the resulting relationship between the dislocation density and the dislocation velocity based on indirect observations inferred from creep and load relaxation experiments. An accurate estimate of any resultant subset of mobile dislocation density is not

possible. Furthermore, given this study is carried out on metals that exhibit an indentation size effect, the density of dislocations are computed using estimates of geometrically necessary and statistically stored dislocations [11, 123, 124].

In this chapter, we strive to understand the specific mechanisms governing thermally activated processes at room temperature for different pure polycrystalline metals in the presence of an ISE. To accomplish this, we employed two indirect methodologies based on transient testing.

The first method employed the traditional creep test in indentation. A test was performed at defined loads between  $0.07\text{ mN}$  and  $10\text{ N}$ . The activation volume,  $V^*$  at each discrete load was calculated using Equation 22, Chapter 4 Section 4.1, and was found to predictably decrease as the hardness, or stress, increases [58, 79, 80]. From each creep curve at the discrete load, the average strain rate was used to approximate the average dislocation velocity from the Orowan Equation 18 (Chapter 1 Section 1.3). It was found that the average strain rate increased with decreasing load. The average geometrically dislocation density was approximated by Equation 11, Chapter 1 Section 1.2, assuming that in the presence of a size effect the geometrically necessary dislocations dominate based on the mechanism based strain gradient plasticity theory established by Nix Gao [20]. We adopted the concept that the GNDs, which are believed to be responsible for the ISE, dominate the crystal plasticity at shallow depths of indentation, and used the GNDs portion of the total dislocation density for the calculation of the ratio of the dislocation velocity at shallow depth of indentation up to  $1.0\ \mu\text{m}$ . However, for deeper depths of indentation, we implemented the total density of dislocations to calculate the ratio of the dislocation velocity. Therefore, the dislocation velocity can anecdotally be estimated relative to the appropriate density of dislocations that dominate at changing depths of indentation. The average dislocation

velocity and the activation volume are plotted versus hardness in Figure 29, Figure 30 and Figure 31 for Al, Ag, and Ni respectively. It should be noted that the average dislocation density i.e., the GNDs for each metal increases with decreasing hardness in agreement with previously published research work [16, 18, 20, 26, 54, 74, 125]. The dislocation densities were found to be on the order of  $10^{13}$  to  $10^{16}$  for these metals in agreement with previously reported values [125]. For Al, there appears to be a consistent trend indicating that as the hardness increases, the average dislocation velocity and the activation volume both decrease.

The bilinear behavior established by Elmustafa and Stone, 2003 and later investigated by Stegall et al., 2012 for additional materials advocates the decrease of the activation volume with hardening due to dislocation-dislocation interaction in indentation creep experiments [54, 58]. Based on this, we articulate that the dislocation velocity exhibits a bilinear behavior when plotted versus hardness using the Orowan's relation Equation 18. Ag and Ni distinctively depict a bilinear behavior in the dislocation velocity with hardness, however Al exhibited a rather linear behavior. This can be explained by the fact that Al exhibits higher stages of work hardening at a much lower applied stress levels.

The second method utilized load relaxation experiments to verify if the trends for increasing hardness and density of dislocations with a corresponding decrease in dislocation velocity were consistent with creep experiments. Table 3 Table 1 lists the results of the load relaxation experiments for two loads tested at 50mN and 500mN with the corresponding creep data for the same loads.

Table 3 Creep versus Load Relaxation

| Material | Creep |      |         |          |          | Relaxation |            |           |           |               |         |
|----------|-------|------|---------|----------|----------|------------|------------|-----------|-----------|---------------|---------|
|          | mN    | H    | $V/b^3$ | $\rho$   | V        | mN         | $\Delta H$ | $V^*/b^3$ | $V_r/b^3$ | $\rho/\rho_0$ | $V/V_0$ |
| Al       | 50    | 0.3  | 172     | 1.00E+15 | 3.50E-09 | 50         | 0.022      | 80        | 159       | 0.46          | 0.21    |
| Al       | 500   | 0.2  | 245     | 3.00E+14 | 1.00E-08 | 500        | 0.017      | 95        | 243       | 0.28          | 0.25    |
| Ni       | 50    | 1.6  | 243     | 3.00E+15 | 5.00E-10 | 50         | 0.082      | 26        | 40        | 0.83          | 0.28    |
| Ni       | 500   | 1    | 400     | 7.00E+14 | 1.00E-09 | 500        | 0.025      | 68        | 144       | 0.37          | 0.53    |
| Ag       | 50    | 0.8  | 370     | 2.00E+15 | 1.00E-09 | 50         | 0.072      | 9         | 41        | 0.31          | 0.50    |
| Ag       | 500   | 0.45 | 653     | 4.00E+14 | 3.00E-09 | 500        | 0.037      | 17        | 87        | 0.24          | 0.50    |

Based on these data and the representative plot in Figure 32, it can clearly be seen that the ratio of the dislocation density increases with increasing hardness while the ratio of the dislocation velocity decreases. It is to reiterate that the dislocation density ratio is a representative of the total density of dislocations and that the ratio of the velocity is derived relative to that population. Based on these observations we articulate that since the dislocation density is very high due to the gradient in strain beneath the indenter resulting in a very small length scale between dislocations, then pinning or locking is exacerbated thereby immobilizing dislocations rapidly leading to strain hardening. This mechanism is in agreement with the description for plastic deformation described by Courtney [122].

Approximations of the measured dislocation velocity using direct methods such as etch pit and microscopy were reported by several researchers [126, 127]. Their research work revealed a dependence of the dislocation velocity on stress. These experiments were generally based on high purity LiF or single crystals having a very low initial dislocation density and were loaded in tension using 3-point bending or the application of controlled stress pulses. A set dislocation density would be induced into the material generally by scratching the surface followed by acid etching to reveal individual dislocations. In order to estimate the movement of

individual dislocations the distance traveled between loadings and successive etches would be measured to determine the dislocation velocity. In the current work, the dislocation velocity is estimated from the strain rate and an estimate of the dislocation density based on Orowan's relation, Equation 18, which tends to decrease with increasing hardness (stress) at shallow depths of indentation. We postulate that the decrease of the dislocation velocity with hardness at shallow depth of indentation can be explained by excessive accumulation of GNDs type dislocations, due to a strain gradient. As the depth of indentation increases, the strain gradient relaxes and the influence of the GNDs density is significantly reduced. The dislocation velocity will eventually reach a saturation level when the material reaches a steady state value of hardness at depths that corresponds to the bulk hardness where the SSDs dominate the crystal plasticity.

## **6.5 Conclusion**

- The dislocation velocity is estimated from the strain rate and an estimate of the dislocation density based on Orowan's relation which tends to decrease with increasing hardness (stress) at shallow depths of indentation.
- The decrease of the dislocation velocity with hardness at shallow depth of indentation can be explained by excessive accumulation of GNDs type dislocations, due to a strain gradient.
- As the depth of indentation increases, the strain gradient relaxes and the influence of the GNDs density is significantly reduced. The dislocation velocity will eventually reach a saturation level when the material reaches a steady state value of hardness at depths that corresponds to the bulk hardness where the SSDs dominate the crystal plasticity.
- Based on the pre-established bilinear behavior and the decrease of the activation volume with hardening due to dislocation-dislocation interaction in indentation creep experiments by

Elmustafa and Stone [58], we demonstrate that the dislocation velocity exhibits a bilinear behavior when plotted versus hardness using the Orowan's relation.

- Ag and Ni distinctively depict a bilinear behavior in the dislocation velocity with hardness, however Al exhibited a rather linear behavior. This can be explained by the fact that Al exhibits higher stages of work hardening at a much lower applied stress levels.

## CHAPTER 7

### THE INDENTATION SIZE EFFECT AND STACKING FAULT ENERGY: ADDITIONAL PERSPECTIVES

#### 7.1 Introduction

The movement of dislocations is the primary cause for the plastic deformation of metals. There are several interfacial energies including those associated with grain boundaries, twin boundaries, and stacking faults which are associated with the crystal rheology that assist or inhibit dislocation movement [128]. The stacking fault energy (SFE) for most FCC metals and alloys is an important interfacial parameter that can assist in dynamic recovery, change in the work hardening rate and results in differences in deformation behavior [29]. In FCC, metals a stacking fault is a break in the sequence of the atomic stacking in the close packed plane and can be formed during plastic deformation [29]. As some dislocations move through the lattice they can disassociate into two component, or partial, dislocations having a Burger's vector smaller than the parent lattice spacing and subsequently will not traverse the slip plane leaving a faulted region [5]. The stacking fault in FCC metals generally takes the form of a single ribbon of HCP. The HCP structure has a higher Gibb's free energy associated with it and influences the FCC structure [4]. The energy associated with the faulted region is the SFE and is described in terms of the distance between the trailing partial dislocations. Metals with high SFE have a narrow distance between the partial dislocations; therefore, the energy needed to slip across planes and around obstacles is available and dynamic recovery is assisted. A low SFE metal possess wide separation between the partials and will inhibit cross slip, facilitate work hardening, and will produce deformation twins [29]. SFE has a direct impact on twinning and there tends to be a competition between slip and deformation twinning, primarily for BCC and HCP metals but also



in some low SFE FCC metals. Deformation twinning (DT) is unique in that it is a mirroring of a portion of the lattice with respect to the surrounding crystal [29]. Twin planes and directions are unique to each crystal system and are dominant in those that possess limited slip systems as in HCP [29]. While the total amount of deformation is negligible due to twinning compared to slip, it can provide orientation changes with respect to the stress that may activate new slip systems facilitating cross slip [29]. Therefore, since the SFE and DT can impact the work hardening of metals, they are of interest when examining mechanisms that influence the ISE.

Elmustafa and Stone investigated the possible effect of SFE on the magnitude of the ISE for two polycrystalline metals, aluminum (high SFE) and  $\alpha$ -brass (low SFE) [53]. This work was based only on two metals, one being a pure metal and one being an alloy. Alpha brass, an FCC and HCP alloy did not comply with the familiar Hume-Rothery rules for solid solutions; therefore, there may be other mechanisms that affect the ISE. Elmustafa and Stone (2003) concluded that there was no clear evidence to support the notion that SFE impacted the ISE for these two metals given the fact that aluminum depicted a higher magnitude of the ISE over the  $\alpha$ -brass [53]. As was discussed in Chapter 3, it was found that alloys and pure metals should be considered separately when comparing the effect of the SFE on the ISE. Therefore, in this work the possible role of SFE on the magnitude of the ISE is further examined using additional metals and alloys having intermediate values of SFE beyond those presented by Elmustafa and Stone [53]. Similarly, Rester et al. performed indentation experiments on several pure FCC single crystals including nickel, copper, and silver [129]. They also reported that the SFE does not significantly impact the magnitude of the ISE.

In this work, we utilized the standard hardness and indentation creep experiments described in previous chapters to assess the possible impact of SFE on the magnitude of the ISE.

It will be shown that the SFE may have a weak correlation with the ISE for the pure metals. When comparing the pure metals with the alloys no direct correlation could be discernable. Also, since  $\alpha$ -brass is an alloy of copper and zinc, with zinc being 30% composition and possessing an HCP structure, we performed scanning electron microscopy around the indented region to examine possible twinning effects.

## 7.2 Experiments

We utilized the same pure metals described in the previous chapters of this dissertation. We also reintroduced the  $\alpha$ -brass and added two more alloys, 7075 aluminum zinc (95/5) and nickel copper (70/30). The alloys were annealed at temperatures suitable to produce grain sizes between 50 and 100  $\mu\text{m}$ . The samples were polished as described in Chapter 3 of this work.

The indentation experiments were performed at room temperature using the same machine capable of loads between 0.07  $mN$  and 10  $N$  and the same tip capable of reaching 30  $\mu\text{m}$ . The indentation creep test protocol as well as the standard load control hardness tests were described in previous chapters.

## 7.3 Results

The metals tested were chosen to provide a range of SFE from very high in the case of aluminum to very low for  $\alpha$ -brass. It is generally accepted to normalize the SFE by the shear modulus  $G$ , and Burger's vector  $b$ . The values for the SFE given in Table 4 were taken from multiple sources [128-131]. Here again it is noted that in Table 4 the pure metals and alloys are separated but the differences in the normalized SFE between each metal system from low to high is nearly the same.

Table 4 Normalized SFE for Pure FCC metals and Alloys

| Alloy           | SFE        | Shear Modulus | Burgers Vector | Normalized SFE | Metal | SFE $\gamma$ | Shear Modulus | Burgers Vector | Normalized SFE |
|-----------------|------------|---------------|----------------|----------------|-------|--------------|---------------|----------------|----------------|
|                 | $\gamma$   | $G$           | $b$            | $(\gamma/Gb)$  |       | $\gamma$     | $G$           | $b$            | $(\gamma/Gb)$  |
| $\alpha$ -Brass | >10        | 37            | 0.26           | 1              | Ag    | 22           | 34            | 0.29           | 2              |
| NiCu            | $\sim$ 100 | 65            | 0.249          | 6              | Ni    | 128          | 76            | 0.249          | 7              |
| AlZn            | $\sim$ 125 | 26            | 0.29           | 17             | Al    | 200          | 26            | 0.29           | 27             |

The LC data were plotted to show the ISE for each pure metal and alloy to a maximum load of 10 N and is given in Figure 33. The hardness data shown in Figure 33 have been normalized to the reduced modulus that was given in Equation 2 (Chapter 1 Section 1.2). Rester et. al. articulated that in order to assess the potential influence of SFE on the ISE the reduced modulus, in lieu of the shear modulus, is an appropriate normalization parameter when using indentation testing given most materials show strong anisotropy [129].

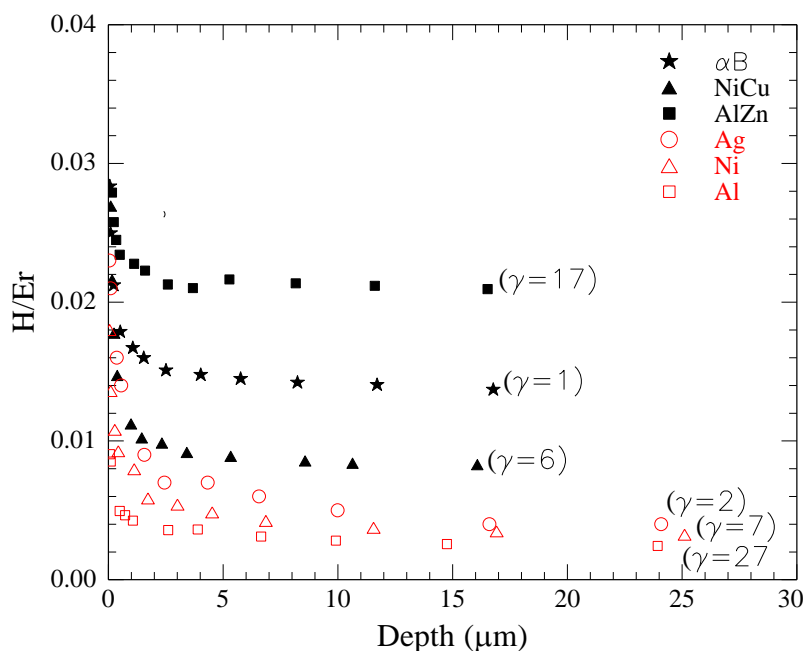


Figure 33 Hardness versus Depth Metals and Alloys

The data of Figure 33 were then used to plot the hardness normalized to the bulk hardness measured at the deepest indentation. This normalization represents the magnitude of the ISE for each metal and is given in Figure 34 and is similar to the one presented by Elmustafa and Stone [53].

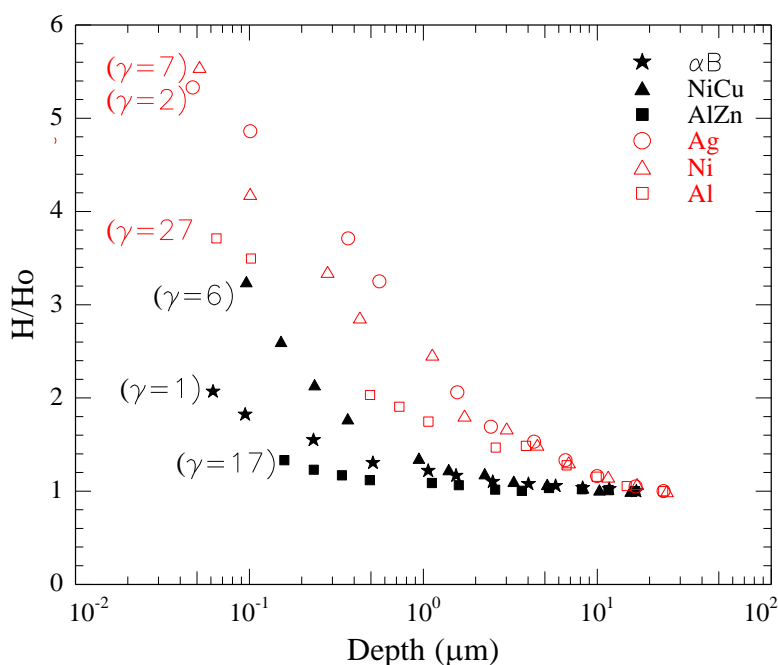


Figure 34 Magnitude of the ISE for Pure Metals and Alloys

The magnitude of the ISE for the pure metals tends to increase with decreasing SFE except for the shallowest depth of  $\sim 50$  nm where it is observed that nickel slightly exceeds the silver sample, 5.55 versus 5.31. In fact it is noted that the magnitude of the silver sample noticeably exceeds the nickel for the shallower depths in the ISE region, except the shallowest data points. The alloys do not show a clear ordering based on SFE given the NiCu sample is exhibiting a much greater magnitude of the ISE over the other two alloys but is less than that of the aluminum. The  $\alpha$ -brass and AlZn samples tend to have a similar magnitude of the ISE despite

the difference in their SFEs. However, if the magnitude of the ISE for  $\alpha$ -brass and AlZn are considered against each other without the NiCu (being a fully substitutional solid solution alloy), then the ordering would be similar to the pure metals where the magnitude of the ISE increases with decreasing SFE.

In addition to hardness versus depth studies for the ISE, the data for each sample were fitted to Elmustafa et al. (2004) Bi-linear Behavior model [59]. This model provides an assessment of the dependence on the GND density through the relation given by  $C_2$  Equation 21 Section .2. The value of  $C_2$  is given by Equation 32;

$$C_2 = \frac{4\Gamma}{b\beta} \quad (32)$$

The data for each metal are fitted to the bilinear model of Elmustafa and Stone and plotted in Figure 35.

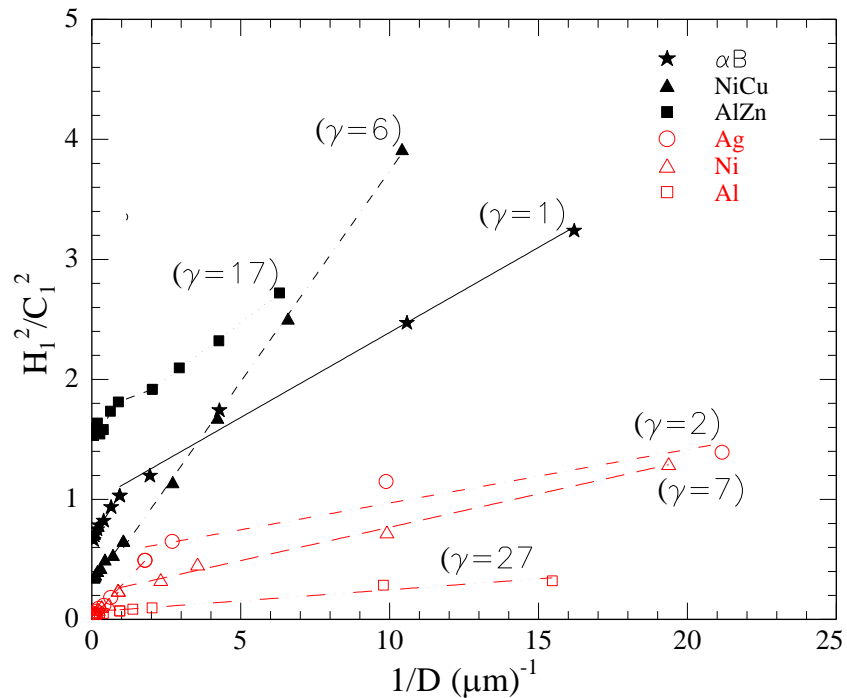


Figure 35 Bi-linear Behavior for pure metals and alloys

To explore the ISE from a kinetics based perspective, indentation creep experiments were used to conduct activation volume analysis similar to that reported by Elmustafa and Stone (2003) [13]. The activation volume presented in previous Chapters  $V^*$  is calculated for each metal and alloy and is plotted versus hardness normalized to the reduced modulus in Figure 36.

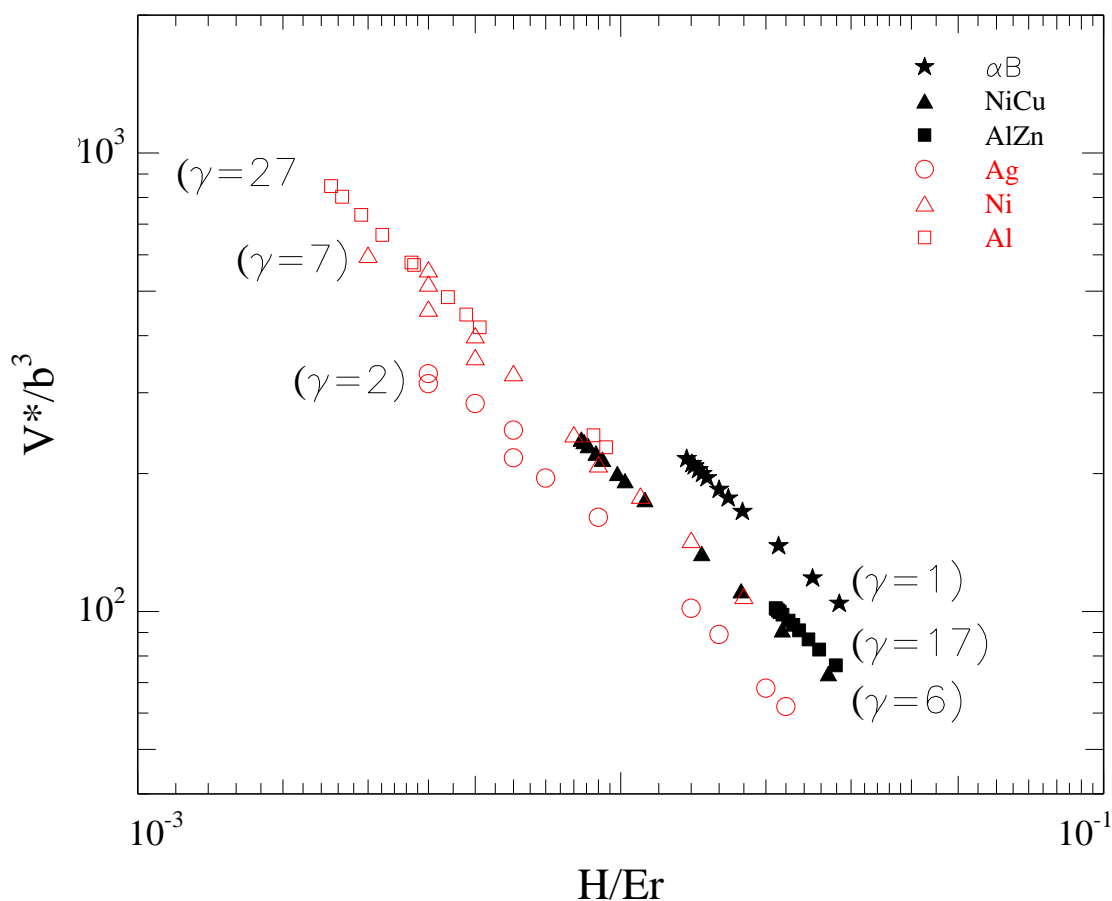


Figure 36  $V^*$  versus Hardness normalized to the Reduced Modulus

#### 7.4 Discussion

Stacking fault energy has a direct impact on FCC metals ability to work harden. Since dislocation mechanisms are responsible for plastic deformation, the dislocation structures are also impacted by the SFE where low SFE metals tend to have banded, linear arrays of

dislocations while high SFE metals possess a cellular dislocation structure that is tangled during deformation [29]. Elmustafa and Stone were the first to postulate that a low SFE metal should have a higher ISE due to restricted cross slip compared to the ISE of a high SFE metal which should be lower due to dynamic recovery [53]. Their analysis concluded that the ISE was not directly impacted by the SFE when comparing pure aluminum and  $\alpha$ -brass in both the annealed and work hardened states. Similarly, Rester et al. conducted indentation experiments on several single crystal FCC metals including silver, copper, and nickel and concluded that the SFE does not show a clear influence on the ISE [129]. They restricted their analysis to comparisons of normalized  $H$  versus depth of indentation and show that all 3 metals depicted exactly the same magnitude of ISE which is unexpected. The current work postulates that the possible influence of SFE on the ISE of a pure metal and alloy cannot be directly compared due to complexities of alloying and that the data must be examined using various techniques.

The samples were tested using the standard load control indentation method at loads ranging from .07  $mN$  to 10  $N$ . The results shown in Figure 33 with the hardness normalized to the reduced modulus versus contact depth depict that the pure metals seem to be ordered based on the respective SFE, whereas the alloys are not. Here the direction of ordering for alloys is opposite to that of the pure metals and the NiCu alloy does not fall between the  $\alpha$ -brass and AlZn. It is noted that the NiCu is a fully substitutional solid solution alloy unlike the mixed FCC HCP alloys. The data in Figure 34 show that the magnitude of the ISE does increase with decreasing SFE for pure metals in a limited fashion. The fact that the magnitude of the ISE for the nickel sample at the shallowest depth slightly increases over the silver could be explained by the fact that the nickel has a much higher shear modulus or it may be that the another process is dominating the silver at very shallow depths of indentation such as deformation twinning. When

the  $\alpha$ -Brass and AlZn are examined in the absence of the NiCu, it was noted that there was some similarity with the pure metals between the ordering based on SFE. This observation underscores the postulate that alloying has a profound effect on the magnitude of the ISE and that it is even more complicated when mixing elements having different crystal structures, such as FCC and HCP. Referring to Figure 35, all the hardness data were fitted using the bilinear behavior model and the trend for the data to organize based on SFE is again observed for pure metals but not for alloys. NiCu is showing a consistent behavior that is similar to the data in Figures 33 and 34 with the slope of the nano-scale data being significantly different from the rest of the samples. Figure 36, shows the change in activation volume,  $V^*$  with hardness, stress, illustrating the impact of thermal activation. The pure metals tend to align based on SFE but again the alloys do not. While there appears to be a weak correlation between SFE and ISE for pure metals based on the analyses performed, the potential influence of alloying on the ISE cannot be understood based on these results. Therefore, a confident conclusion cannot be drawn concerning the SFE impacts on the ISE across all FCC metals. A possible complication could be drawn due to the  $\alpha$ -brass and AlZn not being fully solid solution alloys because of the HCP component in the Zinc. HCP structures have fewer slip systems available during deformation compared to FCC metals and have a tendency to deform by alternate mechanisms such as deformation twinning. It is known that under certain conditions deformation by slip and twinning may become competing processes based on increased strain rate or decreasing temperature. The movement of dislocations through a crystal based on deformation twinning and slip are very different.

To underscore this finding, we performed scanning electron microscopy around the deepest indentations in the  $\alpha$ -brass to see if there was any deformation twinning present. The results are given in Figure 37.



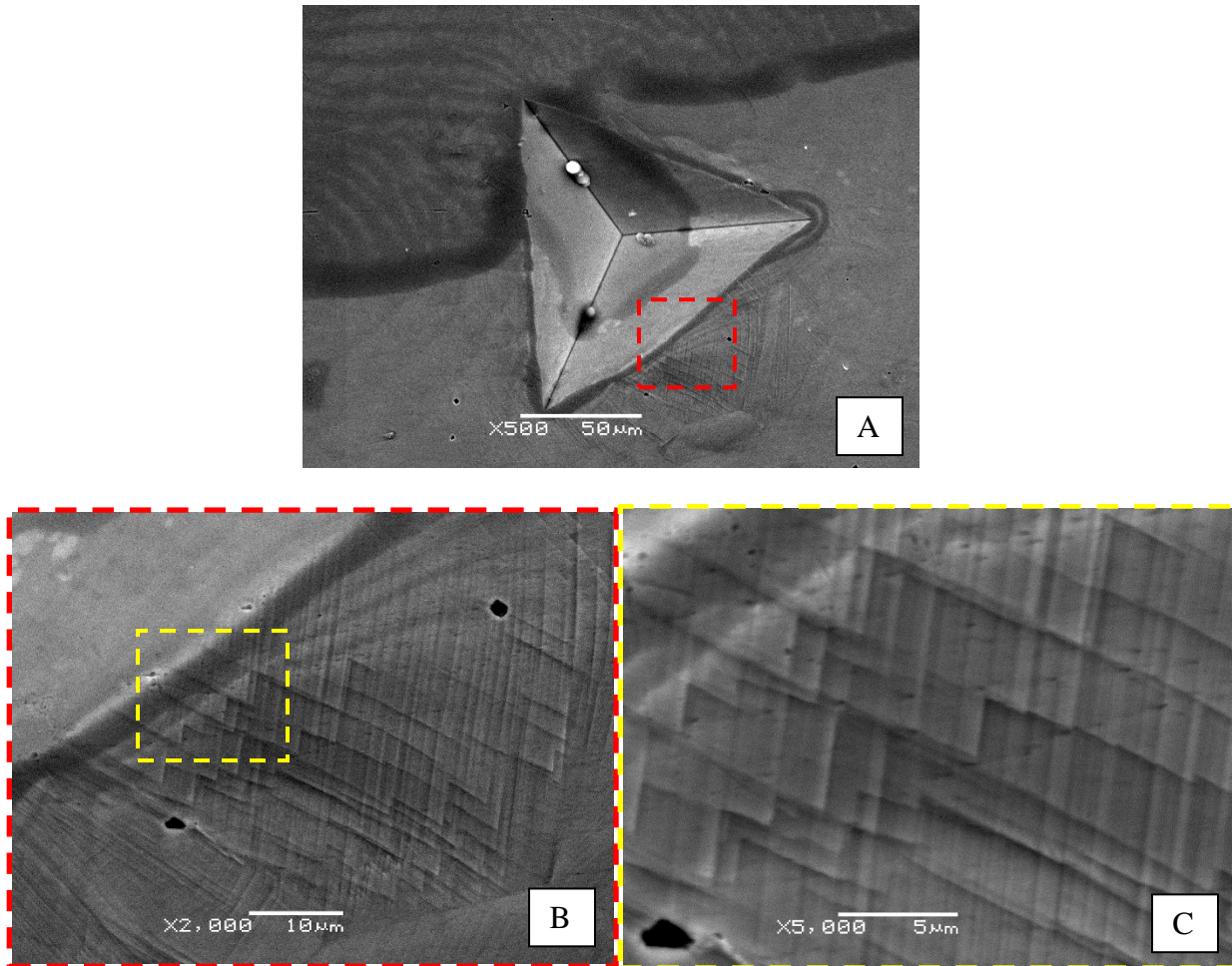


Figure 37 SEM image of  $\alpha$ -Brass indentation

The micrographs shown in Figure 37 “A” was taken using an SEM at 500X. The depth of indentation was  $\sim 17 \mu\text{m}$ . The extent of deformation around all sides of the indentation is clear in “A” while the SEM provided greater details of the possible twinning at higher magnifications shown in “B” and “C”.

Indentations from the aluminum and silver samples at the same load were compared to the  $\alpha$ -brass. It can be clearly seen in Figures 38 and 39 that the aluminum and silver indentations show no sign of deformation twinning at high loads. Twinning in the aluminum sample is not

expected due to the high SFE; however, since silver is a low SFE metal it was possible that deformation twinning was occurring.

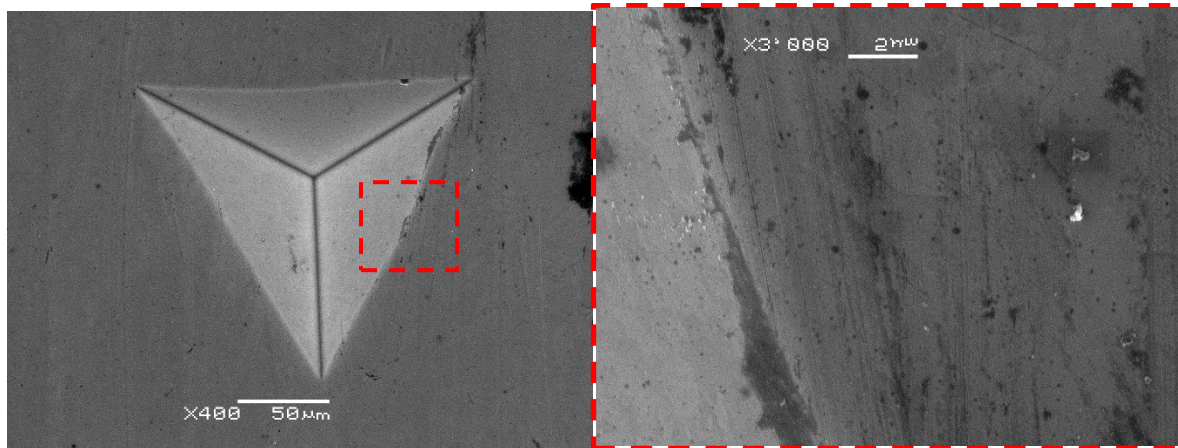


Figure 38 SEM image of aluminum indentation

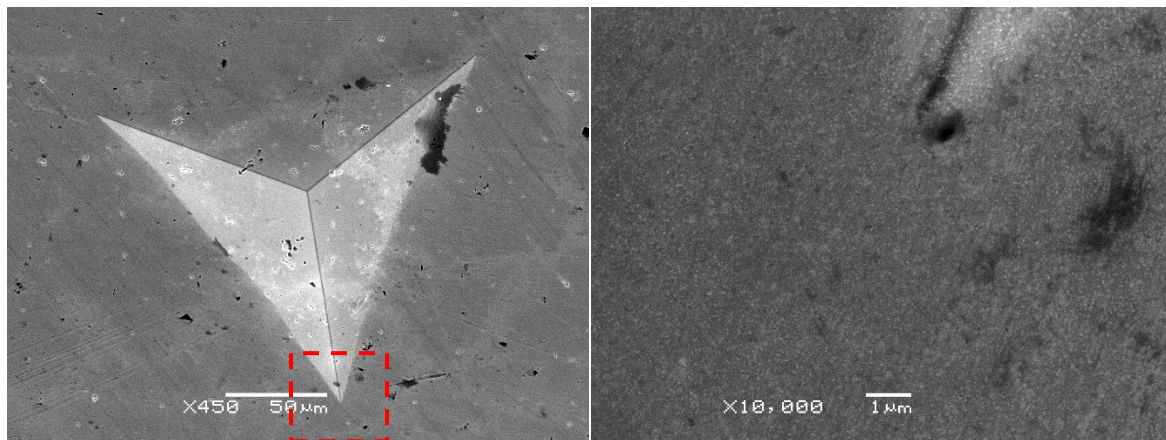


Figure 39 SEM image of silver indentation

The interest in examining the role of deformation twinning for FCC metals has become a topic of interest due to the development of ultrafine and nanoscale grain structures [100, 132-135]. Chen et al. fabricated ultrafine grained Cu and imbedded a high density of nanoscale twins in the grain structure and reported that the ductility and work hardening, from tensile testing, were improved due to the higher density of stored dislocations being influenced by the presence

twinning [135]. Similar results were reported by Lu et al. (2005) for ultrafine Cu samples possessing varying densities of nanoscale twins using indentation and tensile tests [100]. They found that the strain rate sensitivity of the hardness increased significantly, accompanied by a smaller activation volume, for samples having a higher nanoscale twin density and verified through TEM analysis that twinning assisted in the storage and accumulation of dislocations especially around stress gradients [100].

These results coupled with the analysis presented in this chapter would seem to support the proposition that deformation twinning could indeed have some impact on the magnitude of the ISE for the  $\alpha$ -brass. Furthermore, given that deformation twinning is prevalent in lower SFE metals it is speculated that if the silver experiences nano-twinning at very high stresses for low depths of indentation this may explain why the magnitude of the ISE slightly drops below that of the nickel for the shallowest depth of indentation, although no microscopic evidence was found to support that observation. A detailed study that would include extensive HRSEM would be needed to draw any substantive conclusions concerning the specific role twinning, especially at the nanoscale.

## **7.5 Conclusion**

- It is concluded that while a weak correlation of the ISE with SFE is observed for the pure metals tested, the influence of SFE for all metals and alloys cannot be made. It is recommended that a separate study be conducted on an alloy, perhaps a diffusion couple, where the alloying content can be precisely controlled and tested.
- Scanning electron microscopy revealed the presence of deformation twinning at high loads for the  $\alpha$ -brass sample but no evidence of twinning was found for the Ag or Al samples.

## CHAPTER 8

### CONCLUSIONS

The goal of this dissertation is to further examine the fundamental dislocation mechanisms that may be contributing to the indentation size effect. This work successfully addressed each of the objectives given in Chapter 2 by incorporating a qualitative and quantitative approach to each experiment presented in this dissertation. The qualitative component consisted of utilizing a single indentation machine and single tip to conduct all the different experiments. This eliminated any uncertainty in measurements when comparing data for any metal across the nano to micro-range (from 0.07 *mN* to 10 *N*). To the best of my knowledge, this is the first time this type of comprehensive approach, using the same machine and same tip, has been used to conduct experiments using nanoindentation. The work also incorporated a quantitative aspect in that it used several pure polycrystalline metals and alloys that were chosen based on SFE (including 99.999% Aluminum (SFE  $\sim 200$  *mJ/m<sup>2</sup>*), 99.95% Nickel (SFE  $\sim 125$  *mJ/m<sup>2</sup>*), 99.95% Silver (SFE  $\sim 22$  *mJ/m<sup>2</sup>*), and three alloys, alpha brass 70/30, (SFE  $>10$  *mJ/m<sup>2</sup>*), 70/30 NiCu (SFE  $\sim 100$  *mJ/m<sup>2</sup>*), and 7075 AlZn (SFE  $\sim 125$  *mJ/m<sup>2</sup>*), to study the effect on the ISE. The addition of several different metals provided a larger dataset to draw conclusions concerning various aspects that may influence the ISE.

We wanted to verify the existence of an ISE and the bilinear behavior of various FCC metals using single indentation test platform and the same tip for various stress decades. The data derived from the experiments described in Chapter 3 provided verification that aluminum, nickel, silver, and  $\alpha$ -brass exhibited a clear ISE regardless of machine and tip used. This finding removes the doubts concerning the ISE measured using different machines and tips. We verified that the bilinear behavior for pure Al and  $\alpha$ -brass is mechanistic in nature and is observed

regardless of the type of the self-similar indenter tip employed. We confirmed that the CSM protocol produced erroneous data at shallow depths of indentation due to the “tapping effect” for soft metals having high E/H ratios. We conducted new experimental work to support the understanding of this effect in the vicinity of grain boundaries, using different versions of the test method and different tips, to conclude that the apparent hardening/softening behavior at shallow depths for the FCC metals is due to the errors associated with the XP CSM protocol and the so called tapping effect for high E/H metals and not related to the microstructure. Finally, we concluded that despite the SFE of the single metals tested (Al, Ni, and Ag) depicted a limited correlation with the magnitude of the ISE, the  $\alpha$ -brass showed a distinct difference; therefore, additional alloys should be included and examined separately from the pure metals.

Next, we wanted to examine the thermally activated mechanisms that could contribute to the ISE via the kinetics of plastic deformation based on indentation experiments for constant load creep and load relaxation as well as classical uniaxial testing to study the coupled relationship between strain rate, dislocation density, and dislocation velocity. The desire was to provide a new approach to investigate the ISE in terms of the variables that govern Orowan’s equation specifically dislocation velocity and how it changes with  $V^*$ . This work was documented in Chapters 4, 5, and 6.

In Chapter 4 we presented data from indentation creep and uniaxial tensile tests from the same pure metals to examine the dependence of the  $V^*$  across decades of stress. We found that  $V^*/b^3$  from uniaxial testing data compared well with  $V^*/b^3$  data measured using nanoindentation equipped with high capability that reached 10 N for Al, Ag, and Ni FCC metals and that  $V^*/b^3$  vs.  $H$  data extrapolated into literature data from conventional uniaxial testing. This validated the notion that the accumulation of dislocations due to dislocations/dislocations interaction resulted

in smaller activation area swept out by dislocations during activation explains the decrease in  $V^*/b^3$  with strain hardening, i.e. that the ISE possess the same kinetic signature as that observed in uniaxial testing.

In Chapter 5, we developed a new test protocol to perform repeated load relaxation experiments in nanoindentation. The purpose of this work was to develop an experimental technique for indentation, beyond that of single transient creep, capable of generating data to examine the coupled relationship between  $V$ ,  $\rho$ , and  $v$  for metals that exhibit an ISE. We found that the ratio dislocation density decreases with increasing depth of indentation while the dislocation velocity increases. This finding indicated that as the depth of indentation decreases; the velocity of mobile dislocations is directly inhibited by the increase in the dislocation density and is at a minimum consistent with the accepted theory that the ISE is governed by a dislocation mechanism.

In Chapter 6, we used the new load relaxation protocol, in addition to indentation creep experiments for the different pure polycrystalline metals. The goal was to expand our understanding of these observations by examining the fundamental variables for the Orowan equation (including strain rate, dislocation densities, and dislocation velocity) that may contribute to the specific mechanisms governing thermally activated processes and the ISE. We observed that the dislocation velocity, based on the strain rate and an estimate of the dislocation density based on Orowan's relation, tends to decrease with increasing hardness (stress) at shallow depths of indentation. It was concluded that this decrease in velocity can be explained by excessive accumulation of GND's, due to a strain gradient, and as the depth of indentation increases, the strain gradient relaxes and the influence of the GND density is significantly reduced. The dislocation velocity will eventually reach a saturation level when the

material reaches a steady state value of hardness at depths that corresponds to the bulk hardness where the SSDs dominate the crystal plasticity. We have demonstrated for the first time that based on the pre-established bilinear behavior and the decrease of the activation volume with hardening due to dislocation-dislocation interaction in indentation creep experiments by Elmustafa and Stone (2003) that the dislocation velocity exhibits a bilinear behavior when plotted versus hardness using the Orowan's relation. We concluded that Ag and Ni distinctively depict a bilinear behavior in the dislocation velocity with hardness, however Al exhibited a rather linear behavior. This can be explained by the fact that Al exhibits higher stages of work hardening at a much lower applied stress levels.

Lastly, the final objective was to examine the possible contribution of stacking fault energy on the ISE by comparing pure metals over a wide SFE range as well as the effect of alloying. The work detailed in Chapter 7 showed that pure metals weakly tend to align based on their respective SFE when plotting the hardness normalized to the reduced modulus, the hardness normalized to the bulk hardness versus depth, the bilinear behavior, and  $V^*$  versus hardness, but the alloys do not. It is concluded that while a weak correlation of the ISE with SFE is observed for the pure metals tested, a direct influence of SFE for all metals and alloys cannot be made. Surprisingly, we found that the  $\alpha$ -brass sample shows significant deformation twinning around the indentation using an SEM but the contribution of twinning is unclear especially given the limited number of alloys tested.

## **8.1 Future Work**

Additional work could be accomplished to further articulate the specific dislocation structures that are impacting the ISE in the pure metals by performing microscopic

measurements of dislocation movement in the vicinity of indents at different depths. The effect of the SFE on the ISE should continue to be examined by including additional pure metals for comparison including pure copper, gold, platinum, and lead. For investigations on alloys, a possible path to accomplish this would be to use a diffusion couple composed of two pure metals with well-controlled phases having defined alloy content. A second option would be to purchase, or fabricate, a set of specimens with increasing alloy content, such as pure copper and producing additional specimens with increasing zinc content. Also, the possible influence that deformation twinning could have on the ISE could be further examined using specimens with varying zinc content. The implementation of HRSEM or TEM to examine the deformation structures around indentations would be extremely valuable.



## REFERENCES

- [1] G. Revankar, "Introduction to Hardness Testing," in *ASM Handbook*. vol. 8, H. Kuhn and D. Medlin, Eds., ed Metals Park, Ohio: ASM International, 2000, pp. 199-202.
- [2] W. C. Oliver and G. M. Pharr, "An improved technique for determining hardness and elastic modulus using load and displacement sensing indentation experiments," *Journal of Materials Research*, vol. 7, pp. 1564-83, 06/ 1992.
- [3] W. C. Oliver and G. M. Pharr, "Measurement of hardness and elastic modulus by instrumented indentation: advances in understanding and refinements to methodology," *Journal of Materials Research*, vol. 19, pp. 3-20, 01/ 2004.
- [4] M. A. Meyers and K. K. Chawla, *Mechanical Metallurgy Principles and Applications*, 1st ed. Englewood Cliffs, New Jersey: Prentice Hall, 1984.
- [5] F. A. McClintock and A. S. Argon, *Mechanical Behavior of Materials*. Reading, Massachusetts: Addison-Wesley, 1966.
- [6] E. Meyer, "Hardness testing and hardness," *VDI Zeitschrift*, vol. 52, pp. 645-654, 04/25 1908.
- [7] D. Tabor, *The hardness of metals*: Clarendon Press, Oxford University Press, 1951.
- [8] B. W. Mott, *Micro-indentation hardness testing /B. W. Mott*. London: Butterworth, 1956.
- [9] H. Bückle, "PROGRESS IN MICRO-INDENTATION HARDNESS TESTING," *Metallurgical Reviews*, vol. 4, pp. 49-100, 1959/01/01 1959.
- [10] J. B. Pethica, R. Hutchings, and W. C. Oliver, "Hardness measurement at penetration depths as small as 20 nm," *Philosophical Magazine A (Physics of Condensed Matter, Defects and Mechanical Properties)*, vol. 48, pp. 593-606, 10/ 1983.
- [11] M. Qing and D. R. Clarke, "Size dependent hardness of silver single crystals," *Journal of Materials Research*, vol. 10, pp. 853-63, 04/ 1995.
- [12] D. Tabor, "Indentation hardness and its measurement: Some cautionary comments," in *Microindentation Techniques in Materials Science and Engineering, ASTM STP 889*, P. J. Blau and B. R. Lawn, Eds., ed Philadelphia: American Society for Testing and Materials, 1986, pp. 129-159.
- [13] A. A. Elmustafa and D. S. Stone, "Size-dependent hardness in annealed and work hardened -brass and aluminum polycrystalline materials using activation volume analysis," *Materials Letters*, vol. 57, pp. 1072-8, 01/ 2003.
- [14] G. M. Pharr and W. C. Oliver, "Nanoindentation of silver-relations between hardness and dislocation structure," *Journal of Materials Research*, vol. 4, pp. 94-101, 1989.
- [15] N. A. Fleck and J. W. Hutchinson, "A phenomenological theory for strain gradient effects in plasticity," *Journal of the Mechanics and Physics of Solids*, vol. 41, pp. 1825-57, 12/ 1993.
- [16] N. A. Fleck, G. M. Muller, M. F. Ashby, and J. W. Hutchinson, "Strain gradient plasticity: theory and experiment," *Acta Metallurgica et Materialia*, vol. 42, pp. 475-87, 02/ 1994.
- [17] W. J. Poole, M. F. Ashby, and N. A. Fleck, "Micro-hardness of annealed and work-hardened copper polycrystals," *Scripta Materialia*, vol. 34, pp. 559-64, 02/15 1996.

- [18] N. A. Stelmashenko, M. G. Walls, L. M. Brown, and Y. V. Milman, "Microindentations on W and Mo oriented single crystals: An STM study," *Acta Metallurgica et Materialia*, vol. 41, pp. 2855-2865, 1993.
- [19] F. R. N. Nabarro, S. Shrivastava, and S. B. Luyckx, "The size effect in microindentation," *Philosophical Magazine*, vol. 86, pp. 4173-80, 2006.
- [20] W. D. Nix and G. Huajian, "Indentation size effects in crystalline materials: a law for strain gradient plasticity," *Journal of the Mechanics and Physics of Solids*, vol. 46, pp. 411-25, 03/ 1998.
- [21] H. Gao, Y. Huang, W. D. Nix, and J. W. Hutchinson, "Mechanism-based strain gradient plasticity. I. Theory," *Journal of the Mechanics and Physics of Solids*, vol. 47, pp. 1239-63, 06/ 1999.
- [22] J.-Y. Kim, S.-K. Kang, J. R. Greer, and D. Kwon, "Evaluating plastic flow properties by characterizing indentation size effect using a sharp indenter," *Acta Materialia*, vol. 56, pp. 3338-3343, 2008.
- [23] K. Durst, B. Backes, and M. Goken, "Indentation size effect in metallic materials: Correcting for the size of the plastic zone," *Scripta Materialia*, vol. 52, pp. 1093-7, 06/ 2005.
- [24] Y. Huang, F. Zhang, K. C. Hwang, W. D. Nix, G. M. Pharr, and G. Feng, "A model of size effects in nano-indentation," *Journal of the Mechanics and Physics of Solids*, vol. 54, pp. 1668-1686, 2006.
- [25] A. A. Elmustafa and D. S. Stone, "Indentation size effect in polycrystalline F.C.C. metals," *Acta Materialia*, vol. 50, pp. 3641-50, 08/16 2002.
- [26] M. F. Ashby, "The deformation of plastically non-homogeneous materials," *Philosophical Magazine*, vol. 21, pp. 399-424, 02/ 1970.
- [27] A. A. Elmustafa, J. Lou, O. Adewoye, W. O. Soboyejo, and D. S. Stone, "Bilinear behavior in the indentation size effect: a consequence of strain gradient plasticity," in *Surface Engineering 2002 - Synthesis, Characterization and Applications. Symposium, 2-5 Dec. 2002*, Warrendale, PA, USA, 2003, pp. 27-32.
- [28] Y. Huang, H. Gao, W. D. Nix, and J. W. Hutchinson, "Mechanism-based strain gradient plasticity. II. Analysis," *Journal of the Mechanics and Physics of Solids*, vol. 48, pp. 99-128, 01/ 2000.
- [29] G. E. Dieter, *Mechanical Metallurgy*, 3rd ed. New York: McGraw Hill, 1986.
- [30] D. Caillard and J. L. Martin, *Thermally Activated Mechanisms in Crystal Plasticity*. Amsterdam: Pergamon, 2003.
- [31] A. S. Krausz and H. Eyring, *Deformation Kinetics*, 1 ed. New York: John Wiley and Sons, 1975.
- [32] B. David and K. W. D., *Microstructural Characterization of Materials*, 2nd ed. West Sussex, England: John Wiley and Sons, 2008.
- [33] A. J. Wilkinson, G. Meaden, and D. J. Dingley, "High-resolution elastic strain measurement from electron backscatter diffraction patterns: New levels of sensitivity," *Ultramicroscopy*, vol. 106, pp. 307-313, 3// 2006.
- [34] A. J. Wilkinson, "Measurement of elastic strains and small lattice rotations using electron back scatter diffraction," *Ultramicroscopy*, vol. 62, pp. 237-47, 03/ 1996.
- [35] M. Kamaya, A. J. Wilkinson, and J. M. Titchmarsh, "Measurement of plastic strain of polycrystalline material by electron backscatter diffraction," *Nuclear Engineering and Design*, vol. 235, pp. 713-725, 3// 2005.

- [36] J. Jiang, T. B. Britton, and A. J. Wilkinson, "Measurement of geometrically necessary dislocation density with high resolution electron backscatter diffraction: Effects of detector binning and step size," *Ultramicroscopy*, vol. 125, pp. 1-9, 2013.
- [37] T. B. Britton and A. J. Wilkinson, "Measurement of residual elastic strain and lattice rotations with high resolution electron backscatter diffraction," *Ultramicroscopy*, vol. 111, pp. 1395-1404, 7// 2011.
- [38] T. J. Ruggles and D. T. Fullwood, "Estimations of bulk geometrically necessary dislocation density using high resolution EBSD," *Ultramicroscopy*, vol. 133, pp. 8-15, 10/ 2013.
- [39] W. Pantleon, "Resolving the geometrically necessary dislocation content by conventional electron backscattering diffraction," *Scripta Materialia*, vol. 58, pp. 994-7, 06/ 2008.
- [40] M. Rester, C. Motz, and R. Pippan, "The deformation-induced zone below large and shallow nanoindentations: A comparative study using EBSD and TEM," *Philosophical Magazine Letters*, vol. 88, pp. 879-887, 2008.
- [41] M. Rester, C. Motz, and R. Pippan, "Indentation across size scales - A survey of indentation-induced plastic zones in copper {1 1 1} single crystals," *Scripta Materialia*, vol. 59, pp. 742-745, 2008.
- [42] M. Rester, C. Motz, and R. Pippan, "Microstructural investigation of the deformation zone below nano-indenters in copper," in *Fundamentals of Nanoindentation and Nanotribology IV*, 26-29 Nov. 2007, Warrendale, PA, USA, 2008, pp. 29-34.
- [43] N. Zaafarani, D. Raabe, F. Roters, and S. Zaeferrer, "On the origin of deformation-induced rotation patterns below nanoindenters," *Acta Materialia*, vol. 56, pp. 31-42, 2008.
- [44] N. Zaafarani, D. Raabe, R. N. Singh, F. Roters, and S. Zaeferrer, "Three-dimensional investigation of the texture and microstructure below a nanoindent in a Cu single crystal using 3D EBSD and crystal plasticity finite element simulations," *Acta Materialia*, vol. 54, pp. 1863-1876, 2006.
- [45] J. Mayer, L. A. Giannuzzi, T. Kamino, and J. Michael, "TEM sample preparation and FIB-induced damage," *MRS Bulletin*, vol. 32, pp. 400-7, 05/ 2007.
- [46] J. W. Kysar, Y. X. Gan, T. L. Morse, C. Xi, and M. E. Jones, "High strain gradient plasticity associated with wedge indentation into face-centered cubic single crystals: Geometrically necessary dislocation densities," *Journal of the Mechanics and Physics of Solids*, vol. 55, pp. 1554-73, 07/ 2007.
- [47] T. J. Ruggles, "Characterization of geometrically necessary dislocation content with EBSD-based continuum dislocation microscopy," Brigham Young University, USA, Ann Arbor, MI, USA, 2015.
- [48] B. Yang and H. Vehoff, "Dependence of nanohardness upon indentation size and grain size - A local examination of the interaction between dislocations and grain boundaries," *Acta Materialia*, vol. 55, pp. 849-56, 02/ 2007.
- [49] Y. L. Chiu and A. H. W. Ngan, "A TEM investigation on indentation plastic zones in Ni<sub>3</sub>Al(Cr,B) single crystals," *Acta Materialia*, vol. 50, pp. 2677-2691, 2002.
- [50] D. Kiener, K. Durst, M. Rester, and A. Minor, "Revealing deformation mechanisms with nanoindentation," *JOM*, vol. 61, pp. 14-23, 03/ 2009.
- [51] D. E. Kramer, M. F. Savage, A. Lin, and T. Foecke, "Novel method for TEM characterization of deformation under nanoindenters in nanolayered materials," *Scripta Materialia*, vol. 50, pp. 745-9, 03/ 2004.

- [52] S. Graca, P. A. Carvalho, and R. Colaco, "Dislocation structures in nanoindented ductile metals-a transmission electron microscopy direct observation," *Journal of Physics D: Applied Physics*, vol. 44, 2011.
- [53] A. A. Elmustafa and D. S. Stone, "Stacking fault energy and dynamic recovery: Do they impact the indentation size effect?," *Materials Science and Engineering A*, vol. 358, pp. 1-8, 2003.
- [54] D. E. Stegall, M. A. Mamun, B. Crawford, and A. Elmustafa, "Indentation size effect in FCC metals: An examination of experimental techniques and the bilinear behavior," *Journal of Materials Research*, vol. 27, pp. 1543-1552, 2012.
- [55] D. E. Stegall and A. A. Elmustafa, "Activation volume of pure face centered cubic metals using uniaxial testing and nanoindentation equipped with high load capability," *Materials Research Express*, vol. 3, p. 105024, 2016.
- [56] D. E. Stegall, M. A. Mamun, B. Crawford, and A. A. Elmustafa, "Repeated load relaxation testing of pure polycrystalline nickel at room temperature using nanoindentation," *Applied Physics Letters*, vol. 104, p. 041902 (4 pp.), 01/27 2014.
- [57] J. Mencik, "Determination of mechanical properties by instrumented indentation," *Meccanica*, vol. 42, pp. 19-29, / 2007.
- [58] A. A. Elmustafa and D. S. Stone, "Nanoindentation and the indentation size effect: Kinetics of deformation and strain gradient plasticity," *Journal of the Mechanics and Physics of Solids*, vol. 51, pp. 357-381, 2003.
- [59] A. A. Elmustafa, A. A. Ananda, and W. M. Elmahboub, "Bilinear behavior in nano and microindentation tests of fcc polycrystalline materials," *Journal of Engineering Materials and Technology, Transactions of the ASME*, vol. 126, pp. 353-359, 2004.
- [60] W. Tayon, R. Crooks, M. Domack, J. Wagner, and A. A. Elmustafa, "EBSD study of delamination fracture in Al-Li alloy 2090," *Experimental Mechanics*, vol. 50, pp. 135-143, 2010.
- [61] A. H. Almasri and G. Z. Voyiadjis, "Nano-indentation in FCC metals: Experimental study," *Acta Mechanica*, vol. 209, pp. 1-9, 01/ 2010.
- [62] D. Faghihi and G. Z. Voyiadjis, "Size effects and length scales in nanoindentation for body-centred cubic materials with application to iron," *Proceedings of the Institution of Mechanical Engineers, Part N: Journal of Nanoengineering and Nanosystems*, vol. 224, pp. 5-18, 2010.
- [63] G. Z. Voyiadjis and D. Faghihi, "Variable (intrinsic) material length scale for face-centred cubic metals using nano-indentation," *Proceedings of the Institution of Mechanical Engineers, Part N (Journal of Nanoengineering and Nanosystems)*, vol. 225, pp. 123-47, 2010.
- [64] G. Z. Voyiadjis and R. Peters, "Size effects in nanoindentation: an experimental and analytical study," *Acta Mechanica*, vol. 211, pp. 131-53, 04/ 2010.
- [65] G. M. Pharr, J. H. Strader, and W. C. Oliver, "Critical issues in making small-depth mechanical property measurements by nanoindentation with continuous stiffness measurement," *Journal of Materials Research*, vol. 24, pp. 653-66, 03/ 2009.
- [66] J. W. Wyrzykowski and M. W. Grabski, "The Hall-Petch relation in aluminium and its dependence on the grain boundary structure," *Philosophical Magazine A (Physics of Condensed Matter, Defects and Mechanical Properties)*, vol. 53, pp. 505-20, 04/ 1986.

- [67] P. C. Wo and A. H. W. Ngan, "Investigation of slip transmission behavior across grain boundaries in polycrystalline Ni<sub>3</sub>Al using nanoindentation," *Journal of Materials Research*, vol. 19, pp. 189-201, 01/ 2004.
- [68] M. G. Wang and A. H. W. Ngan, "Indentation strain burst phenomenon induced by grain boundaries in niobium," *Journal of Materials Research*, vol. 19, pp. 2478-86, 08/ 2004.
- [69] Y. M. Soifer, A. Verdyan, M. Kazakevich, and E. Rabkin, "Nanohardness of copper in the vicinity of grain boundaries," *Scripta Materialia*, vol. 47, pp. 799-804, 12/09 2002.
- [70] K. E. Aifantis, W. A. Soer, J. T. M. De Hosson, and J. R. Willis, "Interfaces within strain gradient plasticity: Theory and experiments," *Acta Materialia*, vol. 54, pp. 5077-5085, 11// 2006.
- [71] A. J. Beaudoin, A. Acharya, S. R. Chen, D. A. Korzekwa, and M. G. Stout, "Consideration of grain-size effect and kinetics in the plastic deformation of metal polycrystals," *Acta Materialia*, vol. 48, pp. 3409-23, 08/01 2000.
- [72] P. Sayan and J. Ulrich, "Effect of various impurities on the hardness of NaCl crystals," *Crystal Research and Technology*, vol. 36, pp. 1253-62, / 2001.
- [73] T. B. Britton, D. Randman, and A. J. Wilkinson, "Nanoindentation study of slip transfer phenomenon at grain boundaries," *Journal of Materials Research*, vol. 24, pp. 607-15, 03/ 2009.
- [74] G. M. Pharr, E. G. Herbert, and G. Yanfei, "The indentation size effect: A critical examination of experimental observations and mechanistic interpretations," *Annual Review of Materials Research*, vol. 40, pp. 271-92, / 2010.
- [75] S. Pathak, J. Michler, K. Wasmer, and S. R. Kalidindi, "Studying grain boundary regions in polycrystalline materials using spherical nano-indentation and orientation imaging microscopy," *Journal of Materials Science*, vol. 47, pp. 815-823, 2012.
- [76] D. Faghihi and G. Z. Voyiadjis, "Determination of nanoindentation size effects and variable material intrinsic length scale for body-centered cubic metals," *Mechanics of Materials*, vol. 44, pp. 189-211, 2012.
- [77] T. C. Lee, I. M. Robertson, and H. K. Birnbaum, "Prediction of slip transfer mechanisms across grain boundaries," *Scripta Metallurgica*, vol. 23, pp. 799-803, 05/ 1989.
- [78] S. Vadalakonda, R. Banerjee, A. Puthcode, and R. Mirshams, "Comparison of incipient plasticity in bcc and fcc metals studied using nanoindentation," *Materials Science and Engineering A*, vol. 426, pp. 208-213, 2006.
- [79] M. Z. Butt and P. Feltham, "Work hardening of polycrystalline copper and alpha brasses," *Metal science*, vol. 18, pp. 123-126, 1984.
- [80] W. Bochniak, "Mode of deformation and the Cottrell-Stokes law in f.c.c. single crystals," *Acta Metallurgica et Materialia*, vol. 43, pp. 225-33, 01/ 1995.
- [81] W. Bochniak, "Cottrell-Stokes law for f.c.c. single crystals," *Acta metallurgica et materialia*, vol. 41, pp. 3133-3140, 1993.
- [82] E. Sirois and H. K. Birnbau, "Effects of hydrogen and carbon on thermally activated deformation in nickel," *Acta metallurgica et materialia*, vol. 40, pp. 1377-1385, 1992.
- [83] K. Tanoue, "Thermal activation analysis on the plastic deformation satisfied with the Cottrell-Stokes law," *Acta Metallurgica et Materialia*, vol. 40, pp. 1945-50, 08/ 1992.
- [84] K. Tanoue, "Cottrell-Stokes law and scaling loci of stress relaxation curves in copper single crystals," *Scripta Metallurgica et Materialia*, vol. 25, pp. 565-9, 03/ 1991.

- [85] D. S. Stone and K. B. Yoder, "Division of the hardness of molybdenum into rate-dependent and rate-independent components," *Journal of Materials Research*, vol. 9, pp. 2524-33, 10/ 1994.
- [86] M. F. Tambwe, D. S. Stone, A. J. Griffin, H. Kung, Y. C. Lu, and M. Nastasi, "Haasen plot analysis of the Hall-Petch effect in Cu-Nb nanolayer composites," *Journal of Materials Research*, vol. 14, pp. 407-17, 02/ 1999.
- [87] M. Haghshenas and R. J. Klassen, "Indentation-based assessment of the dependence of geometrically necessary dislocations upon depth and strain rate in FCC materials," *Materials Science and Engineering A*, vol. 586, pp. 223-230, 2013.
- [88] I.-C. Choi, Y.-J. Kim, Y. M. Wang, U. Ramamurty, and J.-i. Jang, "Nanoindentation behavior of nanotwinned Cu: Influence of indenter angle on hardness, strain rate sensitivity and activation volume," *Acta Materialia*, vol. 61, pp. 7313-7323, 11// 2013.
- [89] K. W. McElhaney, J. J. Vlassak, and W. D. Nix, "Determination of indenter tip geometry and indentation contact area for depth-sensing indentation experiments," *Journal of Materials Research*, vol. 13, pp. 1300-6, 05/ 1998.
- [90] C. C. Koch, "Ductility in nanostructured and ultra fine-grained materials: Recent evidence for optimism," *Journal of Metastable and Nanocrystalline Materials*, vol. 18, pp. 9-20, 2003.
- [91] S. H. Van and A. Caro, "Molecular dynamics computer simulation of nanophase Ni: Structure and mechanical properties," *Nanostructured Materials*, vol. 9, pp. 669-672, 1997.
- [92] M. A. Meyers, A. Mishra, and D. J. Benson, "Mechanical properties of nanocrystalline materials," *Progress in Materials Science*, vol. 51, pp. 427-556, 2006.
- [93] Q. Zhou, J. Zhao, J. Y. Xie, F. Wang, P. Huang, T. J. Lu, *et al.*, "Grain size dependent strain rate sensitivity in nanocrystalline body-centered cubic metal thin films," *Materials Science and Engineering: A*, vol. 608, pp. 184-189, 7/1/ 2014.
- [94] Y. Wang, Y. Liu, and J. T. Wang, "Investigation on activation volume and strain-rate sensitivity in ultrafine-grained tantalum," *Materials Science and Engineering: A*, vol. 635, pp. 86-93, 5/21/ 2015.
- [95] J. D. Littell, W. K. Binienda, G. D. Roberts, and R. K. Goldberg, "Characterization of damage in triaxial braided composites under tensile loading," *Journal of Aerospace Engineering*, vol. 22, pp. 270-9, 07/ 2009.
- [96] F. R. N. Nabarro, "Cottrell-Stokes law and activation theory," *Acta Metallurgica et Materialia*, vol. 38, pp. 161-4, 02/ 1990.
- [97] O. G. Lademo, O. Engler, J. Aegerter, T. Berstad, A. Benallal, and O. S. Hopperstad, "Strain-rate Sensitivity Of Aluminum Alloys AA1200 And AA3103," *Journal of Engineering Materials and Technology*, vol. 132, p. 041007 (8 pp.), 10/ 2010.
- [98] J. May, H. W. Höppel, and M. Göken, "Strain rate sensitivity of ultrafine-grained aluminium processed by severe plastic deformation," *Scripta Materialia*, vol. 53, pp. 189-194, 7// 2005.
- [99] F. Dalla Torre, H. Van Swygenhoven, and M. Victoria, "Nanocrystalline electrodeposited Ni: Microstructure and tensile properties," *Acta Materialia*, vol. 50, pp. 3957-3970, 2002.
- [100] L. Lu, R. Schwaiger, Z. W. Shan, M. Dao, K. Lu, and S. Suresh, "Nano-sized twins induce high rate sensitivity of flow stress in pure copper," *Acta Materialia*, vol. 53, pp. 2169-79, 04/ 2005.

- [101] J. R. P. Carreker, "Tensile deformation of silver as function of temperature, strain rate, and grain size," *Journal of Metals*, vol. 9, pp. 112-115, 1957.
- [102] H. Mecking, U. F. Kocks, and H. Fischer, "Hardeing, recovery, and creep in FCC Mono- and polycrystals," vol. 1, pp. 334-339, 1976.
- [103] R. W. Rohde and T. V. Nordstrom, "On stress relaxation experiments," *Scripta Metallurgica*, vol. 7, pp. 317-322, 1973.
- [104] F. H. Dalla Torre, E. V. Pereloma, and C. H. J. Davies, "Strain rate sensitivity and apparent activation volume measurements on equal channel angular extruded Cu processed by one to twelve passes," *Scripta Materialia*, vol. 51, pp. 367-71, 2004.
- [105] C. Duhamel, Y. Brechet, and Y. Champion, "Activation volume and deviation from Cottrell-Stokes law at small grain size," *International Journal of Plasticity*, vol. 26, pp. 747-57, 05/ 2010.
- [106] Y. M. Wang, A. V. Hamza, and E. Ma, "Temperature-dependent strain rate sensitivity and activation volume of nanocrystalline Ni," *Acta Materialia*, vol. 54, pp. 2715-2726, 2006.
- [107] X. X. Wu, X. Y. San, Y. L. Gong, L. P. Chen, C. J. Li, and X. K. Zhu, "Studies on strength and ductility of Cu-Zn alloys by stress relaxation," *Materials & Design*, vol. 47, pp. 295-9, 05/ 2013.
- [108] B. Lo Piccolo, P. Spatig, T. Kruml, J. L. Martin, and J. Bonneville, "Characterising thermally activated dislocation mechanisms," in *Dislocations 2000: An International Conference on the Fundamentals of Plastic Deformation, 19-22 June 2000, Switzerland, 2001*, pp. 251-5.
- [109] J. L. Martin, B. Lo Piccolo, T. Kruml, and J. Bonneville, "Characterization of thermally activated dislocation mechanisms using transient tests," *Materials Science and Engineering A*, vol. 322, pp. 118-125, 2002.
- [110] S. Caijun, E. G. Herbert, S. Sangjoon, J. A. LaManna, W. C. Oliver, and G. M. Pharr, "Measurement of power-law creep parameters by instrumented indentation methods," *Journal of the Mechanics and Physics of Solids*, vol. 61, pp. 517-36, 02/ 2013.
- [111] Y. Liu, C. Huang, H. Bei, X. He, and W. Hu, "Room temperature nanoindentation creep of nanocrystalline Cu and Cu alloys," *Materials Letters*, vol. 70, pp. 26-29, 2012.
- [112] D. S. Stone, T. Plookphol, and R. F. Cooper, "Similarity and scaling in creep and load relaxation of single-crystal halite (NaCl)," *Journal of Geophysical Research*, vol. 109, p. 17 pp., 12/10 2004.
- [113] J. K. Mason, A. C. Lund, and C. A. Schuh, "Determining the activation energy and volume for the onset of plasticity during nanoindentation," *Physical Review B (Condensed Matter and Materials Physics)*, vol. 73, pp. 54102-1, 02/01 2006.
- [114] D. Pan and M. Chen, "Rate-change instrumented indentation for measuring strain rate sensitivity," *Journal of Materials Research*, vol. 24, pp. 1466-1470, 2009.
- [115] X. Baoxing, Y. Zhufeng, and C. Xi, "Characterization of strain rate sensitivity and activation volume using the indentation relaxation test," *Journal of Physics D: Applied Physics*, vol. 43, p. 245401 (5 pp.), 05/05 2010.
- [116] D. Stegall and A. A. Elmustafa, "Investigation of the Indentation Size Effect in FCC Metals Using Activation Volume Analysis," in *Supplemental Proceedings*, ed: John Wiley & Sons, Inc., 2012, pp. 747-752.
- [117] M. Z. Butt, P. Feltham, and S. M. Raza, "Stress relaxation in nickel between 15 and 300 K," *Physica Status Solidi (A) Applied Research*, vol. 84, pp. k125-k127, 1984.

- [118] Y. M. Wang, A. V. Hamza, and E. Ma, "Activation volume and density of mobile dislocations in plastically deforming nanocrystalline Ni," *Applied Physics Letters*, vol. 86, pp. 241917-1, 06/13 2005.
- [119] E. Demir, D. Raabe, N. Zaafarani, and S. Zaeferrer, "Investigation of the indentation size effect through the measurement of the geometrically necessary dislocations beneath small indents of different depths using EBSD tomography," *Acta Materialia*, vol. 57, pp. 559-69, 01/ 2009.
- [120] T. R. Bieler, J. Hairong, L. P. Lehman, T. Kirkpatrick, E. J. Cotts, and B. Nandagopal, "Influence of Sn grain size and orientation on the thermomechanical response and reliability of Pb-free solder joints," *IEEE Transactions on Components and Packaging Technology*, vol. 31, pp. 370-81, 06/ 2008.
- [121] Z. H. Cao, L. Wang, K. Hu, Y. L. Huang, and X. K. Meng, "Microstructural evolution and its influence on creep and stress relaxation in nanocrystalline Ni," *Acta Materialia*, vol. 60, pp. 6742-6754, 2012.
- [122] T. H. Courtney, *Mechanical Behavior of Materials*. New York: McGraw Hill, 1990.
- [123] R. B. King, "Elastic analysis of some punch problems for a layered medium," *International Journal of Solids and Structures*, vol. 23, pp. 1657-1664, 1987.
- [124] J. Nye, "Some geometrical relations in dislocated crystals," *Acta metallurgica*, vol. 1, pp. 153-162, 1953.
- [125] Z. Zong, J. Lou, O. O. Adewoye, A. A. Elmustafa, F. Hammad, and W. O. Soboyejo, "Indentation size effects in the nano- and micro-hardness of fcc single crystal metals," *Materials Science and Engineering A*, vol. 434, pp. 178-187, 2006.
- [126] W. G. Johnston and J. J. Gilman, "Dislocation velocities, dislocation densities, and plastic flow in lithium fluoride crystals," *Journal of Applied Physics*, vol. 30, pp. 129-144, 1959.
- [127] R. W. Rohde and C. H. Pitt, "Stress relaxation in nickel single crystals between 77-350K," *Journal of Applied Physics*, vol. 39, pp. 3186-3192, 1968.
- [128] L. E. Murr, *Interfacial Phenomenon in Metals and Alloys*. Reading Massachusetts: Addison Wesley, 1975.
- [129] M. Rester, C. Motz, and R. Pippan, "Stacking fault energy and indentation size effect: Do they interact?," *Scripta Materialia*, vol. 58, pp. 187-190, 2008.
- [130] L. Delehouzee and A. Deruyttere, "Stacking fault density in solid solutions based on copper, silver, nickel, aluminium and lead," *Acta Metallurgica*, vol. 15, pp. 727-734, 1967.
- [131] Y. C. Liu and P. C. J. Gallagher, "Analytical expressions for the composition dependence of stacking fault energies and probabilities in binary silver systems," *Journal of Applied Physics*, vol. 42, pp. 3322-8, 08/ 1971.
- [132] B. Q. Li, B. Li, Y. B. Wang, M. L. Sui, and E. Ma, "Twinning mechanism via synchronized activation of partial dislocations in face-centered-cubic materials," *Scripta Materialia*, vol. 64, pp. 852-5, 05/ 2011.
- [133] N. Bernstein and E. B. Tadmor, "Tight-binding calculations of stacking energies and twinnability in fcc metals," *Physical Review B (Condensed Matter)*, vol. 69, pp. 94116-1, 03/01 2004.
- [134] E. B. Tadmor and N. Bernstein, "A first-principles measure for the twinnability of FCC metals," *Journal of the Mechanics and Physics of Solids*, vol. 52, pp. 2507-2519, 11// 2004.



- [135] X. H. Chen, L. Lu, and K. Lu, "Grain size dependence of tensile properties in ultrafine-grained Cu with nanoscale twins," *Scripta Materialia*, vol. 64, pp. 311-314, 2// 2011.

**APPENDIX A**  
**COPYRIGHT PERMISSIONS**

The content given in Chapters Three, Four, and Five of this dissertation are based on works published in the following Journals. Chapter Seven was adapted from a Conference article.

Chapter 3: D. E. Stegall, M. A. Mamun, B. Crawford, and A. Elmustafa, "Indentation size effect in FCC metals: An examination of experimental techniques and the bilinear behavior," *Journal of Materials Research*, vol. 27, pp. 1543-1552, 2012, MRS Publishing

Chapter 4: D E Stegall and A A Elmustafa, "Activation volume of pure face centered cubic metals using uniaxial testing and nanoindentation equipped with high load capability", *Materials Research Express*, Vol. 3, 10, pp.105024, 2016, IOP Publishing

Chapter 5: D. E. Stegall, M. A. Mamun, B. Crawford, and A. A. Elmustafa, "Repeated load relaxation testing of pure polycrystalline nickel at room temperature using nanoindentation," *Applied Physics Letters*, vol. 104, p. 041902 (4 pp.), 2014, AIP Publishing

Chapter 7: D.E. Stegall, A.A. Elmustafa, "The role of stacking fault energy and deformation twinning on the indentation size effect of FCC pure metals and alloys," in *Supplemental Proceedings*, ed: John Wiley & Sons, Inc., 2012, pp. 739-746.

Individual copyright permissions are given as for each publication.

**CAMBRIDGE UNIVERSITY PRESS LICENSE  
TERMS AND CONDITIONS**

Oct 24, 2016

---

This Agreement between David E Stegall ("You") and Cambridge University Press ("Cambridge University Press") consists of your license details and the terms and conditions provided by Cambridge University Press and Copyright Clearance Center.

|   |  |
|---|--|
| License Number                                    | 3975480801249  |
| License date                                      | Oct 24, 2016   |
| Licensed Content Publisher                        | Cambridge University Press   |
| Licensed Content Publication                      | Journal of Materials Research  |
| Licensed Content Title                            | Indentation size effect in FCC metals: An examination of experimental techniques and the bilinear behavior                     |
| Licensed Content Author                           | David E. Stegall, Md. Abdullah Mamun, Bryan Crawford, Abdelmageed Elmustafa  |
| Licensed Content Date                             | Apr 20, 2012   |
| Licensed Content Volume Number                    | 27   |
| Licensed Content Issue Number                     | 12   |
| Start page  | 1543   |
| End page  | 1552   |
| Type of Use                                       | Dissertation/Thesis  |
| Requestor type                                    | Author   |
| Portion   | Full article   |
| Author of this Cambridge University Press article | Yes  |
| Author / editor of the new work                   | Yes  |
| Order reference number                            | CAO2794  |
| Territory for reuse                               | World  |
| Title of your thesis / dissertation               | An Examination of the Indentation Size Effect in FCC Metals and Alloys from a Kinetics Based Perspective using Nanoindentation |
| Expected completion date                          | Dec 2016   |
| Estimated size(pages)                             | 134  |
| Requestor Location                                | David E Stegall<br>20 Belles Cove Drive<br>Apt H<br><br>Poquoson, VA 23662<br>United States<br>Attn: David E Stegall           |
| Publisher Tax ID                                  | GB823847609  |

|                      |  |
|----------------------|--|
| Billing Type         | Invoice  |
| Billing Address      | David E Stegall<br>20 Belles Cove Drive<br>Apt H<br><br>Poquoson, VA 23662<br>United States<br>Attn: David E Stegall |
| Total                | 0.00 USD   |
| Terms and Conditions |  |

### TERMS & CONDITIONS

Cambridge University Press grants the Licensee permission on a non-exclusive non-transferable basis to reproduce, make available or otherwise use the Licensed content 'Content' in the named territory 'Territory' for the purpose listed 'the Use' on Page 1 of this Agreement subject to the following terms and conditions.

1. The License is limited to the permission granted and the Content detailed herein and does not extend to any other permission or content.
2. Cambridge gives no warranty or indemnity in respect of any third-party copyright material included in the Content, for which the Licensee should seek separate permission clearance.
3. The integrity of the Content must be ensured.
4. The License does extend to any edition published specifically for the use of handicapped or reading-impaired individuals.
5. The Licensee shall provide a prominent acknowledgement in the following format:  
author/s, title of article, name of journal, volume number, issue number, page references, , reproduced with permission.

Other terms and conditions:

v1.0

Questions? [customercare@copyright.com](mailto:customercare@copyright.com) or +1-855-239-3415 (toll free in the US) or +1-978-646-2777.

---

---



DAVID STEGALL &lt;dsteg001@odu.edu&gt;

---

## Permission to use Journal paper in Dissertation

---

**Permissions** <permissions@iop.org>  
To: DAVID STEGALL <dsteg001@odu.edu>

Wed, Oct 26, 2016 at 9:51 AM

Dear David Stegall,

Thank you for your email and for taking the time to seek this permission.

Regarding:

D E Stegall and A A Elmustafa 2016 Mater. Res. Express 3 105024)

When you transferred the copyright in your article to IOP, we granted back to you certain rights, including the right to include the Final Published Version of the article within any thesis or dissertation. Please note you may need to obtain separate permission for any third party content you included within your article.

Please include citation details, "© IOP Publishing. Reproduced with permission. All rights reserved" and for online use, a link to the Version of Record.

The only restriction is that if, at a later date, your thesis were to be published commercially, further permission would be required.

Please let me know if you have any further questions.

In the meantime, I wish you the best of luck with the completion of your dissertation.

Kind regards,

### Copyright & Permissions Team

Contact Details

E-mail: [permissions@iop.org](mailto:permissions@iop.org)

For further information: <http://iopscience.iop.org/page/copyright>

Please see our Author Rights Policy <http://iopublishing.org/author-rights/>

**Please note:** We do not provide signed permission forms as a separate attachment. Please print this email and provide it to your institution as proof of permission.

**Please note:** Any statements made by IOP Publishing to the effect that authors do not need to get permission to use any content are not intended to constitute any sort of legal advice. Authors must make their own decisions as to the suitability of the content they are using and whether they require permission for it to be published within their article.

**AIP PUBLISHING LLC LICENSE  
TERMS AND CONDITIONS**

Oct 24, 2016

This Agreement between David E Stegall ("You") and AIP Publishing LLC ("AIP Publishing LLC") consists of your license details and the terms and conditions provided by AIP Publishing LLC and Copyright Clearance Center.

|                                     |  |
|-------------------------------------|--|
| License Number                      | 3975480992509  |
| License date                        | Oct 24, 2016   |
| Licensed Content Publisher          | AIP Publishing LLC   |
| Licensed Content Publication        | Applied Physics Letters  |
| Licensed Content Title              | Repeated load relaxation testing of pure polycrystalline nickel at room temperature using nanoindentation                      |
| Licensed Content Author             | D. E. Stegall, M. A. Mamun, B. Crawford, et al.  |
| Licensed Content Date               | Jan 27, 2014   |
| Licensed Content Volume Number      | 104  |
| Licensed Content Issue Number       | 4  |
| Type of Use                         | Thesis/Dissertation  |
| Requestor type                      | Author (original article)  |
| Format                              | Print and electronic   |
| Portion                             | Abstract   |
| Number of Abstracts                 | 1  |
| Will you be translating?            | No   |
| Order reference number              | CAO2794  |
| Title of your thesis / dissertation | An Examination of the Indentation Size Effect in FCC Metals and Alloys from a Kinetics Based Perspective using Nanoindentation |
| Expected completion date            | Dec 2016   |
| Estimated size (number of pages)    | 134  |
| Requestor Location                  | David E Stegall<br>20 Belles Cove Drive<br>Apt H<br><br>Poquoson, VA 23662<br>United States<br>Attn: David E Stegall           |
| Billing Type                        | Invoice  |
| Billing Address                     | David E Stegall<br>20 Belles Cove Drive<br>Apt H<br><br>Poquoson, VA 23662   |

United States  
Attn: David E Stegall

Total 0.00 USD

[Terms and Conditions](#)

AIP Publishing LLC -- Terms and Conditions: Permissions Uses

AIP Publishing hereby grants to you the non-exclusive right and license to use and/or distribute the Material according to the use specified in your order, on a one-time basis, for the specified term, with a maximum distribution equal to the number that you have ordered. Any links or other content accompanying the Material are not the subject of this license.

1. You agree to include the following copyright and permission notice with the reproduction of the Material: "Reprinted from [FULL CITATION], with the permission of AIP Publishing." For an article, the credit line and permission notice must be printed on the first page of the article or book chapter. For photographs, covers, or tables, the notice may appear with the Material, in a footnote, or in the reference list.
2. If you have licensed reuse of a figure, photograph, cover, or table, it is your responsibility to ensure that the material is original to AIP Publishing and does not contain the copyright of another entity, and that the copyright notice of the figure, photograph, cover, or table does not indicate that it was reprinted by AIP Publishing, with permission, from another source. Under no circumstances does AIP Publishing purport or intend to grant permission to reuse material to which it does not hold appropriate rights.  
You may not alter or modify the Material in any manner. You may translate the Material into another language only if you have licensed translation rights. You may not use the Material for promotional purposes.
3. The foregoing license shall not take effect unless and until AIP Publishing or its agent, Copyright Clearance Center, receives the Payment in accordance with Copyright Clearance Center Billing and Payment Terms and Conditions, which are incorporated herein by reference.
4. AIP Publishing or Copyright Clearance Center may, within two business days of granting this license, revoke the license for any reason whatsoever, with a full refund payable to you. Should you violate the terms of this license at any time, AIP Publishing, or Copyright Clearance Center may revoke the license with no refund to you. Notice of such revocation will be made using the contact information provided by you. Failure to receive such notice will not nullify the revocation.
5. AIP Publishing makes no representations or warranties with respect to the Material. You agree to indemnify and hold harmless AIP Publishing, and their officers, directors, employees or agents from and against any and all claims arising out of your use of the Material other than as specifically authorized herein.
6. The permission granted herein is personal to you and is not transferable or assignable without the prior written permission of AIP Publishing. This license may not be amended except in a writing signed by the party to be charged.
7. If purchase orders, acknowledgments or check endorsements are issued on any forms containing terms and conditions which are inconsistent with these provisions, such inconsistent terms and conditions shall be of no force and effect. This document, including the CCC Billing and Payment Terms and Conditions, shall be the entire agreement between the parties relating to the subject matter hereof.

This Agreement shall be governed by and construed in accordance with the laws of the State of New York. Both parties hereby submit to the jurisdiction of the courts of New York County for purposes of resolving any disputes that may arise hereunder.

V1.1

Questions? [customer@copyright.com](mailto:customer@copyright.com) or +1-855-239-3415 (toll free in the US) or +1-978-646-2777.



**AIP PUBLISHING LLC LICENSE  
TERMS AND CONDITIONS**

Oct 24, 2016

This Agreement between David E Stegall ("You") and AIP Publishing LLC ("AIP Publishing LLC") consists of your license details and the terms and conditions provided by AIP Publishing LLC and Copyright Clearance Center.

|                                     |  |
|-------------------------------------|--|
| License Number                      | 3975481133159  |
| License date                        | Oct 24, 2016   |
| Licensed Content Publisher          | AIP Publishing LLC   |
| Licensed Content Publication        | Applied Physics Letters  |
| Licensed Content Title              | Repeated load relaxation testing of pure polycrystalline nickel at room temperature using nanoindentation                      |
| Licensed Content Author             | D. E. Stegall, M. A. Mamun, B. Crawford, et al.  |
| Licensed Content Date               | Jan 27, 2014   |
| Licensed Content Volume Number      | 104  |
| Licensed Content Issue Number       | 4  |
| Type of Use                         | Thesis/Dissertation  |
| Requestor type                      | Author (original article)  |
| Format                              | Print and electronic   |
| Portion                             | Figure/Table   |
| Number of figures/tables            | 6  |
| Order reference number              | CAO2794  |
| Title of your thesis / dissertation | An Examination of the Indentation Size Effect in FCC Metals and Alloys from a Kinetics Based Perspective using Nanoindentation |
| Expected completion date            | Dec 2016   |
| Estimated size (number of pages)    | 134  |
| Requestor Location                  | David E Stegall<br>20 Belles Cove Drive<br>Apt H<br><br>Poquoson, VA 23662<br>United States<br>Attn: David E Stegall           |
| Billing Type                        | Invoice  |
| Billing Address                     | David E Stegall<br>20 Belles Cove Drive<br>Apt H<br><br>Poquoson, VA 23662<br>United States<br>Attn: David E Stegall           |

Total 0.00 USD

[Terms and Conditions](#)

AIP Publishing LLC -- Terms and Conditions: Permissions Uses

AIP Publishing hereby grants to you the non-exclusive right and license to use and/or distribute the Material according to the use specified in your order, on a one-time basis, for the specified term, with a maximum distribution equal to the number that you have ordered. Any links or other content accompanying the Material are not the subject of this license.

1. You agree to include the following copyright and permission notice with the reproduction of the Material: "Reprinted from [FULL CITATION], with the permission of AIP Publishing." For an article, the credit line and permission notice must be printed on the first page of the article or book chapter. For photographs, covers, or tables, the notice may appear with the Material, in a footnote, or in the reference list.
2. If you have licensed reuse of a figure, photograph, cover, or table, it is your responsibility to ensure that the material is original to AIP Publishing and does not contain the copyright of another entity, and that the copyright notice of the figure, photograph, cover, or table does not indicate that it was reprinted by AIP Publishing, with permission, from another source. Under no circumstances does AIP Publishing purport or intend to grant permission to reuse material to which it does not hold appropriate rights.  
You may not alter or modify the Material in any manner. You may translate the Material into another language only if you have licensed translation rights. You may not use the Material for promotional purposes.
3. The foregoing license shall not take effect unless and until AIP Publishing or its agent, Copyright Clearance Center, receives the Payment in accordance with Copyright Clearance Center Billing and Payment Terms and Conditions, which are incorporated herein by reference.
4. AIP Publishing or Copyright Clearance Center may, within two business days of granting this license, revoke the license for any reason whatsoever, with a full refund payable to you. Should you violate the terms of this license at any time, AIP Publishing, or Copyright Clearance Center may revoke the license with no refund to you. Notice of such revocation will be made using the contact information provided by you. Failure to receive such notice will not nullify the revocation.
5. AIP Publishing makes no representations or warranties with respect to the Material. You agree to indemnify and hold harmless AIP Publishing, and their officers, directors, employees or agents from and against any and all claims arising out of your use of the Material other than as specifically authorized herein.
6. The permission granted herein is personal to you and is not transferable or assignable without the prior written permission of AIP Publishing. This license may not be amended except in a writing signed by the party to be charged.
7. If purchase orders, acknowledgments or check endorsements are issued on any forms containing terms and conditions which are inconsistent with these provisions, such inconsistent terms and conditions shall be of no force and effect. This document, including the CCC Billing and Payment Terms and Conditions, shall be the entire agreement between the parties relating to the subject matter hereof.

This Agreement shall be governed by and construed in accordance with the laws of the State of New York. Both parties hereby submit to the jurisdiction of the courts of New York County for purposes of resolving any disputes that may arise hereunder.

V 1.1

Questions? [customer@copyright.com](mailto:customer@copyright.com) or +1-855-239-3415 (toll free in the US) or +1-978-646-2777.

**AIP PUBLISHING LLC LICENSE  
TERMS AND CONDITIONS**

Oct 24, 2016

This Agreement between David E Stegall ("You") and AIP Publishing LLC ("AIP Publishing LLC") consists of your license details and the terms and conditions provided by AIP Publishing LLC and Copyright Clearance Center.

|                                     |  |
|-------------------------------------|--|
| License Number                      | 3975490682173  |
| License date                        | Oct 24, 2016   |
| Licensed Content Publisher          | AIP Publishing LLC   |
| Licensed Content Publication        | Applied Physics Letters  |
| Licensed Content Title              | Repeated load relaxation testing of pure polycrystalline nickel at room temperature using nanoindentation                      |
| Licensed Content Author             | D. E. Stegall, M. A. Mamun, B. Crawford, et al.  |
| Licensed Content Date               | Jan 27, 2014   |
| Licensed Content Volume Number      | 104  |
| Licensed Content Issue Number       | 4  |
| Type of Use                         | Thesis/Dissertation  |
| Requestor type                      | Author (original article)  |
| Format                              | Print and electronic   |
| Portion                             | Excerpt (> 800 words)  |
| Will you be translating?            | No   |
| Order reference number              | CA02794  |
| Title of your thesis / dissertation | An Examination of the Indentation Size Effect in FCC Metals and Alloys from a Kinetics Based Perspective using Nanoindentation |
| Expected completion date            | Dec 2016   |
| Estimated size (number of pages)    | 134  |
| Requestor Location                  | David E Stegall<br>20 Belles Cove Drive<br>Apt H<br><br>Poquoson, VA 23662<br>United States<br>Attn: David E Stegall           |
| Billing Type                        | Invoice  |
| Billing Address                     | David E Stegall<br>20 Belles Cove Drive<br>Apt H<br><br>Poquoson, VA 23662<br>United States<br>Attn: David E Stegall           |
| Total                               | 0.00 USD   |

## Terms and Conditions

### AIP Publishing LLC -- Terms and Conditions: Permissions Uses

AIP Publishing hereby grants to you the non-exclusive right and license to use and/or distribute the Material according to the use specified in your order, on a one-time basis, for the specified term, with a maximum distribution equal to the number that you have ordered. Any links or other content accompanying the Material are not the subject of this license.

1. You agree to include the following copyright and permission notice with the reproduction of the Material: "Reprinted from [FULL CITATION], with the permission of AIP Publishing." For an article, the credit line and permission notice must be printed on the first page of the article or book chapter. For photographs, covers, or tables, the notice may appear with the Material, in a footnote, or in the reference list.
2. If you have licensed reuse of a figure, photograph, cover, or table, it is your responsibility to ensure that the material is original to AIP Publishing and does not contain the copyright of another entity, and that the copyright notice of the figure, photograph, cover, or table does not indicate that it was reprinted by AIP Publishing, with permission, from another source. Under no circumstances does AIP Publishing purport or intend to grant permission to reuse material to which it does not hold appropriate rights. You may not alter or modify the Material in any manner. You may translate the Material into another language only if you have licensed translation rights. You may not use the Material for promotional purposes.
3. The foregoing license shall not take effect unless and until AIP Publishing or its agent, Copyright Clearance Center, receives the Payment in accordance with Copyright Clearance Center Billing and Payment Terms and Conditions, which are incorporated herein by reference.
4. AIP Publishing or Copyright Clearance Center may, within two business days of granting this license, revoke the license for any reason whatsoever, with a full refund payable to you. Should you violate the terms of this license at any time, AIP Publishing, or Copyright Clearance Center may revoke the license with no refund to you. Notice of such revocation will be made using the contact information provided by you. Failure to receive such notice will not nullify the revocation.
5. AIP Publishing makes no representations or warranties with respect to the Material. You agree to indemnify and hold harmless AIP Publishing, and their officers, directors, employees or agents from and against any and all claims arising out of your use of the Material other than as specifically authorized herein.
6. The permission granted herein is personal to you and is not transferable or assignable without the prior written permission of AIP Publishing. This license may not be amended except in a writing signed by the party to be charged.
7. If purchase orders, acknowledgments or check endorsements are issued on any forms containing terms and conditions which are inconsistent with these provisions, such inconsistent terms and conditions shall be of no force and effect. This document, including the CCC Billing and Payment Terms and Conditions, shall be the entire agreement between the parties relating to the subject matter hereof.

This Agreement shall be governed by and construed in accordance with the laws of the State of New York. Both parties hereby submit to the jurisdiction of the courts of New York County for purposes of resolving any disputes that may arise hereunder.

V1.1

Questions? [customercare@copyright.com](mailto:customercare@copyright.com) or +1-855-239-3415 (toll free in the US) or +1-978-646-2777.

---



DAVID STEGALL &lt;dsteg001@odu.edu&gt;

---

**NON RIGHTSLINK**

---

**Wiley Global Permissions** <permissions@wiley.com>  
To: DAVID STEGALL <dsteg001@odu.edu>

Thu, Nov 3, 2016 at 12:12 PM

Dear David:

Thank you for your request.

Permission is hereby granted for the use requested subject to the usual acknowledgements (author, title of material, title of book/journal, ourselves as publisher). You should also duplicate the copyright notice that appears in the Wiley publication; this can be found on the copyright page if the material is a book or within the article if it is a journal.

Any third party material is expressly excluded from this permission. If any of the material you wish to use appears within our work with credit to another source, authorization from that source must be obtained.

This permission does not include the right to grant others permission to photocopy or otherwise reproduce this material except for accessible versions made by non-profit organizations serving the blind, visually impaired and other persons with print disabilities (VIPs).

Sincerely,

---

Manager, Copyright & Permissions

Wiley

---

111 River Street  
Hoboken, NJ 07030-5774  
U.S.  
[permissions@wiley.com](mailto:permissions@wiley.com)

**JOHN WILEY AND SONS LICENSE  
TERMS AND CONDITIONS**

Oct 24, 2016

---

This Agreement between David E Stegall ("You") and John Wiley and Sons ("John Wiley and Sons") consists of your license details and the terms and conditions provided by John Wiley and Sons and Copyright Clearance Center.

|                                     |  |
|-------------------------------------|--|
| License Number                      | 3975490761823  |
| License date                        | Oct 24, 2016   |
| Licensed Content Publisher          | John Wiley and Sons  |
| Licensed Content Publication        | Wiley eBooks   |
| Licensed Content Title              | The Role of Stacking Fault Energy and Deformation Twinning on the Indentation Size Effect of FCC Pure Metals and Alloys        |
| Licensed Content Author             | David Stegall,A.A. Elmustafa   |
| Licensed Content Date               | Jun 7, 2012  |
| Licensed Content Pages              | 8  |
| Type of use                         | Dissertation/Thesis  |
| Requestor type                      | Author of this Wiley chapter   |
| Format                              | Print and electronic   |
| Portion                             | Full chapter   |
| Will you be translating?            | No   |
| Order reference number              | CA02794  |
| Title of your thesis / dissertation | An Examination of the Indentation Size Effect in FCC Metals and Alloys from a Kinetics Based Perspective using Nanoindentation |
| Expected completion date            | Dec 2016   |
| Expected size (number of pages)     | 134  |
| Requestor Location                  | David E Stegall<br>20 Belles Cove Drive<br>Apt H<br><br>Poquoson, VA 23662<br>United States<br>Attn: David E Stegall           |
| Publisher Tax ID                    | EU826007151  |
| Billing Type                        | Invoice  |
| Billing Address                     | David E Stegall<br>20 Belles Cove Drive<br>Apt H<br><br>Poquoson, VA 23662<br>United States<br>Attn: David E Stegall           |
| Total                               | 0.00 USD   |
| Terms and Conditions                |  |

**TERMS AND CONDITIONS**

This copyrighted material is owned by or exclusively licensed to John Wiley & Sons, Inc. or one of its group companies (each a "Wiley Company") or handled on behalf of a society with which a Wiley Company has exclusive publishing rights in relation to a particular work (collectively "WILEY"). By clicking "accept" in connection with completing this licensing transaction, you agree that the following terms and conditions apply to this transaction (along with the billing and payment terms and conditions established by the Copyright Clearance Center Inc., ("CCC's Billing and Payment terms and conditions"), at the time that you opened your RightsLink account (these are available at any time at <http://mvaccount.copyright.com>).

### Terms and Conditions

- The materials you have requested permission to reproduce or reuse (the "Wiley Materials") are protected by copyright.
- You are hereby granted a personal, non-exclusive, non-sub licensable (on a stand-alone basis), non-transferable, worldwide, limited license to reproduce the Wiley Materials for the purpose specified in the licensing process. This license, **and any CONTENT (PDF or image file) purchased as part of your order**, is for a one-time use only and limited to any maximum distribution number specified in the license. The first instance of republication or reuse granted by this license must be completed within two years of the date of the grant of this license (although copies prepared before the end date may be distributed thereafter). The Wiley Materials shall not be used in any other manner or for any other purpose, beyond what is granted in the license. Permission is granted subject to an appropriate acknowledgement given to the author, title of the material/book/journal and the publisher. You shall also duplicate the copyright notice that appears in the Wiley publication in your use of the Wiley Material. Permission is also granted on the understanding that nowhere in the text is a previously published source acknowledged for all or part of this Wiley Material. Any third party content is expressly excluded from this permission.
- With respect to the Wiley Materials, all rights are reserved. Except as expressly granted by the terms of the license, no part of the Wiley Materials may be copied, modified, adapted (except for minor reformatting required by the new Publication), translated, reproduced, transferred or distributed, in any form or by any means, and no derivative works may be made based on the Wiley Materials without the prior permission of the respective copyright owner. **For STM Signatory Publishers clearing permission under the terms of the [STM Permissions Guidelines](#) only, the terms of the license are extended to include subsequent editions and for editions in other languages, provided such editions are for the work as a whole in situ and does not involve the separate exploitation of the permitted figures or extracts**, You may not alter, remove or suppress in any manner any copyright, trademark or other notices displayed by the Wiley Materials. You may not license, rent, sell, loan, lease, pledge, offer as security, transfer or assign the Wiley Materials on a stand-alone basis, or any of the rights granted to you hereunder to any other person.
- The Wiley Materials and all of the intellectual property rights therein shall at all times remain the exclusive property of John Wiley & Sons Inc, the Wiley Companies, or their respective licensors, and your interest therein is only that of having possession of and the right to reproduce the Wiley Materials pursuant to Section 2 herein during the continuance of this Agreement. You agree that you own no right, title or interest in or to the Wiley Materials or any of the intellectual property rights therein. You shall have no rights hereunder other than the license as provided for above in Section 2. No right, license or interest to any trademark, trade name, service mark or other branding

("Marks") of WILEY or its licensors is granted hereunder, and you agree that you shall not assert any such right, license or interest with respect thereto

- NEITHER WILEY NOR ITS LICENSORS MAKES ANY WARRANTY OR REPRESENTATION OF ANY KIND TO YOU OR ANY THIRD PARTY, EXPRESS, IMPLIED OR STATUTORY, WITH RESPECT TO THE MATERIALS OR THE ACCURACY OF ANY INFORMATION CONTAINED IN THE MATERIALS, INCLUDING, WITHOUT LIMITATION, ANY IMPLIED WARRANTY OF MERCHANTABILITY, ACCURACY, SATISFACTORY QUALITY, FITNESS FOR A PARTICULAR PURPOSE, USABILITY, INTEGRATION OR NON-INFRINGEMENT AND ALL SUCH WARRANTIES ARE HEREBY EXCLUDED BY WILEY AND ITS LICENSORS AND WAIVED BY YOU.
- WILEY shall have the right to terminate this Agreement immediately upon breach of this Agreement by you.
- You shall indemnify, defend and hold harmless WILEY, its Licensors and their respective directors, officers, agents and employees, from and against any actual or threatened claims, demands, causes of action or proceedings arising from any breach of this Agreement by you.
- IN NO EVENT SHALL WILEY OR ITS LICENSORS BE LIABLE TO YOU OR ANY OTHER PARTY OR ANY OTHER PERSON OR ENTITY FOR ANY SPECIAL, CONSEQUENTIAL, INCIDENTAL, INDIRECT, EXEMPLARY OR PUNITIVE DAMAGES, HOWEVER CAUSED, ARISING OUT OF OR IN CONNECTION WITH THE DOWNLOADING, PROVISIONING, VIEWING OR USE OF THE MATERIALS REGARDLESS OF THE FORM OF ACTION, WHETHER FOR BREACH OF CONTRACT, BREACH OF WARRANTY, TORT, NEGLIGENCE, INFRINGEMENT OR OTHERWISE (INCLUDING, WITHOUT LIMITATION, DAMAGES BASED ON LOSS OF PROFITS, DATA, FILES, USE, BUSINESS OPPORTUNITY OR CLAIMS OF THIRD PARTIES), AND WHETHER OR NOT THE PARTY HAS BEEN ADVISED OF THE POSSIBILITY OF SUCH DAMAGES. THIS LIMITATION SHALL APPLY NOTWITHSTANDING ANY FAILURE OF ESSENTIAL PURPOSE OF ANY LIMITED REMEDY PROVIDED HEREIN.
- Should any provision of this Agreement be held by a court of competent jurisdiction to be illegal, invalid, or unenforceable, that provision shall be deemed amended to achieve as nearly as possible the same economic effect as the original provision, and the legality, validity and enforceability of the remaining provisions of this Agreement shall not be affected or impaired thereby.
- The failure of either party to enforce any term or condition of this Agreement shall not constitute a waiver of either party's right to enforce each and every term and condition of this Agreement. No breach under this agreement shall be deemed waived or excused by either party unless such waiver or consent is in writing signed by the party granting such waiver or consent. The waiver by or consent of a party to a breach of any provision of this Agreement shall not operate or be construed as a waiver of or consent to any other or subsequent breach by such other party.
- This Agreement may not be assigned (including by operation of law or otherwise) by you without WILEY's prior written consent.



- Any fee required for this permission shall be non-refundable after thirty (30) days from receipt by the CCC.
- These terms and conditions together with CCC's Billing and Payment terms and conditions (which are incorporated herein) form the entire agreement between you and WILEY concerning this licensing transaction and (in the absence of fraud) supersedes all prior agreements and representations of the parties, oral or written. This Agreement may not be amended except in writing signed by both parties. This Agreement shall be binding upon and inure to the benefit of the parties' successors, legal representatives, and authorized assigns.
- In the event of any conflict between your obligations established by these terms and conditions and those established by CCC's Billing and Payment terms and conditions, these terms and conditions shall prevail.
- WILEY expressly reserves all rights not specifically granted in the combination of (i) the license details provided by you and accepted in the course of this licensing transaction, (ii) these terms and conditions and (iii) CCC's Billing and Payment terms and conditions.
- This Agreement will be void if the Type of Use, Format, Circulation, or Requestor Type was misrepresented during the licensing process.
- This Agreement shall be governed by and construed in accordance with the laws of the State of New York, USA, without regards to such state's conflict of law rules. Any legal action, suit or proceeding arising out of or relating to these Terms and Conditions or the breach thereof shall be instituted in a court of competent jurisdiction in New York County in the State of New York in the United States of America and each party hereby consents and submits to the personal jurisdiction of such court, waives any objection to venue in such court and consents to service of process by registered or certified mail, return receipt requested, at the last known address of such party.

## **WILEY OPEN ACCESS TERMS AND CONDITIONS**

Wiley Publishes Open Access Articles in fully Open Access Journals and in Subscription journals offering Online Open. Although most of the fully Open Access journals publish open access articles under the terms of the Creative Commons Attribution (CC BY) License only, the subscription journals and a few of the Open Access Journals offer a choice of Creative Commons Licenses. The license type is clearly identified on the article.

### **The Creative Commons Attribution License**

The [Creative Commons Attribution License \(CC-BY\)](#) allows users to copy, distribute and transmit an article, adapt the article and make commercial use of the article. The CC-BY license permits commercial and non-

### **Creative Commons Attribution Non-Commercial License**

The [Creative Commons Attribution Non-Commercial \(CC-BY-NC\) License](#) permits use, distribution and reproduction in any medium, provided the original work is properly cited and is not used for commercial purposes.(see below)

### **Creative Commons Attribution-Non-Commercial-NoDerivs License**

The [Creative Commons Attribution Non-Commercial-NoDerivs License](#) (CC-BY-NC-ND) permits use, distribution and reproduction in any medium, provided the original work is properly cited, is not used for commercial purposes and no modifications or adaptations are made. (see below)

### **Use by commercial "for-profit" organizations**

Use of Wiley Open Access articles for commercial, promotional, or marketing purposes requires further explicit permission from Wiley and will be subject to a fee.

Further details can be found on Wiley Online Library

<http://olabout.wiley.com/WileyCDA/Section/id-410895.html>

**Other Terms and Conditions:**

**v1.10 Last updated September 2015**

Questions? [customercare@copyright.com](mailto:customercare@copyright.com) or +1-855-239-3415 (toll free in the US) or +1-978-646-2777.

---

---

## VITA

David Earl Stegall

David E. Stegall obtained his B.S. Mechanical Engineering degree from Old Dominion University in 1996. He went on to complete a M.E. in Mechanical Engineering from Old Dominion University in 2000. Later, he earned a MBA from Old Dominion University in 2004. He completed the requirements for a Ph.D. in Mechanical Engineering in 2016.

David joined the nanomechanical properties research group under the direction of Dr. A.A. Elmustafa and began to investigate the indentation size effect (ISE) phenomena in face centered cubic metals and alloys. This research was primarily concerned with the development of novel experimental indentation methods that could be used to examine the fundamental dislocation behavior associated with the ISE in metals. He has coauthored four refereed journal articles and four conference proceedings articles during his research at Old Dominion University.

Prior to joining the Ph.D. program at Old Dominion University, he has worked in various capacities as an engineer in research and test in the aerospace, shipbuilding, and manufacturing industries for over 20 years.